Addendum

P 1, add paragraph to beginning of Section 1.1: "Cloud seeding is defined as the anthropogenic perturbation of in-cloud microphysics with the intent of increasing precipitation efficiency. In the case of Tasmania this is achieved by initiating a phase change from supercooled liquid to ice. This changes the environment such that after seeding an individual cloud will have ice and water coexisting at the same temperature, as the saturation vapour pressure is lower over ice, relative to water, ice crystals will increase in mass drawing water from the surrounding liquid droplets."

P 1, 4 lines from top: sentence starting with: "The following chapters ..." change to "The later chapters focus on clouds and climate close to Tasmania"

P 1, 13 lines from top: insert "Finally, in Chapter 5, a climatology ..."

P 2, para 2, Reference for the US National Academy of Sciences Report: NRC, 2003: Critical Issues in Weather Modification Research. Washington, D. C.: National Academy Press.

P 8, line 6, add sentence to end of line "Ultimately the WRF model is used to study the environment within which clouds with large amounts of supercooled liquid water form."

P 8, line 10: change sentence "The case studies presented within Chapter 3 are further utilised within Chapter 4 as the basis for the sensitivity study." to "The case studies presented within Chapter 3 are further utilised within Chapter 4 as the basis for the sensitivity study, the fact that no significant changes are observed between the various experiments increases confidence in the results."

P 8, 1 line from bottom: replace "spacial" with "spatial"

P 18, end of first paragraph add "Further, rainfall totals for the HECA and CSIRO targets behave in a similar fashion (Figure 2.3) indicating the same processes operate throughout the region."

P 22, 8 lines from bottom: replace "calender" with "calendar"

P 26, Figure 2.6: add sentence to end of figure caption "The NE and SE controls are separated along 42S"

P 33, line 4: replace sentence with "It might be argued that a complete compilation of the efficacy of cloud seeding may be obtained with a field programme that examines the microphysics of cloud systems, experimental results from Tasmania 1 and 2, and this work"

P 34, line 9: add sentence "The two case studies were chosen as they represented ideal conditions, where supercooled liquid drops were the dominant hydrometeor species (2006) and less ideal conditions where supercooled liquid and ice (mixed phase) already coexisted (2007)."

P 34, line 11: should read "..followed by the model evaluation.."

P 39, line 13: change "...poor skill initial and boundary conditions..." to "...large errors in the initial and boundary conditions ..."

P 41, line 1: change to "These alternate configurations of the WRF model in general produced results which represented the observations with less skill than the standard configuration"

P 43, Figure 3.5: change “Thermodynamic and wind profiles” to “Thermodynamic (temperature and dew point) and wind profiles”

P 47, line 15: change “... were common, the task here ...” to “were common. The task here is to use the WRF model to simulate ...”

P 47, 3 lines from bottom: change sentence “The absorption coefficients are $0.14500\mathrm{m}^2\mathrm{g}^{-1}$, 0.07350, 0.00234, and 0.00033 ...” to “ the absorption coefficients are $0.14500\mathrm{m}^2\mathrm{g}^{-1}$, $0.07350\mathrm{m}^2\mathrm{g}^{-1}$, $0.00234\mathrm{m}^2\mathrm{g}^{-1}$ and $0.00033\mathrm{m}^2\mathrm{g}^{-1}$ ...”

P 50, 9 lines from bottom: should read “WRF predicts a lower number of pixels above 273 K, then predicts a higher number between 250-273 K”

P 51, Table 3.1: change table heading to “Mean, median and standard deviation of cloud top temperatures (K) together with cloud fraction estimated for both case studies using satellite observations (obs) and w.r.t model with domain 5”

P 54, line 6: change “measured with a hot-wire probe” to “measured with a King hot-wire probe”.

P 55, line 16: change sentence starting with “Further, as the model ice category is initiated with density of 890km m^{-3} and the aircraft measurements were made at temperatures >-20°C where mixed phase conditions ...” to “Further, as the model ice category is initiated with density of 890km m^{-3} and the aircraft measurements were made at temperatures >-20°C, mixed phase conditions ...”

P 55, last line: change “The uncertainty in this quantity is of greater importance during the 2007 case due to its more mixed phase nature” to “The uncertainty due to the presence of ice is considered to be of greater importance during the 2007 case, where larger quantities of ice were measured”. Further add sentence ”It is also noted that certain hot-wire probes underestimate liquid water content in the presence of large drops (correspondence with Warren King, designer of the King hot-wire probe). This effect results in the probe under sampling in high liquid water conditions”.

P 56, line 10: change “Regarding moist fields ...” to “Regarding moist fields (i.e. all liquid and frozen hydrometeors) ...”

P 62, 12 lines from bottom: replace “scalers” with “scalars”

P 64, 4 lines from bottom: change sentence “2006 was especially well represented.” to “2006 was especially well represented, however the model did tend to produce greater quantities (mass) of liquid and frozen hydrometeors relative to the aircraft observations. It is noted however that there is considerable potential for the aircraft observations to under sample w.r.t to these measurements, both the hot-wire and the CAS fail to accurately sample hydrometeors greater than 50μm in diameter.”

P 65, line 5: replace sentence “The final aim is to use the conclusions drawn from the model results to predict thermodynamic and in-cloud microphysical structure for two more case studies.” With ”Ultimately, the intent of this section is to increase confidence in the conclusions drawn from the previous chapter, essentially the microphysical representation of these cloud structures plays a minor role in determining the presence of supercooled liquid water.”

P 66, Figure 4.1: change start of caption to read “Plots showing domain averaged cloud fraction ..”

P 79, 10 lines from bottom: change “schemes” to scheme’s”

P 90, 6 lines from bottom: change “objected” to “objects”

P 92, 10 lines from bottom: Change “There are currently three separate inferences of cloud phase within the MODIS cloud product, the bispectral IR, which uses inherent ...” to “There are currently three separate inferences of cloud phase within the MODIS cloud product. The first algorithm uses the bispectral IR method which exploits inherent ..."

P 93, line 3 add after ".., respectively", "(no smoothing has been implemented on this data, the results are simply contoured to enhance interpretability)."

P 104, 9 lines from top: replace "spacial" with "spatial"

General Declaration

Monash University
Monash Research Graduate School

Declaration for thesis based or partially based on conjointly published or unpublished work

General Declaration

In accordance with Monash University Doctorate Regulation 17/ Doctor of Philosophy and Master of Philosophy (MPhil) regulations the following declarations are made:

I hereby declare that this thesis contains no material which has been accepted for the award of any other degree or diploma at any university or equivalent institution and that, to the best of my knowledge and belief, this thesis contains no material previously published or written by another person, except where due reference is made in the text of the thesis.

This thesis includes one original paper published in a peer reviewed journal and one unpublished publication. The core theme of the thesis is cloud seeding over Tasmania and clouds over Tasmania and the Southern Ocean. The ideas, development and writing up of all the papers in the thesis were the principal responsibility of myself, the candidate, working within the School of Mathematical Sciences under the supervision of Steven T. Siems.

In the case of chapters 2 and 3 my contribution to the work involved performing all of the analysis and the writing up for publication.

Thesis chapter	Publication title	Publication status	Nature and extent of candidate's contribution
2	On the Analysis of a Cloud Seeding Data Set over Tasmania	Published	80%
3 & 4	A Modelling Case Study of Mixed Phase Clouds over the Southern Ocean and Tasmania	Returned for revision	90%

I have renumbered sections of submitted or published papers in order to generate a consistent presentation within the thesis.

Signed: ....[redacted]..

Date: ...2/8/09.............................

Cloud seeding over Tasmania: A long-term evaluation and modelling plausibility study

by

Anthony E. Morrison

A Dissertation Submitted in

Fulfillment of the

Requirements for the Degree of

Doctor of Philosophy

in

Applied Mathematics

at

Monash University, Melbourne

August 2009

Cloud seeding over Tasmania: A long-term evaluation and modelling plausibility study

by

Anthony E. Morrison

A Dissertation Submitted in

Fulfillment of the

Requirements for the Degree of

Doctor of Philosophy

in

Applied Mathematics

at

Monash University, Melbourne

August 2009

Abstract

Cloud seeding over Tasmania: A long-term evaluation and modelling plausibility study

by

Anthony E. Morrison

Monash University, Melbourne, 2009
Under the Supervision of Associate Professor Steve T. Siems

Initially, an analysis of cloud seeding activity for the period 1960-2005 over a hydro-electric catchment (target) area located in central Tasmania is presented. The analysis is performed using a double ratio on monthly area averaged rainfall for the months May-October. Results indicate that increases in monthly precipitation are observed within the target area relative to nearby controls during periods of cloud seeding activity. Ten independent tests were performed and all double ratios found are above unity with values that range from 5-14%. Nine out of ten confidence intervals are entirely above unity and overlap in the range of 6-11%. Nine tests obtain levels of significance greater than the 0.05 level. If the Bonferroni adjustment is made to account for multiple comparisons, six tests are found to be significant at the adjusted alpha level.

Secondly, the cloud structure associated with two frontal passages/cloud seeding events over the Southern Ocean and Tasmania is investigated. The Weather Research and Forecasting (WRFV2.2.1) model is evaluated using remote sensed and in-situ observations within the post frontal airmass. The evaluated cases are then used to investigate numerically the prevalence of supercooled and mixed phase clouds over Tasmania and the ocean to the west. The simulations produce marine stratocumulus like clouds with maximum heights of between 3 and 5km. These are capped by weak temperature and strong moisture inversions. When the inversion is at temperatures warmer than -10°C, WRF produces wide spread supercooled cloud fields with little glaciation. This is consistent with the limited in-situ observations. When the inversion is at higher altitudes, allowing cooler cloud tops, glaciated (and to a lesser extent mixed phase) clouds are more common. The sensitivity of the simulations to certain bulk microphysical assumptions is explored, the findings indicate the results are relatively insensitive to the parameters investigated.

Finally, a MODIS based climatology of Southern Ocean clouds south of mainland Australia is presented, for the region 30-60S and 100-160E. Particular emphasis is placed on observations of supercooled clouds. Results are compared with those from the North Pacific region (30-60N, 160-220E) as a point of comparison. The findings presented are consistent with an earlier study by Mace et al. (2007), between 40-60% of clouds that exist over the Southern Ocean west of Tasmania are low with tops <3km and cloud top temperatures ∼0°C. Supercooled clouds are more common at the high latitudes, the island of Tasmania (situated in the lower latitude bands) modifies clouds sufficiently so that these resemble more closely those within the higher latitude bands. Little annual variability is observed. The North Pacific region resembles the Southern Ocean, however a greater seasonal variability is observed. In general, a supercooled cloud top is observed ∼20% of the total time over the Southern Ocean and North Pacific. Mixed phase clouds are more rare, occurring <10% of the total time. Over western Tasmania, supercooled clouds exist ∼25% of the time during winter months.

For all teachers, with eternal gratitude

Table of Contents

1 Introduction **1**
1.1 Cloud seeding over Tasmania . . . 1
1.2 Southern Ocean Clouds . . . 5
1.3 Aims Summary . . . 9

2 On the Analysis of a Cloud Seeding Data Set over Tasmania **10**
2.1 Historical Review . . . 10
2.1.1 Tasmania 1, 1964, 1966, 1968, 1970-71 . . . 11
2.1.2 Tasmania 2, 1979-83 . . . 13
2.1.3 Recent Cloud Seeding . . . 14
2.2 Climate and Meteorology . . . 16
2.3 Data Preparation . . . 17
2.4 Double Ratio Analysis . . . 27
2.5 Data Analysis Discussion . . . 31

3 WRF model evaluation **34**
3.1 Case Study Meteorology . . . 34
3.2 Numerical Modelling of Clouds . . . 35
3.2.1 Model Configuration . . . 37
3.3 Evaluation . . . 41
3.3.1 Atmospheric Profiles . . . 42
3.3.2 Satellite Observations . . . 47
3.3.3 Radar . . . 51
3.3.4 Aircraft Microphysics Observations . . . 52
3.4 Evaluation Summary . . . 63

4 Numerical investigation **65**
4.1 Evolution of Mixed Phase Clouds . . . 65
4.2 Summary: Evolution of Mixed Phase Clouds . . . 75
4.3 Model Results: Sensitivity to Changes in CCN, Ice Initiation Parameterisation and Microphysics Routine . . . 77
4.3.1 Sensitivity of In-cloud Conditions . . . 79
4.3.2 Broad Scale Cloud Evolution Sensitivity . . . 83
4.4 Summary: Sensitivity Analysis . . . 87

5 Southern Ocean Cloud Climatology **92**
5.1 Data Preparation . . . 92
5.2 Results . . . 94
5.2.1 Southern Ocean Climatology . . . 94
5.2.2 MODIS Bow Tie Effect . . . 101
5.2.3 Pacific Ocean Comparison . . . 103

5.2.4 Clouds over Tasmania 107
5.3 Summary: MODIS Cloud Climatology 109

6 Conclusions **112**

Bibliography **115**

Appendix **125**

List of Figures

2.1 Map showing the locations of the CSIRO and HECA target areas. Also shown are the static controls used in Tasmania 1 & 2. NW - northwest, N - north, E - eastern subsidiary and SW - southwest. . . 12

2.2 Frequency of occurrence indicating the approximate position of the seeding track relative to the target area: west, northwest, southwest or other, for the period 2002-05. Four distances are shown 0-25km, 26-50km, 51-75km and >75km. The column labeled other contains no data (i.e. not documented) and tracks anywhere else over Tasmania. 17

2.3 (a) Time series of the number of rain gauges operating in the HECA target area 1960-2005. (b) Quantity of precipitation that fell during the months May-October 1960-2005 for both the HECA and CSIRO targets. Years in which winter seeding occurred are shaded. Note: average number of sites used to construct HECA (CSIRO) area average is 20 (12). 19

2.4 Graph of number of seeding events per month and number of of months seeded (1960-2005). 21

2.5 Correlation maps for (a) HECA and (b) CSIRO target areas for the 50% threshold filter. Correlation is for unseeded periods only. Regions containing highly correlated sites closely resemble target perimeter. 24

2.6 Map of Tasmania highlighting the location of long-lived sites 25, 50 & 75% (small grey circles, small red stars and small black crosses, respectively) for the period 1960-2005. The HECA and CSIRO target areas together with the control areas are defined (Note: any sites inside a control area within 25km of the target perimeter are not included in the control region). Sites marked using a large black star are Bureau of Meteorology high quality sites. 26

2.7 Double ratios and confidence intervals for the HECA (left) & CSIRO (right) targets vs. the west (W), northwest (NW), high quality (HQ), northeast (NE) and southeast (SE) controls. The bootstrap probabilities for obtaining a double ratio higher than the actual is shown above the horizontal axis. 28

3.1 MSLP analyses provided by the Bureau of Meteorology, Melbourne, Australia. Upper: 0000UTC 09/08/2006. Lower: 0000UTC 04/10/2007. 36

3.2 Left: IR satellite image taken by the Terra satellite at 2350 UTC 08/08/2006. Right: IR satellite image taken by the Terra satellite at 0010 UTC 04/10/2007. 37

3.3 Map of Tasmania with seeding track overlaid, (a) 09/08/2006 and (b) 04/10/2007. Dark grey indicates seeding burners are aflame, lighter grey is the flight track. Atmospheric profiles were acquired by the plane over two regions for both case studies at approximately (42S,145E) and (42S,146E), indicated by the dots. 38
3.4 Map showing WRF domains 1-5. Melbourne and Sydney airports are show. Domain 1 (d1) has grid a spacing of 81km and time step of 360 seconds, daughter nests have grid spacing and time-step 1/3 of the parent. 40
3.5 Thermodynamic and wind profiles as measured by aircraft and model. Model predicted temperature profiles extend the full height of the sounding - thick line, aircraft soundings - thin line. Wind profiles are shown on the right. (a) Upwind profile 08/08/2006, (42S,145E). Aircraft sounding 23:00 UTC, model sounding 23:00 UTC, (b) Downwind profile 09/08/2006, (42S,146E). Aircraft sounding 00:25 UTC, model sounding 00:00 UTC. 43
3.6 As in Figure 3.5. (a) Upwind profile 04/10/2007, (42.11S,145.17E). Aircraft sounding 2:30 UTC (thin line), model sounding 3:00 UTC (thick line), model sounding 5:00 UTC (dashed line), wind barbs shown for 5:00 UTC model sounding. (b) Downwind profile 04/10/2007, (42.18S,146.14E). Aircraft sounding 3:00 UTC (thin line), model sounding 3:00 UTC (thick line), model sounding 5:00 UTC (dashed line), wind barbs shown for 5:00 UTC model sounding. 44
3.7 Thermodynamic and wind profiles supplied to the WRF model using the FNL Reanalysis data. The bold line indicates the sounding closest to the observation times, the dashed line indicates the next available sounding, 6 hours later. Wind barbs on the right are associated with the bold sounding, barbs on the left are for the dashed sounding. (a) FNL upwind profile 09/08/2006 00:00 and 06:00, (42S,145E), (b) FNL upwind profile 04/10/2007 00:00 and 06:00, (42S,145.17E). . . . 46
3.8 Cloud top temperatures. (a) 23:50 08/08/2006 MODIS, (b) 00:05 04/10/2007 MODIS, (c) 00:00 09/08/2006 WRF domains 3, 4 and 5 and (d) 02:00 04/10/2007 WRF domains 3, 4 and 5. 48
3.9 Satellite retrieved and WRF simulated cloud top temperatures for both case studies. Only the region defined by the finest resolution domain is used. One observation time is shown. (a) August 2006, the closest model time and one hour after are shown. (b) October 2007, the closest model time, one and two hours delay are also show. 49
3.10 Radar reflectivities from the West Takone radar in north west Tasmania for 16:00 08/08/2006 UTC. Precipitation associated with the frontal cloud band is shown. Plots (a) and (c) are observations, (b) and (d) are WRF simulated fields. Constant altitude plan position indicator (CAPPI) is at a height of 3km, cross sections are taken at 40.5S. 53

3.11 Liquid water traces and histograms from the August 2006 case study. The averages shown in (a) i and ii are over all seeding tracks. Measurements were taken at $\sim$ 2.5km altitude at temperatures between -8 and -18°C. 58
3.12 Liquid water traces and histograms from October 2007 case study. The averages shown in (a) i and ii are over the all seeding tracks. Measurements were taken at $\sim$3km altitude at a temperature of approx. -10°C. 59
3.13 August 2006 case study. CAS small hydrometeor mixing ratio trace and WRF cloud ice + water mixing ratio trace together with histogram showing the relative frequency of encountering specific mixing ratios. Measurements taken in conjunction with Figure 3.11. 60
3.14 As in Figure 3.13 for the October 2007 case study. 61

4.1 Plots showing cloud fraction, mean (solid) and median (dashed) TFH and TSLW for both case studies within the finest resolution domain. The simulation start time is indicated by the dates at the top of the plot and the first time shown on the horizontal axis (in UTC). 66
4.2 Cross sections across 42S for domain 4 showing the Southern Ocean (140-145E) and Tasmania (145-148E). Filled contours show liquid hydrometeors ($q_c + q_r$), grey contours show frozen hydrometeors ($q_i + q_s + q_g$) the first contour is 0.05g/kg larger contours are in steps of 0.5g/kg. The solid black line indicates the height of the freezing layer. (a) 15:00 08/08/2006 UTC frontal, (b) 23:00 08/08/2006 postfrontal, (c) 15:00 03/10/2007 prefrontal and (d) 01:00 04/10/2007, postfrontal. 69
4.3 Evolution of SLW over land (a) and (b), and Ocean (c) and (d) for the finest resolution domain only during the August 2006 event. Horizontal axis is hours since 12:00 07/08/2006 UTC. Specifically, plots (a) and (c) are histograms showing the time evolution of the ratio of TSLW to sum of TSLW + total frozen hydrometeors (RSACH) for incloud regions only. SLW is integrated from the freezing layer to the top of the model, frozen hydrometeors are integrated throughout the entire model depth, both variables have units kg m^{-2}. In cloud regions are defined as having total liquid/solid hydrometeor contents $>$ 0.05kg m^{-2}. Plots (b) and (d) show the evolution of the mean (solid) and median (dot) TSLW with mean (dash) and median (dash dot) TFH content over land and ocean respectively. 71
4.4 As in Figure 4.3, starting 12:00 02/10/2007. 72
4.5 Histograms of cloud-top temperature for August 2006 (a and b) and October 2007 (c and d) case studies. Plots (a) and (c) show CTT over land, (b) and (d) over Ocean. 74

4.6 Ice nucleation by deposition and condensation freezing. Three parameterisations are shown by Cooper, Fletcher and Meyers. Note: maximum number is set to 500/L, ice does not form until temperatures are below -8°C, or the supersaturation w.r.t. ice >8%. The curve representing the Meyers parameterisation assumes the maximum possible ice supersaturation i.e. water saturation. 78
4.7 Histograms showing distributions of in-cloud supercooled liquid water and small hydrometeor contents for the 2006 case. Measurements were taken at ∼ 2.5km altitude at temperatures between -8 and -18°C. Observation hydrometeor content assumes particles observed by the CAS probe have an average density of 1000kg m^{-3}. The smaller plots show the observations and the numerical experiment Nc=30, this was found to most accurately reproduce the observations (Table 4.1). The first bin is 0.01-0.1g/kg, the remaining bins are 0.1g/kg in width with the smaller value shown. 82
4.8 Histograms showing distributions of in-cloud supercooled liquid water and small hydrometeor contents for the October 2007 case. Measurements were taken at ∼3km altitude at a temperature of approx. -10°C. Observation hydrometeor content assumes particles observed by the CAS probe have an average density of 400kg m^{-3}. The smaller plots show the observations and the numerical experiment Nc=30, this was found to most accurately reproduce the observations (Table 4.1). The first bin is 0.01-0.1g/kg, the remaining bins are 0.1g/kg in width with the smaller value shown. 82
4.9 cloud-top temperature time evolution histograms for sim. starting 07/08/2006. Top left - standard configuration Nc=75, top right - Meyers, center left - standard configuration Nc=150, center right - Fletcher, bottom left - standard configuration Nc=30 and bottom right - Lin. 85
4.10 CTT time evolution histograms for sim. starting 02/10/2007. Top left - standard configuration Nc=75, top right - Meyers, center left - standard configuration Nc=150, center right - Fletcher, bottom left - standard configuration Nc=30 and bottom right - Lin. 86
4.11 Ratio of TSLW to TSLW+TFH evolution histograms for sim. starting 07/08/2006. Top left - standard configuration Nc=75, top right - Meyers, center left - standard configuration Nc=150, center right - Fletcher, bottom left - standard configuration Nc=30 and bottom right - Lin. 88
4.12 Ratio of TSLW to TSLW+TFH time evolution histograms for sim. starting 02/10/2007. Top left - standard configuration Nc=75, top right - Meyers, center left - standard configuration Nc=150, center right - Fletcher, bottom left - standard configuration Nc=30 and bottom right - Lin. 89

5.1 Cloud top phase from the MODIS instrument of the Terra satellite 23:50 08/08/2006 (hour:minute dd/mm/yyyy, UTC). A cold front is shown east of Tasmania, much of this cloud mass is glaciated. A post frontal trough line is observed over the west of Tasmania. This image is for the August 2006 case as described in detail in the previous chapters. 95
5.2 Planar view cloud-top phase and cloud fraction DJF (summer), -30 to -60S, 100-160E. Water pixels represent all water clouds at temperatures above 0°C, SLW (supercooled liquid water) is water clouds at temperatures < 0°C. Relative frequency is to the number of observations, i.e. the Southern Ocean south of Tasmania has clouds present $> 90\%$ of the time, over Tasmania an ice cloud is observed $\sim$25% of the time. As such, the sum of water, SLW, ice, mixed and uncertain pixels equals the cloud fraction in the top left plot. 97
5.3 Planar view cloud-top phase and cloud fraction MAM (autumn). . . . 98
5.4 Planar view cloud-top phase and cloud fraction JJA (winter). 99
5.5 Planar view cloud-top phase and cloud fraction SON (spring). 100
5.6 Histograms showing the relative frequency of cloud-top phase decomposed into temperatures. The colder bin edge is shown and the bin width is 5°C. Left: summer. Right: winter. The occurrence is relative to the total time, i.e. the sum of all temperature bins is equal to the fraction of time a cloud is observed. 100
5.7 Histograms showing the relative frequency of cloud-top phase decomposed into temperature 5°C temperature bins, the colder bin edge is shown. Left: summer. Right: winter. Top: 30-40S, middle 40-50S and bottom 50-60S. The occurrence is relative to the total time, i.e. the sum of all temperature bins is equal to the fraction of time a cloud is observed within a specific latitude band. 102
5.8 Relative frequency of occurrence for specific CTPs during winter (JJA), 30-60S, 100-160E, 2006-2008 inclusive. Solid line uses the entire field of view, the dashed line uses only pixels near to the nadir ($\leq 5 \times 10$km), total cloud cover is 0.88 and 0.87 respectively. 103
5.9 Planar view cloud-top phase and cloud fraction JJA (northern hemisphere summer) 2006-2008 inclusive. 30-60N, 160-220E, as described in Figure 5.2. 105
5.10 Planar view cloud-top phase and cloud fraction DJF (northern hemisphere winter) 2006-2008 inclusive, as described in Figure 5.9. 106
5.11 Histograms showing the relative frequency of occurrence of CTT and CTP during the summer months for the Southern Ocean (solid line) and the summer months for the north Pacific (dashed), 2006-2008 inclusive. 107
5.12 As in Figure 5.11 for the winter months. 108

5.13 Histograms showing the relative frequency of occurrence for specific CTTs and CTPs during the winter months for the region immediately to the west of Tasmania (dashed), over the west coast of Tasmania (dashed) and immediately to the east (dot). 108

1 Upwind soundings comparison 23:00 08/08/2006. Standard configuration is shown in Figure 3.5 (a). Top middle - Meyers, top right - Fletcher, bottom left - Standard Configuration Nc=150, bottom middle - Standard Configuration Nc=30 and bottom right - Lin. . . . 134
2 Upwind soundings comparison aircraft, 03:00, model 05:00 04/10/2007. Standard configuration is shown in Figure 3.6 (a). Top middle - Meyers, top right - Fletcher, bottom left - Standard Configuration Nc=150, bottom middle - Standard Configuration Nc=30 and bottom right - Lin. 135
3 Downwind soundings comparison 00:00 09/08/2006. Standard configuration is shown in Figure 3.5 (b). Top middle - Meyers, top right - Fletcher, bottom left - Standard Configuration Nc=150, bottom middle - Standard Configuration Nc=30 and bottom right - Lin. . . . 136
4 Downwind soundings comparison, aircraft 03:00, model 05:00 04/10/2007. Standard configuration is shown in Figure 3.6 (b). Top middle - Meyers, top right - Fletcher, bottom left - Standard Configuration Nc=150, bottom middle - Standard Configuration Nc=30 and bottom right - Lin. 137
5 Planar view cloud-top temperature for 00:00 09/08/2006. (a) is for the standard configuration, (b) standard config. with CCN = 150, (c) standard config. CCN=30, (d) Meyers, (e) Fletcher and (f) Lin. . 138
6 Planar view cloud-top temperature for 02:00 04/10/2007. (a) is for the standard configuration, (b) standard config. with CCN = 150, (c) standard config. CCN=30, (d) Meyers, (e) Fletcher and (f) Lin. . 139
7 Cross sections across 42S for the August 2006 case, for domain 4 showing the Southern Ocean (140-145E) and Tasmania (145-148E). Filled contours show liquid hydrometeors (q_c+q_r), grey contours show frozen hydrometeors ($q_i + q_s + q_g$) the first contour is 0.05g/kg larger contours are in steps of 0.5g/kg. The solid black line indicates the height of the freezing layer. The standard configuration is shown in Figure 4.2, plots (a) and (b). 15:00 is during the passage of the frontal cloud band, 23:00 is postfrontal. Top right - Meyers, center left - standard configuration Nc=150, center right - Fletcher, bottom left - standard configuration Nc=30 and bottom right - Lin. 140
8 As in Figure 7 for October 2007. The standard configuration is shown in Figure 4.2, plots (c) and (d). 15:00 03/10/07 is prefrontal, 01:00 04/10/2007 is postfrontal. Top right - Meyers, center left - standard configuration Nc=150, center right - Fletcher, bottom left - standard configuration Nc=30 and bottom right - Lin. 141

List of Tables

2.1 Seeding history. 11
2.2 Average rainfall (mm) for all months (May-October 1960-2005), only seeded months (S.), non-seeded months (N.S.) and lightly months (L.S.) (1-2 seeds) for both the CSIRO and HECA targets for the 25, 50 and 75% longevity filters. 23
2.3 Correlations between control areas and target areas, W - west control, NW - northwest control, NE - northeast, SE - southeast and HQ - high quality. Also shown is the average rainfall (May-October 1960-2005), average seeded rainfall and average unseeded rainfall (mm) for each control. 25

3.1 Mean, median and standard deviation of cloud-top temperature (°K) together with cloud fraction for both case studies for domain 5. . . . 51

4.1 Comparison of the observed and simulated in-cloud mixing ratio fields for the various numerical experiments. The Kolmogorov-Smirnov test is used for the comparison. The null hypothesis is that the samples are drawn from the same population, 0 indicates that the null hypothesis cannot be rejected at the 0.05 level. The model variables that are compared with the hot-wire probe are q_c and q_r, with the CAS, q_c and q_i, as detailed in Section 3.3.4. The columns titled CAS use a density of 1000kg m^{-3} for objects viewed by the CAS. 80

5.1 Comparison of the various cloud top phases for the Southern Ocean and the north Pacific. The fractions shown are relative to the total number of observations, hence, the sum of Warm, SLW , ice, mixed and uncertain cloud top phases is the total cloud cover (i.e. 1-clear). . 111

A1 Table showing the different analyses performed. The experiment number is on the left, numbers indicated with an asterisk are the tests presented in Chapter 2. Columns from the left are: the experiment reference number, period, sites included (B - Bureau of Meteorology, H - Hydro Tasmania), longevity threshold (0.25, 0.50 and 0.75) and target area (HECA). The following columns detail the average numbers of sites used throughout the analysis for: T - target (HECA), W - west, NW - north west, HQ - high quality, NE - north east and finally SE - south east. 127
A2 As in TableA1 for the CSIRO target. 127
A3 Table showing the results for the tests described in Table A1. Results indicated with an asterisk indicate tests presented in Chapter 2. No results are presented for test no. 9, due to incomplete data. 128
A4 Table showing the results for the tests described in Table A2. Results indicated with an asterisk indicate tests presented in Chapter 2. . . . 129

A5 Table showing double ratios and probabilities of occurrence for the period 1950/1960-1985 and 1980-2005. The data used to create these results included both BoM and HT sites, with a threshold longevity criteria of 0.5 (either 1950-2005 or 1960-2005). 130
A6 Table showing the results using successively greater number of seeded events to define a seeded month for the HECA target. Results are for the 50% longevity threshold, 1960-2005 including both Hydro Tasmania and BoM sites. Columns from the left are either double ratio or significance, no. of seeded events used to define a seeded month, number of seeded months in the seeded sample then results relative to the west, northwest, high quality, northeast and southeast controls. 130
A7 As in Table A6 for the CSIRO target. 131
A8 August 2006 case. Mean, median and standard deviation of cloud-top temperature (°K) together with cloud fraction for domain 5. Results are shown for the observations and all numerical sensitivity experiments. 142
A9 October 2007 case. Mean, median and standard deviation of cloud-top temperature (°K) together with cloud fraction for domain 5. Results are shown for the observations and all numerical sensitivity experiments. 143

Acknowledgements

I would like to acknowledge the guidance, patience, and all round companionship of Associate Professor Steve Siems, 'Steve' a most excellent supervisor. Professor Mike Manton 'Mike', what more can i say? The name says it all. Finally, Alex Nazarov for his guidance, support and unique 'Alexness'.

Further, the team at Hydro Tasmania, in particular Christina Nebel, Greg Carson and Mark DeHoog and Blair Trewin at the Bureau of Meteorology are thanked for their support and for simply being themselves.

Finally, but by no means least i wish to thank my family and friends. In particular Melanie, Simon, Guido and my brothers Iain and Alex. You all get an extra special mention for putting up with my strange living habits.

The only thing you take with you is your knowledge, make sure to share.

Student

Chapter 1

Introduction

There are two points of focus within this thesis, first, cloud seeding over Tasmania and second, clouds over the Southern Ocean and Tasmania. Chapter 2 focuses solely on the former and is a long-term analysis of Tasmanian precipitation records, evaluating precipitation totals during seeded and unseeded periods. The following chapters primarily deal with the latter. Chapter 3 is devoted entirely to presenting observations of two cloud seeding flights made over the western region of Tasmania together with selected satellite and radar observations. These are then used to evaluate the Weather Research and Forecasting (WRF) numerical weather predication model in a pristine environment. Within Chapter 4 the WRF model is used as a tool to understand the processes and environment which together create mixed phase and supercooled clouds around Tasmania. The sensitivity of the model results to certain assumptions made within bulk microphysics packages is investigated. Finally, a climatology of Southern Ocean clouds (south of Australia) obtained by satellite is presented. Comparisons with the northern Pacific are also presented. The final chapter is a summary of the numerous conclusions that can be drawn from the material presented herein.

1.1 Cloud seeding over Tasmania

The practice of cloud seeding has remained a point of contention in the scientific community for over half a century. Early laboratory experiments were able to readily demonstrate precipitation enhancement mechanisms through the conversion of supercooled water to ice by the introduction of suitable ice nuclei (Schaefer, 1946), and these laboratory experiments were followed by a field demonstration on individual clouds by Kraus and Squires (1947). However, the extension of cloud seeding impacts from individual clouds to a sustained precipitation increase over a substantial surface area has proven to be an elusive goal, especially at the high level of proof required by the wider scientific community.

The 2003 U.S. National Academies of Science report, entitled "Critical issues in weather modification research", includes an abridged history of the development of various methods of cloud seeding with numerous references to static glaciogenic (of both cumulus and winter orographic regimes), dynamic glaciogenic and hygroscopic seeding field experiments. In spite of these considerable research efforts spanning decades, the National Research Council (NRC) report goes on to highlight the persistence of key uncertainties, which are broadly classified as "cloud/precipitation microphysics issues, cloud dynamic issues, cloud modelling issues and seeding related issues". The NRC report ultimately concludes that "there still is no convincing scientific proof of the efficacy of intentional weather modification efforts".

Boe et al. (2004) noted that the definition of "convincing scientific proof" was ambiguous, leading to Garstang et al. (2005) further clarifying that scientific proof was defined as an understanding of "processes that can be replicated by predictable, detectable and verifiable results". Ultimately on the question of verification it was recognised that "the level of noise in natural systems compared to the magnitude of the signal has made verification of either the enhancement of rain or snowfall or the reduction of hail extremely difficult."

In principle it is possible to overcome large variability by extending a trial so that the accepted 5% significance level (or further) can be achieved. In practice it is not clear what would constitute a suitable period given that precipitation shows variability on the time scale of hours to decades. A very practical time limit arises over the ability to maintain a consistent, extended scientific experiment. Finite funding, changing personnel, changing technology and a changing environment all serve to prohibit field work from being sustained over decades. Long-running cloud seeding projects, such as in Israel (Gabriel and Rosenfeld, 1990; Nirel and Rosenfeld, 1995), the Sierra Nevada (Reynolds and Dennis, 1986; Deshler et al., 1990) and Thailand (Silverman and Sukarnjanasat, 2000) can become operational making it difficult to observe and quantify any positive effect over extended periods of time. Moreover, statistical significance is not sufficient to provide "acceptable proof": associated physical observations of expected changes in cloud properties need to be documented to complement any statistical evaluation.

Australia, the driest inhabitable continent, invested heavily in cloud seeding research into the 1980s. As in the United States, within this decade funding for such research all but ceased due to a lack of convincing scientific proof. Ryan and King (1997) present an account of the many cloud seeding research programs dating back to 1947 conducted by the Commonwealth Scientific and Industrial Research Organisation (CSIRO). A remarkable result reported in the literature was over the island of Tasmania (Smith et al., 1979), where cloud seeding was found to produce a statistically significant increase in surface rainfall over a target of approx. $2500 km^2$. Specifically a 30% increase was found in the autumn months (April, May & June) with weaker increases (that failed to reach high levels of significance) observed in the winter months and early spring. Given the inability of the CSIRO to produce such positive results elsewhere (except in the Snowy Mountains (Smith et al., 1963)), the results were met with some widespread scepticism, leading to a second Tasmanian cloud seeding experiment being conducted a decade later. For this second field experiment Ryan and King (1997) report a 37% increase in surface rainfall over the months of April through October under specific synoptic conditions.

In spite of two positive field experiments, cloud seeding in Tasmania still fails to meet the standard of "convincing scientific proof" amongst the wider scientific community for a variety of reasons. Many of the key uncertainties identified in the NRC report are well illustrated in these experiments. There was no ability to directly observe the in-situ microphysical response to the cloud seeding as was done in Deshler et al. (1990) within orographic clouds over the Sierra Nevada or Rosenfeld and Woodley (1989) in summer convective clouds over west Texas; for example, remote sensing technology such as radar or satellite observations was unavailable. The definition of controls employed in Tasmania 1 (1964-71) and the changes to the controls for Tasmania 2 (1979-83) opened legitimate questions about the robustness of the statistical formulation. Indeed, simply the poor documentation of the synoptic meteorology has led to some confusion: the 2003 NRC report lists these Tasmanian experiments as examples of winter orographic cloud seeding, while a closer examination of the meteorology indicates that Tasmania fails to meet this classification.

These key questions about Tasmania 1 and 2 cannot be addressed some 25 years after the last fieldwork was undertaken. However, the extended but intermittent record of cloud seeding over the central plateau of Tasmania creates a unique data set that has the potential to offer insight into the effectiveness of long-term cloud seeding in this region. The notion is further encouraged by the fact that over the last 50 years the catchment area has remained relatively untouched with respect to human influences and economic development; it is protected as the Tasmanian Wilderness World Heritage Area.

From the period of 1960 through 2005, some form of cloud seeding has taken place during 24 of the 46 winter seasons. If the reported 30% increase found in the first Tasmanian experiment is accepted at face value then it is reasonable to expect a positive signal in the monthly rain gauge records. For example, if 90% of the rainfall were to occur in the ten wettest days of a given month and half of these days were seeded, then one would expect to see 13.5% increase in the overall monthly rainfall. Simply seeding any five random days within a month with a 30% increase should still lead to an increase of 5% in the overall monthly rainfall. If seeding were largely ineffective, then one might expect to find no positive effect in the monthly records. With a long enough time record, any meaningful signal should be detectable and found to be statistical significant. The results and analysis of this research are presented in Chapter 2.

1.2 Southern Ocean Clouds

The Southern Ocean and its accompanying air mass are among the most pristine environments on earth. A recent satellite climatology employing CLOUDSAT (Mace et al., 2007) concludes that the majority of clouds over this region can broadly be categorised into two types. The most common are low and shallow having bases and tops below 3km. The less prevalent type is relatively deeper clouds having bases below 3km and tops between 5-10km. Immediately west of Tasmania between 50-60% of the time cloud top is <3km and ∼40% of the time cloud top is between 5-10km. Further, typically between 70-100% of the Southern Ocean is covered in hydrometeors. These findings are consistent with Bennartz (2007) who found that up to 89% of clouds over this region were likely to be precipitating. Microphysical conditions are found to be homogeneous showing little variability over the entire region.

In addition to satellite climatologies, in-situ microphysical observations have been documented by many authors. The Southern Ocean Cloud Experiments used aircraft measurements to investigate the organisation of convection and evolution of the droplet size distribution in stratocumulus clouds (Boers et al., 1997). Jensen et al. (2000) investigated the dynamics of marine boundary layer clouds and Yum and Hudson (2004) studied the differences between summer and winter cloud condensation nuclei (CCN) and other microphysical characteristics. The Aerosol Characterisation Experiments (ACE-1) encountered a variety of cloud types from frontal cloud bands to shallow cumulus in the region 40°S to 55°S, investigating diverse aspects of the marine boundary layer from cloud droplet concentrations (Boers and Krummel, 1998) to turbulent mixing (Russell et al., 1998). Long-term ground based CCN climatologies exist from the northwest coast of Tasmania (Gras, 1995) and show that concentrations are usually between 10-110 cm^{-3} with an average of around 70 cm^{-3}, consistent with Bennartz (2007).

In-situ observations of mixed phase clouds with particular interest in supercooled liquid water (SLW) have been documented by two cloud seeding experiments over the island of Tasmania, 1964-71 (Smith et al., 1979) and 1979-83 (Ryan and King, 1997). Interestingly, both experiments reported increases in precipitation associated with cloud seeding periods. Further, a recent 46 year study (1960-2005) by Morrison et al. (2009) finds consistent increases in precipitation. Quantitative records of SLW were obtained by aircraft during the 1979-83 experiment. It was found that extended regions (5 minute averages) of supercooled liquid water (SLW) with values $>0.3gm^{-3}$ between -6 and -8°C were common. This is a large amount of SLW relative to similar studies in other parts of the world; e.g. eastern Canada where SLW contents of $\sim 0.1gm^{-3}$ were common within a similar temperature range (Guan et al., 2001, 2002; Vaillancourt et al., 2003), or the Sierra Nevada where the most common peak SLW content (per flight track) was $\sim 0.1gm^{-3}$ (Deshler and Reynolds, 1990). Given that both Tasmanian cloud seeding experiments observed mixed phase conditions, the obvious question is then: in which situations and environments do these conditions occur, and by what processes are they formed and maintained?

These questions are of particular importance to the climate community, the IPCC working group I reports that clouds in general represent the greatest uncertainty in climate model forecasts, IPCC: Solomon et al. (2007). This has in part motivated the many earth observing satellites such as CLOUDSAT (Stephens et al., 2002) which has limited ability identifying cloud phase within the cloud interior (Austin, 2008).

Over the last decade the microphysical parameterisations within mesoscale numerical weather prediction models have become able to predict the mixing ratios and occasionally number concentrations of a number of hydrometeor species (Lin et al., 1983; Ferrier, 1994; Walko et al., 1995; Meyers et al., 1997; Reisner et al., 1998; Tremblay et al., 2001; Thompson et al., 2004; Morrison and Pinto, 2005; Thompson et al., 2007). Numerous examples regarding the modelling mixed phase clouds in the northern hemisphere exist, e.g. over the North American continent, most notably Reisner et al. (1998) attempted to forecast supercooled water in the Colorado Rocky Mountains and Guan et al. (2001, 2002) and Vaillancourt et al. (2003) freezing drizzle and aircraft icing events over south-eastern Canada. Further north within the Arctic, Jiang et al. (2000) and Morrison and Pinto (2005) have modelled mixed phase Arctic stratus. The analysis presented in Chapters 3 and 4 uses the Thompson bulk microphysics package (Thompson et al., 2007), hereafter TMP, to model mixed phase clouds over the Southern Ocean and Tasmania. The scheme, originally based on Reisner et al. (1998) uses a single moment for 4 hydrometeor species (cloud water, rain, snow and graupel) and a double moment for ice. It was initially developed for the forecasting of SLW regarding the prediction of air-frame icing events. Unlike many other microphysics routines, the TMP was tested in both shallow and deep cold cloud conditions ensuring the scheme is able to produce both supercooled and glaciated conditions. As the majority of clouds over the Southern Ocean are relatively low and shallow (Mace et al., 2007), the region may be an ideal place to test the TMP in a pristine environment.

The initial objectives of this research are first, to present observations from two cloud seeding flights made over the western region of Tasmania. Secondly, to evaluate the Weather Research and Forecasting (WRF) NWP model (Michalakes et al., 1999; Skamarock et al., 2005) employing the Thompson microphysics routine (Thompson et al., 2004, 2007) using these in-situ observations and selected satellite and radar observations. Described are two case studies, one during August 2006 characterised by large amounts of SLW, little ice and a relatively small amount of precipitation. The second case is during October 2007, this had lower concentrations of SLW, greater concentrations of ice and relatively larger amounts of precipitation. This analysis is presented in Chapter 3.

Further research into the simulations is presented in Chapter 4. Here, the situations under which mixed phase conditions occur in the model are investigated. Further, the sensitivity to various assumptions regarding the bulk parameterisation of in-cloud processes is assessed. Specifically, how do the model simulated clouds over the Southern Ocean change when the number of cloud condensation nuclei is changed and the rate of ice initiation is increased/decreased. A much earlier bulk microphysics scheme developed by Lin et al. (1983) is also evaluated as a comparison. The case studies presented within Chapter 3 are further utilised within Chapter 4 as the basis for the sensitivity study.

The final objective is to present a satellite climatology of Southern Ocean clouds. Specifically, cloud top temperature and phase according the Moderate Resolution Imaging Spectroradiometer (MODIS) instrument (Platnick et al., 2003) on-board the Terra earth observing satellite. A climatology over the Southern Ocean south of Australia is presented, further as a point of comparison, results for the north Pacific between Russia and the North American continent are detailed. The intention here is to extend the work by Mace et al. (2007) and Bennartz (2007) over the the Southern Ocean, specifically looking into the spacial patterns of, and seasonal variability of specific cloud top phases. This work is presented in Chapter 5.

1.3 Aims Summary

Summarised, the aims of this thesis are:

Chapter 2

1. Analyse the monthly rainfall records over Tasmania (1960-2005) for a detectable signal with respect to the act of cloud seeding.

2. Evaluate whether any such signal is statistically significant.

Chapter 3

3. Present observations from two cloud seeding flights made over the western region of Tasmania.

4. Evaluate the Weather Research and Forecasting (WRF) NWP model and the TMP regarding the ability to simulate in-situ and remote-sensed observations.

Chapter 4

5. Investigate numerically the situations under which SLW is observed in the model and the processes by which it is maintained.

6. Investigate the sensitivity of the model results to alternate microphysical parameterisations.

Chapter 5

7. To present a satellite climatology of Southern Ocean clouds that answers the question: how often do supercooled clouds exist over Tasmania?

Conclusions

Finally a summary of the various conclusions is presented together with possible directions for future research.

Chapter 2

On the Analysis of a Cloud Seeding Data Set over Tasmania

The objectives of this chapter are firstly to analyse the monthly rainfall records over Tasmania for a detectable signal with respect to the act of cloud seeding, and secondly to evaluate whether any such signal is statistically significant. As the various seeding periods were never designed to be analyzed as a single, long-running time series, numerous caveats exist to this approach. In section 2.1 a review of the various seeding efforts over central Tasmania are presented. This is followed by a discussion of the meteorology and climatology in Section 2.2. In Section 2.3 the preparation of the rainfall observations are detailed. In Section 2.4 the double ratio technique is employed to quantify a signal with respect to cloud seeding. A bootstrap analysis is then undertaken to establish the statistical significance of this signal. Finally results are more fully discussed in Section 2.5.

2.1 Historical Review

The island of Tasmania has been the target of both experimental and operational cold cloud seeding dating back to the 1960s (Table 3.1). Glaciogenic seeding research projects led by CSIRO were conducted between 1964-1971 and 1979-83 (Tasmania 1 & 2 as defined in Ryan and King (1997)). A third trial was conducted between 1992-94 solely by the island's hydroelectric energy company Hydro Tasmania (HT), formally the Hydro Electric Commission of Tasmania (HEC), although no results from this research period have been published. Two periods of operational cloud seeding have also been conducted from 1988-1991 and 1998-present.

Table 2.1: Seeding history.

Seeding Period	Mode	Seeding Agent	No. Winters Seeded
1964-1971	Research	Silver Iodide	5
1979-1983	Research	Silver Iodide	5
1988-1991	Operational	Silver Iodide	4
1992-1994	Research	Dry Ice	3
1998-2005	Operational	Silver Iodide	7

2.1.1 Tasmania 1, 1964, 1966, 1968, 1970-71

Tasmania 1 was conducted as a randomised experiment during all months of the year, over a target area of approximately 2500km^2 located in central Tasmania. This original target area is referred to as the CSIRO target. The primary analysis was defined as the double ratio of target rainfall relative to a number of controls: northwest, north and southeast of the target area (Smith et al., 1979). See Figure 2.1 for a map showing the location of these various regions. Seeding units were defined in pairs of duration 12-18 days, with each pair having the seeded and non seeded part randomly assigned. The analysis was separated into seasons and implemented independently on both a western and eastern half of the target area. The seeding agent used at that time was an acetone solution of silver and sodium iodide and was released by a single aircraft 30 minutes upwind (as defined at the seeding level) of the target area for cumulus clouds and 45 minutes upwind for stratiform clouds. The criteria used in defining suitable conditions were that cloud-tops contained supercooled liquid water (SLW) at a temperature colder than -5°C for stratiform clouds and -10°C for cumuliform clouds. Further to this, clouds had to be deep, compact and without excessive clear air volumes. At this time reliable quantitative instruments for measuring the liquid content of a cloud were not available, but it was noted in Smith et al. (1979) that airframe icing was usual and often severe,

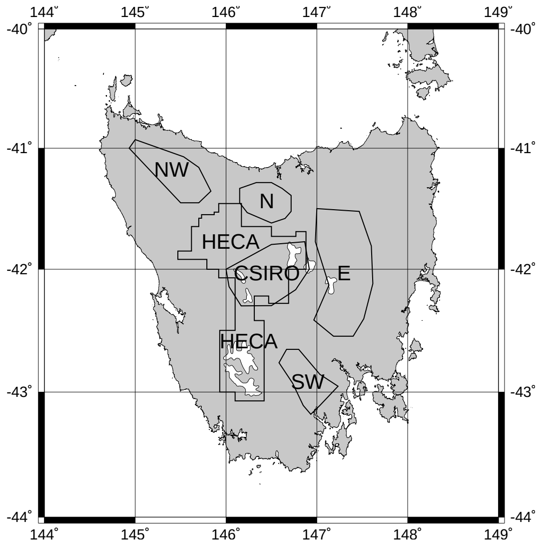

Figure 2.1: Map showing the locations of the CSIRO and HECA target areas. Also shown are the static controls used in Tasmania 1 & 2. NW - northwest, N - north, E - eastern subsidiary and SW - southwest.

occurring about three-quarters of the seeding time. The average seeding time was close to 8 hours per month for the whole experiment, however it is noted that this figure increased steadily from 3.2 hours for months during the initial year to 14.2 hours during the final year.

Precipitation increases of up to 30% during autumn (March, April and May) were published in Smith et al. (1979) as defined by the double ratio between the eastern half of a target area and an average of two controls based to the north and southeast of the target area. Weaker evidence was present indicating a probable 23% increase in the western half of the target area during autumn and a possible 13% increase in winter, however these results were never published in the reviewed literature as they did not reach the required level of significance. Interestingly, it was noted that the observed increase occurred when deep prefrontal stratiform clouds were present, rather than orographically forced clouds which are commonly studied with respect to static glaciogenic cloud seeding (Long and Huggins, 1992; Deshler et al., 1990; Rauber and Grant, 1987).

2.1.2 Tasmania 2, 1979-83

Based on knowledge gained during Tasmania 1, the operations and science plan for Tasmania 2 were revised in a number of respects. Seeding was limited strictly to the months of April-September with a randomization scheme having a seed/no seed ratio of 2:1. The seeding unit was reduced from 12-18 day blocks to a single calendar day. Further constraints were added to the definition of a suitable day i.e. for stratiform clouds, cloud-top temperature $\leq -5°$C, depth be 1/3 terrain clearance of base, supercooled water at the seeding level > 0.1g/m^3 or failing that, 2mm of ice accreted in 5 minutes on an icing rod of 2mm diameter and winds at seeding height $<$ 130km/h. For cumulus clouds, cloud-top colder than -12°C, depth greater than height of base, supercooled water at the -10°C level > 0.5g/m^3 or alternatively 1mm of ice accreted on an icing rod 2mm in diameter during one pass, bases be flat and 'firm' with tops extending vertically and wind speed at cloud base $<$ 100km/h. It is noted in Shaw et al. (1984) that this tightening up of criteria drastically reduced the number of suitable days available for seeding. For example, the average number of suitable days during autumn and winter was 52 for Tasmania 1. In Tasmania 2, the average was 18. Further modifications to the experimental procedure were that stratiform clouds should be seeded 1 hour upwind instead of 45 minutes as was the case in Tasmania 1 and that the seeding solution be modified from silver and sodium iodide to silver and ammonium iodide due to improved nucleating abilities at warmer temperatures.

By 1979 it was possible to quantify cloud water content and so Tasmania 2 was able to record the microphysical mixed phase conditions that were actually encountered by the aircraft. Shaw et al. (1984) and Ryan and King (1997) state that the most frequent liquid water content measured with a 5 minute time constant was $\sim$0.3g/m^3, occurring between -6° and -8°C. This is a large amount of supercooled water relative to studies like Deshler and Reynolds (1990) where the most common peak supercooled water content (per flight track) was ∼0.1 g/m^3 in a similar temperature range.

While the target area defined did not change between Tasmania 1 and 2, a second set of "floating" controls were introduced for the evaluation of Tasmania 2 in addition to the original fixed controls used in Tasmania 1. The motive for the introduction of floating controls was based on previous Australian cloud seeding experiments where it was found that correlations between rain gauges depended on wind direction. On any experimental day 3 floating controls were defined; 1. directly upwind of the target, 2. left of the target when looking into the wind and 3. right of the target. The final data set consisted of 66 days where the average seeding time per month was ∼2.7 hours. The results indicated good evidence of an effect in the western half of the target area and some evidence of a possible effect in the eastern half. If the full 66 days are included in the analysis using the double ratio to estimate the change in rainfall due to seeding, a 30% increase is observed with a P-value of 0.007 in target west. Relative to the fixed controls the estimated increase is only 12% and is not significant. If the analysis is restricted to days where the wind direction is between 231° and 300 ° (the preferred sector), the estimated increase relative to the floating controls increases to 37%.

2.1.3 Recent Cloud Seeding

Given the two positive field experiments reported by the CSIRO, the HEC undertook operational cloud seeding in the years of 1988-1991. The same seeding guidelines were employed for this period as with Tasmania 2, except that no randomization was undertaken and no efforts to quantify results were made. The decision to seed was made in response to low reservoir levels in the hydro electric catchment area (HECA).

The third trial (1992-94), according to Ryan and King (1997), was run solely by the HEC in a similar manner to that of Tasmania 2. Results for this trial have not been published, however there were a total of 61 seeded flights over the 3 year period with an average of 5 hours seeding per month May - November (log files from HT). The seeding agent used during this period was dry ice.

The current operational program has been running since September 1998. In essence it has many similarities with Tasmania 2 in that clouds are usually only seeded if they meet criteria for supercooled water, temperature, wind speed and concentrations of ice crystals. However, these are less strict than those in Tasmania 2. The decision to fly is based on satellite observations of cloud-top temperature. Operations are often undertaken in post frontal conditions to avoid flying when lightning is present, which has been found to be more common in pre-frontal systems. A significant difference between the recent years of operational seeding and earlier research activities is that the target area has been expanded from the original CSIRO target to the new hydro electric catchment area (here after, HECA) (Figure 2.1). This is an increase of around 5000km^2. Due to the increased size of the region intended for precipitation augmentation individual seeding operations now focus on specific catchments within the HECA. A typical seeding flight would target up to two of these individual catchment areas.

Suitable clouds are predominantly associated with cold fronts moving across the Southern Ocean and are usually tracked continuously from April to November. Numerical products are supplied by CSIRO in the form of CCAM (Conformal-cubic global Atmospheric Model) output (McGregor and Dix, 2007) and include height at -10°C, total cloud cover, average cloud water and ice, and magnitude of vertical wind shear. Cloud microphysical properties are assessed in flight using a CSIRO King probe for liquid water, and a Droplet Measurement Technologies (DMT) Cloud Aerosol and Precipitation Spectrometer (CAPS) probe (Baumgardner et al., 2001) for measuring particle numbers. The decision to seed is based on there being supercooled liquid water (SLW) present for extended periods of time and minimal ice. Only about one out four flights actually meet this last criterion (and are seeded). On average there are 32 seeded flights a year between April and November with an average of 5 hours seeding per month.

2.2 Climate and Meteorology

The meteorological conditions under which cloud seeding is performed in Tasmania are determined by the passage of fronts in the Southern Ocean. Tasmania is situated between 40°and 44°S and year round receives a large fraction of its precipitation from frontal cloud systems as they sweep east over southern Australia. Between 50-70 cold fronts usually pass over Tasmania every year and SLW is frequently observed in these clouds in both the pre and postfrontal airmass (Long and Huggins, 1992; Ryan and King, 1997). A more detailed description of the meteorology for two specific cloud seeding events is presented in Section 3.1.

Tasmania can broadly be described as having a fairly mountainous west coast with peaks that reach approx. 1.5km, a central plateau (where the CSIRO target is mostly located) that has an elevation of close to 1km and a relatively low lying eastern region. The extent of the island is around 250km in the north-south direction and 300km at the widest point east-west. As a front passes over Tasmania from west to east precipitation often occurs over the western and central regions. The year round monthly average precipitation on the west coast is 180mm, with a low of 100mm in February and high of 250mm during July. The central plateau receives between 90-180mm per month and the eastern region between 50-80mm.

Figure 2.2 shows the locations of the seeding track relative to the HECA for the period 2002-05. It is observed that the majority of the time during seeding conditions the prevailing wind direction is from either the west, northwest or southwest, however approximately 25% of the time the wind direction is not in these sectors.

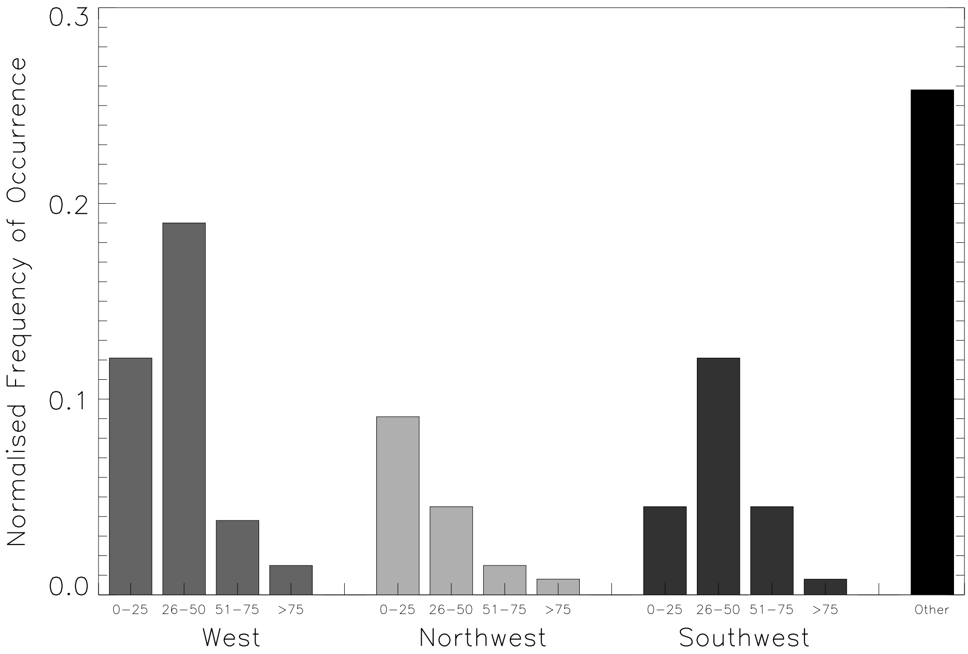

Figure 2.2: Frequency of occurrence indicating the approximate position of the seeding track relative to the target area: west, northwest, southwest or other, for the period 2002-05. Four distances are shown 0-25km, 26-50km, 51-75km and >75km. The column labeled other contains no data (i.e. not documented) and tracks anywhere else over Tasmania.

The northwest conditions are typically pre-frontal.

2.3 Data Preparation

The purpose of any useful cloud seeding project is to increase annual or at least seasonal rainfall to a measurable extent over a region of economic significance. This investigation attempts to identify a significant increase in rainfall due to cloud seeding by taking a calendar month as the basic unit of time. A monthly averaged rainfall is defined as the arithmetic mean from all long-lived surface rain gauge sites operating anywhere within a specified region. If a station has any missing records within the given calendar month, that specific station is discarded for the entire month.

A shortcoming of using this minimalist definition of an area-averaged rainfall is that the spatial distribution of rain gauges may not be adequate to sample the spatial variability of rainfall in the target area, and so the estimated rainfall may not be a fair representation of the area average. However, a comparison of the site-averaged values with a grid based estimate from the Commonwealth Bureau of Meteorology provides some confidence in this simple approach.

Figure 2.3 shows that a number of rain gauges have only become operational since 1998, particularly those maintained by HT (for completeness precipitation totals are also shown). These new HT records contain no information on non-seeded periods and thus offer no insight into the science. As a means of removing these (or other) short-lived sites, a longevity filter is used on individual sites. Each individual site was filtered at three levels, those having operated for a minimum of 25, 50 and 75% of the total time 1960 to 2005. This filtering is independent of the act of seeding. As the various tests were found to be relatively insensitive to this filter all discussion from here on will refer to the 50% threshold, unless otherwise specified. This longevity filter was chosen as it represented a balance between adequate spacial sampling with regard to number of gauges and minimal temporal evolution of the rain gauge network (i.e. the coming and going of individual sites). To further expand this, the analysis was also performed using only the Bureau of Meteorology sites, as there may be a perception that these sites are of a higher standard. The omission of the HT sites has no qualitative impact or systematic bias.

Using a calendar month as a seeding unit has a number of advantages. Firstly, there are no ambiguities in the definition of seeded periods; if the aircraft made even a single seeding mission in a given month, that calendar month is a seeded month. Secondly, the use of a broad temporal average greatly reduces the variability of the data set, which should allow for statistical significance to be more easily established.

It is noted that months with only one or two seeding flights are retained as seeded months, even though it is difficult to imagine that such limited seeding could

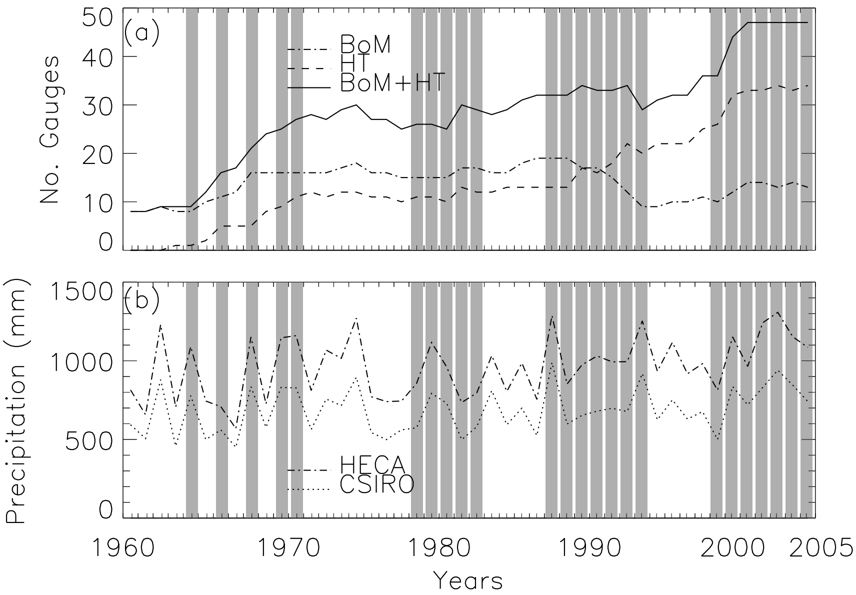

Figure 2.3: (a) Time series of the number of rain gauges operating in the HECA target area 1960-2005. (b) Quantity of precipitation that fell during the months May-October 1960-2005 for both the HECA and CSIRO targets. Years in which winter seeding occurred are shaded. Note: average number of sites used to construct HECA (CSIRO) area average is 20 (12).

have any impact on monthly rainfall totals. Indeed, these lightly seeded months have a lower average rainfall than the overall average for the 46 year period. This is not surprising as these lightly seeded months are likely to have had few seeding opportunities and thus correspondingly poor rainfall. They must be retained as seeded months however, to prevent a bias of the data towards months with wetter conditions.

A non-seeded month primarily means that the aircraft was not in operation, regardless of the meteorology. The seeding history reveals that even during periods of poor regional rainfall, the aircraft will still have seeded at least once in a given month if it were available. For example, there is not a single non-seeded winter month in the most recent operational period, even though it has been widely reported that southeast Australia has been suffering from a drought over this period (although this is not the case for some regions in Tasmania) (Watkins and Trewin, 2007; National Climate Centre, Bureau of Meteorology, 2006). Over the full seeding history, there are only 7 non-seeded winter months (Jun - Aug) immediately adjacent to a seeded month. It is likely that these missed months were primarily a result of operational rather than meteorological factors. In contrast, there are 16 winter months that have been seeded only a single time, and 10 winter months that have been seeded only twice.

Only months with more than 60 flights over the full 46 years are included in the analysis, so that the treatment of months is consistent. Figure 2.4 shows the number of seeded months and seeded missions for 1960-2005. It is observed that almost no seeding occurs in the summer and early autumn (Dec - Mar). As discussed in section 2.1, seeding was only attempted in the summer period during Tasmania 1. These summer months are excluded in the present analysis, simply due to under-sampling with respect to the seeded sample. While the months of April and November have a greater number of seeded units (relative to the summer months), these are also excluded from the present analysis. During operational periods if the aircraft was ready to fly during late April and suitable conditions were present, seeding missions would have begun early. Similarly November is omitted as yearly operations were often ended if meteorological conditions were poor early in the month. Hence, the inclusion of these months could introduce a bias towards favourable meteorological conditions. Note that October has fewer seeding months than May - September, but this is only because October was explicitly not seeded during Tasmania 2, i.e. the decision was operational rather than meteorological.

Limiting the analysis to months May-October, 1960-2005, the data set now encompasses a total of 276 months of which 130 have been seeded. Table 2.2 shows the average rainfalls for both the CSIRO target and the HECA. As detailed in section 2, the target area has incrementally expanded from an original size of 2500 km^2 (CSIRO) to 7500 km^2 (HECA) over the periods of operational cloud seeding.

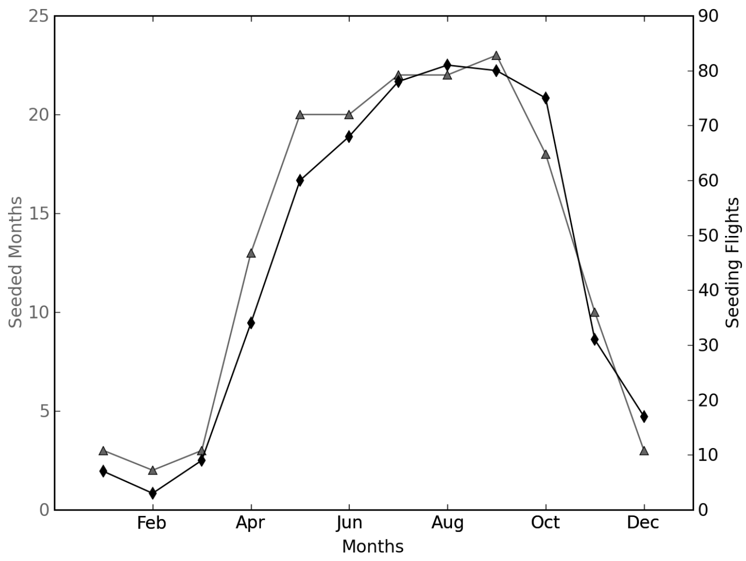

Figure 2.4: Graph of number of seeding events per month and number of of months seeded (1960-2005).

Qualitatively the average rainfall in the two targets behave similarly over the duration of the experiment (Figure 2.3). As the western portion of the HECA target is at a higher elevation than the original CSIRO target, rain gauges in this area experience a greater rainfall on average. Thus while it is possible to define a time-dependent, expanding target region, such sophistication raises ambiguity. A more straightforward approach is to simply analyze the two limits for the target region.

The difference in elevation (and observed rainfall) across the target combined with the time-dependent nature of the rain gauge network could introduce a further bias. For example, a rain gauge operating at high elevation during limited periods would lead to greater area average rainfalls during those periods, whether seeded or not. While the longevity filter already in place should act to minimize this type of bias, this effect must still be explicitly assessed. The test designed to assess this potential caveat involved substituting the observed monthly rainfall for each rain gauge with idealised data unbiased with regard to the act of seeding.

Specifically, each individual rain gauge is interrogated for its rainfall totals for all months having a complete set of data. These data were then compared against a number of ideal distributions. It was found that a log normal distribution most accurately represented the real data with approx. 80% of the months exceeding the 0.05 significance level, tested using the Jarque-Bera test of the null hypothesis that a given sample comes from a specific distribution (Jarque and Bera, 1980). Idealized random data were then created for the monthly rainfall for each site. These data were then analysed for the same values as seen in Table 2.2. One thousand data sets were created and analysed for the period of 1960-2005 with no overall bias being present i.e. no large difference between seeded and non-seeded periods.

As an initial examination of the data, the monthly rainfall is averaged over the seeded and non-seeded months (Table 2.2). Looking at the 50% longevity filter on the data, both the HECA and CSIRO targets find roughly a 20% increase in rainfall during periods of cloud seeding compared to non-seeded periods. The assumption that this increase is due to seeding may be misleading as the differences may simply reflect decadal variations in rainfall in the target area. The double ratio (Gabriel, 1998) has been a common analysis tool employed in cloud seeding research in order to account for temporal variations in rainfall. In order to perform a double ratio a control region must be defined as having an area average monthly rainfall during non-seeded periods that is highly correlated with the target (either the HECA or CSIRO) and that is not affected by the act of seeding. As the primary unit of time is one calender month, it is not possible to say that the control areas used are not affected by the seeding, as over the course of a month it is entirely possible to have winds that span the full 360°(Figure 2.2). Indeed, the act of seeding 60 minutes upwind of the target, as was done in Tasmania 2, often led to the seeding tracks lying off the west coast of Tasmania.

Correlation maps of monthly rainfall totals for individual rain gauges with respect to both the HECA and CSIRO targets during non-seeded months (Figure 2.5) are used to define the controls. Excluding the increased correlation observed for the

Table 2.2: Average rainfall (mm) for all months (May-October 1960-2005), only seeded months (S.), non-seeded months (N.S.) and lightly months (L.S.) (1-2 seeds) for both the CSIRO and HECA targets for the 25, 50 and 75% longevity filters.

	Months	CSIRO	CSIRO	CSIRO	HECA	HECA	HECA
	No.	25%	50%	75%	25%	50%	75%
All Months	276	118.0	113.9	127.0	162.6	160.2	171.3
S. Months	130	131.7	124.7	139.4	179.4	175.9	185.6
N.S. Months	146	105.9	104.3	115.9	147.6	146.3	158.6
L.S. Months	60	117.7	112.5	125.0	159.6	157.0	164.6

southern portion of the HECA little difference is observed in the overall correlation pattern regarding either the HECA or CSIRO target. In defining control regions within Tasmania, only stations outside of the HECA target were considered. In an effort to minimize any potential extra area effects of the seeding an approx. 25km buffer was added around the HECA target. Controls were only defined outside of this buffer region. The correlation map may roughly be broken up into four broad geographic regions: west, northwest, northeast and southeast (here after W, NW, NE & SE control regions) of the target. In addition to these four geographically based controls, a fifth control has been defined using 10 “high-quality” (here after HQ) rain gauges developed by Lavery et al. (1997) (Figure 2.6). None of these 10 sites resides within the HECA or CSIRO target although one of the sites does reside within the 25 km buffer zone to the southeast of the target. The remaining nine HQ sites are found within the four regional controls as follows: W (1), NW (3), NE (3) and SE (2).

The surface rainfall observations for the five different controls were prepared in a manner identical to that for the two targets. Similar to Table 2.2, the monthly rainfall for the five controls may be averaged over seeded and non-seeded months, Table 2.3. Only the 50% longevity threshold data are presented. Whereas both the HECA and CSIRO targets realised an ∼20% gain in rainfall during seeded periods, the controls; W, NW, NE and SE display gains of 14.1, 10.5 and 5.1 and 6.5%,

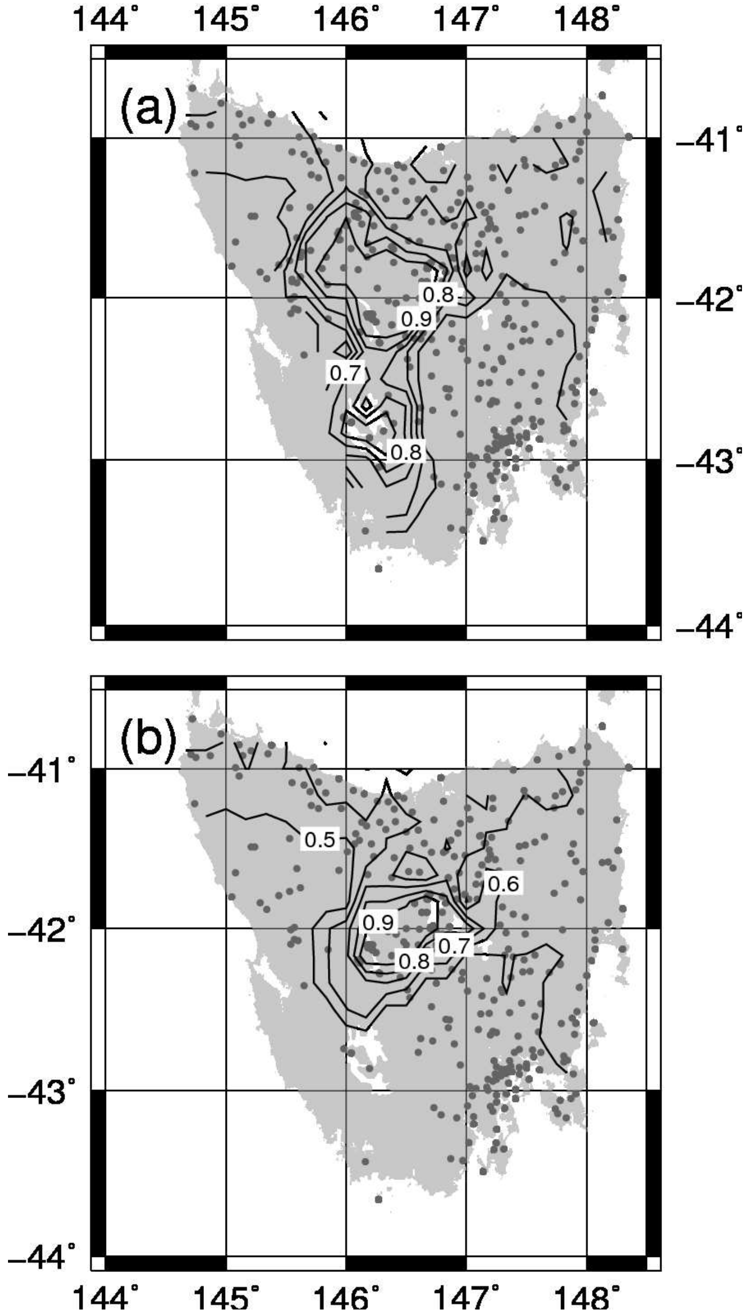

Figure 2.5: Correlation maps for (a) HECA and (b) CSIRO target areas for the 50% threshold filter. Correlation is for unseeded periods only. Regions containing highly correlated sites closely resemble target perimeter.

Table 2.3: Correlations between control areas and target areas, W - west control, NW - northwest control, NE - northeast, SE - southeast and HQ - high quality. Also shown is the average rainfall (May-October 1960-2005), average seeded rainfall and average unseeded rainfall (mm) for each control.

	W	NW	NE	SE	HQ
Correlation with HECA	0.87	0.76	0.66	0.51	0.85
Correlation with CSIRO	0.79	0.74	0.73	0.64	0.87
Average Rainfall	223.11	127.19	84.01	63.29	95.51
Seeded Rainfall	238.76	133.91	86.21	65.40	98.38
Non-seeded Rainfall	209.17	121.21	82.05	61.41	92.96

respectively. These results show that rainfall is greater during seeded periods over the whole of Tasmania and suggests that underlying temporal variations in rainfall should not be neglected.

Using only the 146 non-seeded months, the correlation between each control with either target is presented in Table 2.3. Based strictly on the geometry of the control regions, it is not surprising that the W control demonstrates a higher correlation than the other regional controls. The NW, NE and SE controls are larger in size and contain more sites at a further distance from the target. The SE control is not particularly well correlated with either target in comparison to the W and NW. When swapping from the larger HECA target to the smaller CSIRO target, the correlation with the W control drops from 0.87 to 0.79, while the correlation increases for the NE and SE controls. This is consistent with the geometry of the controls. The CSIRO target is not as mountainous as the HECA and so shows a higher correlation with the relatively low lying NE and SE controls. The HECA being relatively more mountainous exhibits a higher correlation with other like regions, those being the W and NW.

One might expect that the HQ control would roughly act as a weighted average of the four regional controls. This is not the case, as the HQ control displays only a weak enhancement during the seeded months (5.8%) but maintains a high

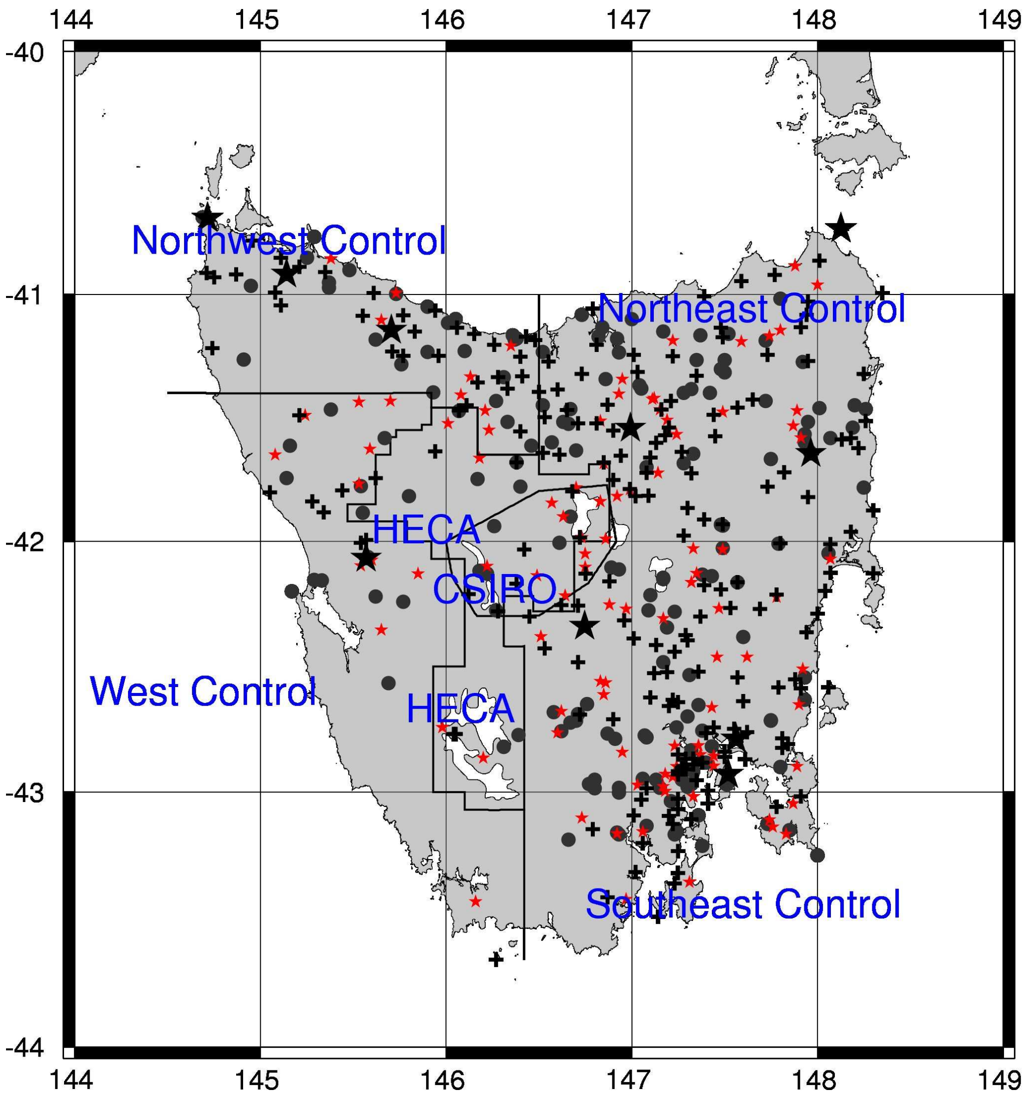

Figure 2.6: Map of Tasmania highlighting the location of long-lived sites 25, 50 & 75% (small grey circles, small red stars and small black crosses, respectively) for the period 1960-2005. The HECA and CSIRO target areas together with the control areas are defined (Note: any sites inside a control area within 25km of the target perimeter are not included in the control region). Sites marked using a large black star are Bureau of Meteorology high quality sites.

correlation with both the larger HECA target (0.85) and the smaller CSIRO target (0.87).

2.4 Double Ratio Analysis

Given that the four regional controls find rainfall enhancements from 5 to 14% (Table 2.3) during seeded months, the increase of 20% during seeded months found for the two targets (Table 2.2) cannot be taken at face value. The conventional means of removing temporal variations in rainfall is to use the double ratio (Gabriel, 1998). If the target rainfall for month i is T_i and the control rainfall is C_i and the summation over all seeded (unseeded) months is $\sum_s$ ($\sum_u$) then the double ratio d is defined as

$$d = \frac{\sum_s T_i / \sum_s C_i}{\sum_u T_i / \sum_u C_i}, \tag{2.1}$$

or alternatively,

$$1.0 = \frac{\sum_s (T_i/d) / \sum_s C_i}{\sum_u T_i / \sum_u C_i}. \tag{2.2}$$

The ten possible double ratios (Figure 2.7) range from as little as 1.047 (CSIRO vs. W) to as large as 1.145 (HECA vs. NE). These values, while considerably less than the 20% found in Table 2.2, are economically meaningful sense given the large target area. The double ratio suggests that over the 46 year period, cloud seeding increased rainfall in the target between 5 and 14% relative to nearby controls.

As a means to estimate the bounds within which the true double should exist, 95% confidence intervals may be defined for these double ratios following the method of Shaw et al. (1984). The estimated increase associated with a double ratio d is

$$(1 - \frac{1}{d}) \sum_s T_i = \sum_s T_i - \sum_u T_i \frac{\sum_s C_i}{\sum_u C_i}. \tag{2.3}$$

If (d_1, d_2) is a $100(1-\alpha)\%$ confidence interval for d, then $((1-\frac{1}{d_1}),(1-\frac{1}{d_2}))$ is the

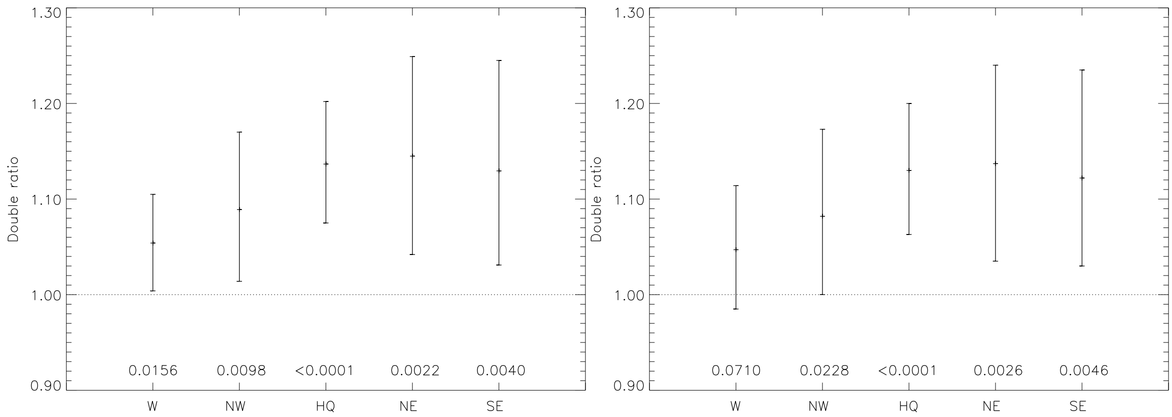

Figure 2.7: Double ratios and confidence intervals for the HECA (left) & CSIRO (right) targets vs. the west (W), northwest (NW), high quality (HQ), northeast (NE) and southeast (SE) controls. The bootstrap probabilities for obtaining a double ratio higher than the actual is shown above the horizontal axis.

$100(1-\alpha)\%$ confidence interval for the increase. Suppose that in Eqn. 2.2, instead of dividing T_i by d, T_i is divided by some δ, any double ratio calculated is therefore $d(\delta)$, with $d(\delta) < 1$ if $\delta > d$ and $d(\delta) > 1$ if $\delta < d$. It is therefore possible to associate a permutation estimate of the probability of a $d(\delta)$ different from 1.0, here defined as $p(\delta)$. The required confidence limits d_1 and d_2 are therefore the two solutions of $p(\delta) = \alpha/2$ and are found numerically. In essence, two questions are asked. Firstly, at what value for δ does the probability of obtaining a double ratio $d(\delta)$ greater than 1 exceed 97.5%? Secondly, at what value of δ does the probability of obtaining a double ratio $d(\delta)$ greater than 1 drop below 2.5%? The value of δ is found by trial and error and the probabilities are assessed using a standard bootstrap technique (Efron and Tibshirani, 1993).

It is observed that all of the confidence intervals lie above a value of one when using the HECA target [Figure 2.7(a)], and all overlap between about 6 and 11%. It is interesting to note that while the HECA-HQ double ratio is comparable to the HECA-SE and HECA-NE values, the confidence interval is smaller. This reflects the higher correlation that the HECA target has with the HQ control over the NE and SE controls. Appropriately, the confidence interval broadens as the correlation drops. The confidence intervals when employing the CSIRO target [Figure 2.7(b)] are comparable with the exception that the the 95% confidence interval for the CSIRO-W does extend below 1.00.

While these confidence intervals suggest that the positive response to cloud seeding is physically consistent across all regions, they do not rigorously define the statistical significance of the result. This is because the confidence intervals address the uncertainty in the calculated double ratio. They cannot address the question "how likely is it that this double ratio could occur by purely random processes?" A bootstrap analysis (Efron and Tibshirani, 1993) is undertaken for this purpose. For this analysis 10,000 bootstrap samples were calculated for the double ratio. Each bootstrap sample is constructed by randomly drawing (with replacement) a month from the full pool of 276 months 130 times. The pair of target and control from these 130 selected months are defined as "seeded". Similarly, 146 "non-seeded" months are defined by 146 independent draws from the full 276 data pool, i.e. replacement is enforced. This bootstrap sample double ratio is then compared with the true double ratio measured. The number of times that a bootstrap sample exceeds the true value is simply counted to define the significance level. If 500 of the 10,000 bootstrap samples exceed the true double ratio, then it is stated that the gain is at the 95% significance level. Of the ten combinations possible (Figure 2.7), only one fails to reach the 95% level (the CSIRO-W is at 92.9%). In the case of the HECA target, all five comparisons surpass the 98% level. Both the HECA-HQ and CSIRO-HQ double ratio surpass the 99.99% level of significance.

As there is more than one comparison being employed, the chances of obtaining a statistically significant result of a double ratio being different from 1.0 are greatly increased. This is because multiple statistical inferences are being considered simultaneously. Applying the Bonferroni adjustment (Weisstein, Accessed 2008) for multiple comparisons to a 95% significance level for 10 tests produces an alpha of 0.005. In this test 6 out of the 10 comparisons pass at the required level of significance.

These high levels of significance must ultimately be tempered since, strictly speaking, the monthly rainfall does exhibit both a month-to-month and year-to-year autocorrelation. The bootstrap analysis assumes that all 276 single ratios are independent of one another. Ideally the monthly cloud seeding would have taken place completely randomly across the six months and 46 years. Operationally this is simply not practical. The month-to-month seasonally adjusted autocorrelation at lag one over the full 276 months for the HECA (CSIRO) target is 0.129 (0.105), after transforming to a standard normal distribution. This is comparable to the month-to-month autocorrelation found over the full 12 month, 46 year data set. The year-to-year autocorrelation at lag one was calculated to be -0.043 and -0.140 for the HECA and CSIRO targets respectively (once again, after transforming to a standard normal distribution). It is noted that autocorrelations less than 0.2 are generally not considered particularly strong.

It is possible to eliminate any month-to-month correlation by analysing the months individually; instead of one data set of 276 months, six separate data sets of 46 months may be tested. This approach has two drawbacks. Firstly, the concern about multiple comparisons is magnified. Instead of 10 tests there are now 60, the two target areas compared against the six months and 5 control regions. Secondly, the reduced sample size makes it much more difficult to reach statistical significance. The results of this analysis remain consistent with those presented thus far. However, due to reduced sample size and the issue regarding multiple comparisons the results show much greater variability and are considerably less significant. Further Results not presented in Morrison et al. (2009) are presented in Appendix A.

2.5 Data Analysis Discussion

An analysis of the surface rainfall data over Tasmania for the period of 1960-2005 readily finds that, on average, more rainfall did occur during months in which seeding took place within target and control regions. The intermittent nature of the seeding (both experiment and operational) over this extended period provides a unique data set that may ultimately help demonstrate that cloud seeding can be viable over an economically meaningful area.

A standard double ratio calculation finds that the rainfall over the target was between 5 and 13% greater than over nearby “control” regions with a satisfactory level of statistical significance being reached (using a bootstrap analysis) in many of the tests. Further to this, it is thought that the consistency in the findings lends much to the credibility. Both Tasmania 1 & 2 present analyses indicating an increase in precipitation associated with seeding, the present analysis is consistent with these.

As the cloud seeding projects over Tasmania were never designed as a single long-term field experiment, numerous caveats to this approach exist. Evolving target boundaries, changing seeding strategies and technologies and evolving surface sites all limit the finding. More importantly, the seeding was not undertaken randomly on a monthly basis. Month-to-month and year-to-year correlations exist within the rainfall observations, which although small, violate assumptions of the bootstrap analysis.

Another major caveat to this approach is in the definition of “control” areas from which to define a double ratio. Control areas are supposed to be highly correlated with the target area during non-seeded periods, but free of any immediate effect of cloud seeding. When examining the data on a monthly time scale, there is no location within Tasmania that is not either downwind of the target or upwind where seeding commonly occurs. A 25 km buffer zone was enforced around the larger target in an effort to minimise any potential extra-area effect of seeding. It is interesting to note that the closest control with the highest chance of extra-area effects consistently shows the lowest double ratio with the least significance.

Further to this, the effects of both wind shear and frontal deformation on the targeting and dispersion of seeding agent remain very legitimate questions. Any extra-area effects would ultimately serve to diminish the double ratio and underestimate the effectiveness of the cloud seeding. It is also noted that operational constraints during seeding periods such as aircraft/instrument maintenance, personnel limitations, inaccurate forecasting and restrictions near lightning also lead to an underestimation of the potential efficiency.

Bearing in mind these caveats, this analysis provides some support for the hypothesis that cloud seeding may be physically plausible over Tasmania. This analysis cannot however, provide "convincing scientific proof" even when coupled with the research of the Tasmania 1 and 2 experiments. Many of the key uncertainties identified in the U.S. National Academies of Science report still remain. Most notably, the basic microphysical state of these precipitating frontal systems over the Southern Ocean is essentially unknown. These are not wintertime orographic clouds, as denoted by the National Academies of Science; these cloud systems reside within the high wind shear "roaring forties". Moreover the atmosphere over the Southern Ocean is pristine with little terrestrial or anthropogenic influences evident on the time scale of days to weeks. Recent observations suggest that even boundary layer clouds over the Southern Ocean are notably different from pristine maritime boundary layer clouds observed in the Northern Hemisphere (Bennartz, 2007). The conclusions reached from glaciogenic seeding efforts over the Western United States (Deshler and Reynolds, 1990; Deshler et al., 1990) are unlikely to be applicable over Tasmania.

The cloud systems over the Southern Ocean cover over 10% of the earth's surface yet remain largely unexplored. The unique dynamics and microphysics of these systems present a particular challenge in understanding the targeting, dispersion, and physical response of the clouds to glaciogenic cloud seeding. Obviously such challenges may only be addressed through further fieldwork. If any such fieldwork were to establish the immediate effect of cloud seeding, then it might be argued that, together with the fieldwork of Tasmania 1 (Smith et al., 1979), 2 (Ryan and King, 1997) and the present analysis, a complete argument for the efficacy of cloud seeding has been presented.

Chapter 3

WRF model evaluation

The objectives of this chapter are first, to present observations from two cloud seeding flights made over the western region of Tasmania and second, to evaluate the Weather Research and Forecasting (WRF) NWP model employing the TMP (Thompson microphysics package) (Thompson et al., 2007) regarding the ability to simulate these in-situ observations together with selected satellite and radar observations. Detailed are two case studies, the 8th August 2006 characterised by large amounts of SLW, little ice and a relatively small amount of precipitation and a more mixed phase event, the 4th October 2007 which showed lower concentrations of SLW, greater concentrations of ice and relatively larger amounts of precipitation. The following sections are organised as follows. First, the meteorology of the individual case studies are presented, this is followed by the evaluation which focuses on thermodynamic profiles, cloud-top structure, radar and in-situ aircraft observations.

3.1 Case Study Meteorology

Located at the northern boundary of the Southern Ocean storm tracks, the year round meteorology of Tasmania is dominated by the passage of fronts (Simmonds and Keay, 2000; Ryan et al., 1985). Both case studies evaluated herein are of winter-time frontal passages over Tasmania.

The MSLP analysis for 9th August 2006 00:00 UTC (hereafter, 2006) shows a high pressure cell over the border between Western and South Australia (Figure 3.1). To the south-east of this feature is a cold front associated with a mid-latitude cyclone south of Tasmania. The frontal cloud band is readily observable in a IR satellite image (Figure 3.2). To the west of the front is a cloud free band and behind this is a line of convection associated with a trough. In-situ aircraft observations indicated these clouds had tops >3km and bases <1.5km. These cells were the target of the cloud seeding research aircraft. Maximum SLW content (5 minute average) between -8 and -18 °C was ~$0.3gkg^{-3}$. The flight track is shown in Figure 3.3(a).

The MSLP analysis chart (Figure 3.1) for the 4th October 2007 00:00 UTC (hereafter, 2007) shows a high pressure cell situated over the border of Victoria, New South Wales and South Australia. The cold front occupies a small latitude band being confined between the high pressure cell to the north and two distinct low pressure centres situated to the southwest of Tasmania at approx. 50°S. The frontal cloud band occupies a much smaller zonal width as the prefrontal airmass is much colder, relative to the 2006 case (Figure 3.2). Typical of this region marine boundary layer clouds are observed in the pre and postfrontal airmass. The aircraft sampled clouds within the trailing edge of the frontal cloud band. Cloud tops were 2.5-3.5km with bases <1.5km. The conditions regarding seeding suitability during this event were less favourable, due to a greater fraction of mixed phase clouds being present. Maximum SLW was ~$0.1gkg^{-1}$ (5 minutes) at approx. -10 °C, a second seeding track was sought further south to find more appropriate conditions; these did not occur (Figure 3.3(b)).

3.2 Numerical Modelling of Clouds

The numerical model chosen to simulate clouds over the Southern Ocean and Tasmania is the Advanced Research WRF (ARW) version 2.2.1 (Michalakes et al., 1999; Skamarock et al., 2005). The model is suitable for applications which range from meters to thousands of kilometres and is used both within the research community and operationally. It has been used to study a wide range of atmospheric phenom-

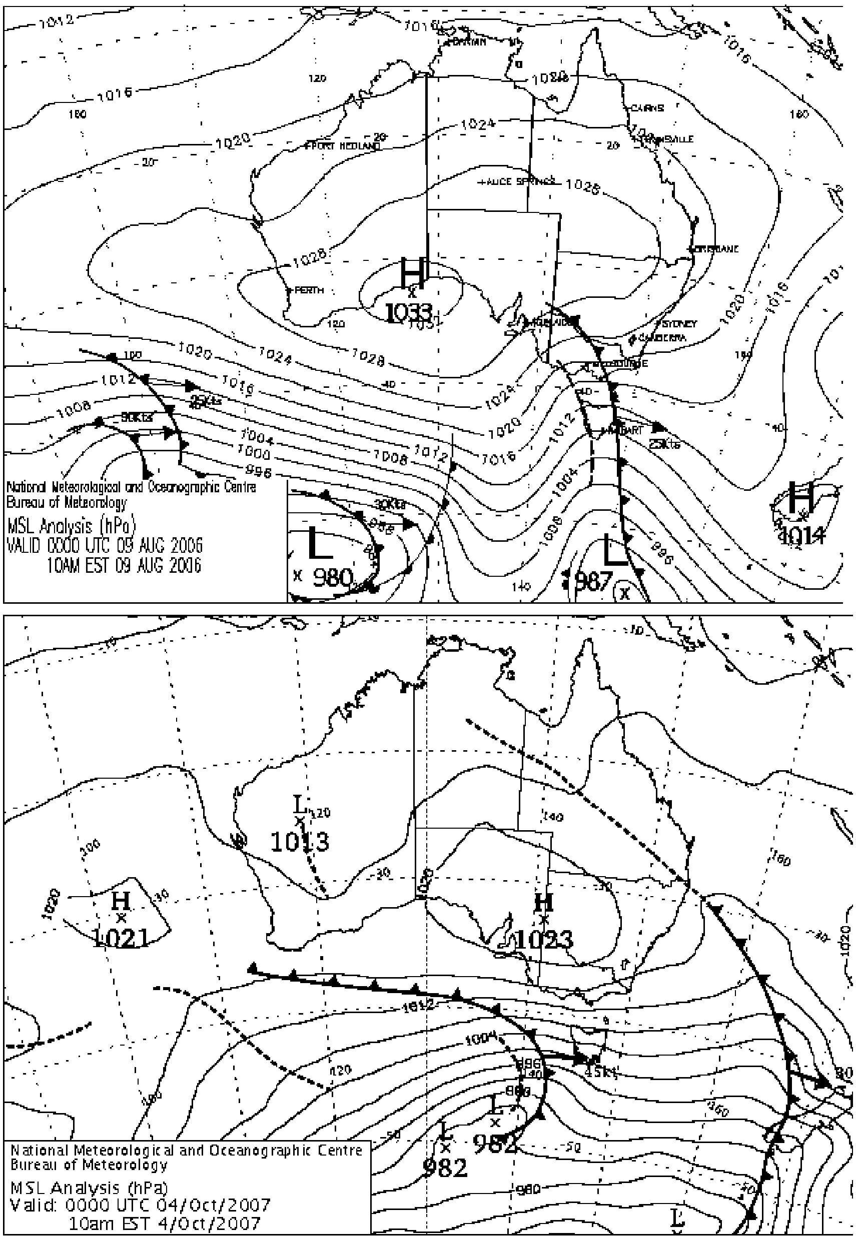

Figure 3.1: MSLP analyses provided by the Bureau of Meteorology, Melbourne, Australia. Upper: 0000UTC 09/08/2006. Lower: 0000UTC 04/10/2007.

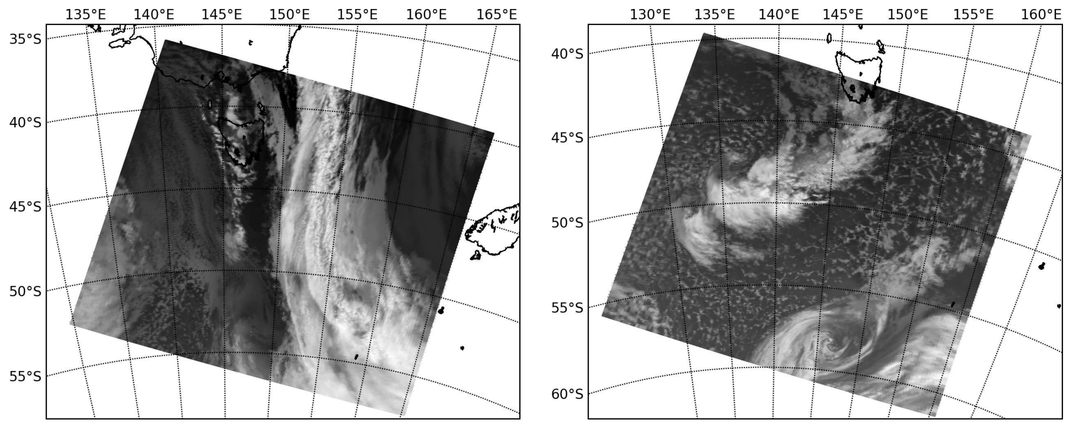

Figure 3.2: Left: IR satellite image taken by the Terra satellite at 2350 UTC 08/08/2006. Right: IR satellite image taken by the Terra satellite at 0010 UTC 04/10/2007.

ena from Asian pollution intensifying storm tracks in the Pacific (Zhang et al., 2007) and tropical convection in general (Wapler et al., 2008) to Arctic meteorology (Hines and Bromwich, 2008).

The WRF core is a fully compressible non-hydrostatic Eulerian solver. The horizontal model grid is an Arakawa 'staggered' C-grid that allows multiple nested domains, one way nesting is used herein. The vertical coordinate is terrain-following hydrostatic pressure with the top of the model being a constant pressure surface. The lateral boundary conditions employed herein are specified by a global model (described further in Section 3.2.1), the nested grid lateral boundary conditions are specified by the coarser resolution domain. The top boundary condition is a gravity wave absorbing (diffusion or Rayleigh damping), vertical velocity (ω)= 0 condition and the bottom boundary condition is free-slip. Vertical nesting is not permitted.

3.2.1 Model Configuration

The WRF model is a non-hydrostatic Eulerian solver developed by multiple government agencies in the U.S. (Michalakes et al., 1999). The model was configured with 64 η levels with a vertical resolution of 40m at the surface extending to 2km for the upper levels. The outer domain (dx = 81km and dt = 360s) was set-up to

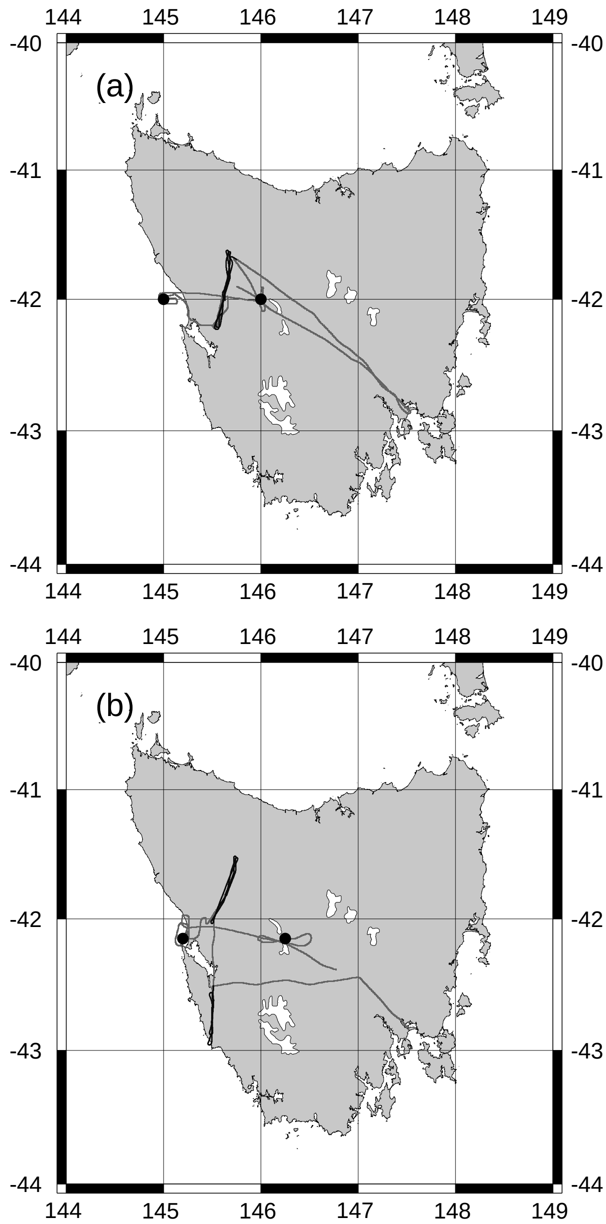

Figure 3.3: Map of Tasmania with seeding track overlaid, (a) 09/08/2006 and (b) 04/10/2007. Dark grey indicates seeding burners are aflame, lighter grey is the flight track. Atmospheric profiles were acquired by the plane over two regions for both case studies at approximately (42S,145E) and (42S,146E), indicated by the dots.

to cover the whole of Australia and the associated portion of the Southern Ocean down to approximately 60°S (Figure 3.4). Four daughter nests were utilised with the innermost domain centred over central western Tasmania ($dx = 1$km and $dt = 4$s). The domain was chosen to incorporate as much of the large scale dynamical features involved in the current analysis into the WRF grid with minimal information needed from the domain boundaries.

All simulations herein are 42 hours in length and were initialised at 22:00 local time (12:00 UTC) with a minimum of 30 hours spin up until the event of interest. Numerous experiments were utilised to investigate the optimal spin up time together with horizontal and vertical resolution, some of these results are mentioned in the following paragraphs. It was decided to use a longer spin up and larger outer domain as this configuration more accurately represented thermodynamic profiles from Hobart and off the west coast of Tasmania. This is in large part due to poor skill initial and boundary conditions within the National Centers for Environmental Prediction Global Forecast System (GFS) final (FNL) data set south of mainland Australia and over the Southern Ocean. The closest radiosonde station data assimilated into this data west of Tasmania and south of mainland Australia is Port-aux-Francais (49S,70E), ~5000km west of Tasmania. This issue is explored further in Section 3.3.1.

The model was configured with short-wave radiation parameterised using Dudhia (1989) and long-wave radiation as described in Mlawer et al. (1997). Boundary layer processes are represented using the Mellor-Yamada-Janjic scheme (Mellor and Yamada, 1982) and interactions between the earth's surface, boundary layer and radiation schemes are parameterised using the Noah land surface model (Ek et al., 2003). Alternative parameterisations were investigated, e.g. the Betts-Miller-Janjic (Janjic, 2000) convective parameterisation scheme was implemented in the two outer domains and the YSU non-local boundary layer scheme developed by Hong et al.

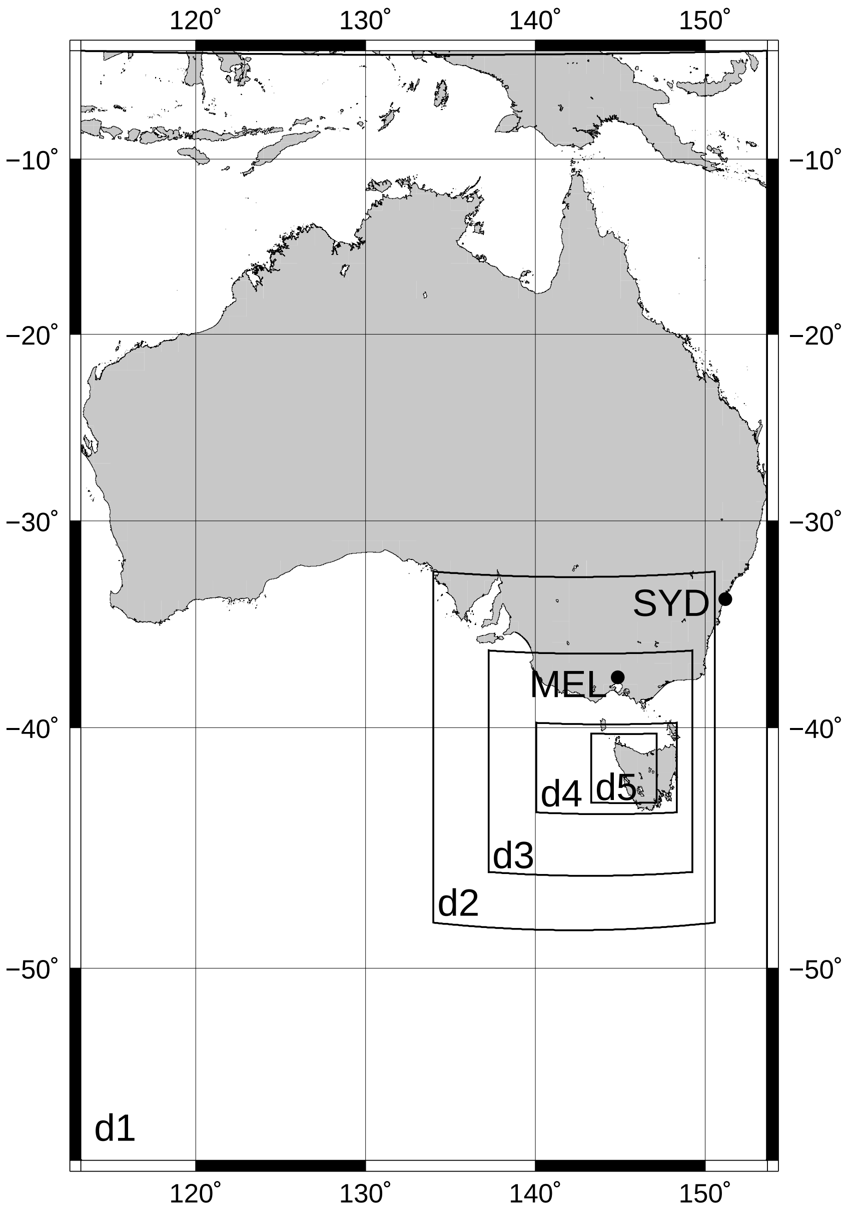

Figure 3.4: Map showing WRF domains 1-5. Melbourne and Sydney airports are show. Domain 1 (d1) has grid a spacing of 81km and time step of 360 seconds, daughter nests have grid spacing and time-step 1/3 of the parent.

(2006) was also implemented. These alternative configurations of the WRF model either under-performed or were no better than the standard configuration. It should be noted that model results presented herein were produced with no convective parameterisation in the outer domains.

The TMP is used to describe cloud processes (Thompson et al., 2007). This scheme is a bulk microphysics parameterisation that is double moment for ice and single moment for cloud water, rain, snow and graupel. The number of cloud droplets (a proxy variable for Cloud Condensation Nuclei, CCN) activated upon reaching saturation is pre-set by the user, this was set to 75cm^{-3}, consistent with direct measurements of CCN made at Cape Grim in northwest Tasmania (Gras, 1995). Ice initiation is parameterised as described in Cooper and Lawson (1984) and does not form until temperatures are $<$ -8°C or supersaturation w.r.t. ice is $>$ 8%. A more thorough investigation regarding the sensitivity of these simulations to microphysical parameterisations is presented in Chapter 4, further, a more detailed description of the code is also presented.

3.3 Evaluation

The model evaluation focuses mainly on cloud structure, with a brief examination of precipitation structure using radar. Comparisons with surface observations are not discussed as they do not add any extra insight into cloud structure. Satellite observations collected by the Moderate Resolution Imaging Spectroradiometer (MODIS) instrument on the Terra satellite managed by NASA (Justice et al., 1998) are used in a broad scale evaluation. For the 2006 case study, model simulated radar reflectivities are compared with observations from the West Takone radar site in northwest Tasmania. The radar data for 2007 were not available, no radar evaluation is possible for this event. Only a cursory examination of the radar data for the 2006 case is presented.

The principal observations used in the evaluation are in-situ aircraft observations obtained by Hydro Tasmania's (HT) cloud seeding research aircraft, a Cessna Conquest which flew between 20:22 08/08/06 and 01:01 09/08/06 (hour:minute day/month/year, UTC) and 23:52 03/10/07 and 03:12 04/10/07 (Figure 3.3). The flight objectives were to encounter SLW between -5 and -15°C for the purposes of cloud seeding. The aircraft had on board a Droplet Measurement Technologies (DMT) Cloud Aerosol and Precipitation Spectrometer (CAPS) probe (Baumgardner et al., 2001) which incorporates a hot-wire liquid water sensor, a Cloud Aerosol Probe (CAS) that measures particles within size range 0.5-50μm and a Cloud Imaging Probe (CIP) 25μm-1.55mm. Unfortunately no data were available for the CIP and hot-wire on the CAPS during either case study. There were two additional hot-wire probes attached to the fuselage, a DMT and CSIRO King hot-wire probe. In addition the plane also collected thermodynamic measurements: relative humidity, temperature and pressure.

3.3.1 Atmospheric Profiles

Aircraft observed soundings are produced both off the west coast of Tasmania (hereafter the upwind sounding) and over the central plateau (downwind) for comparison with WRF simulated soundings (Figures 3.5 and 3.6). The model soundings are produced at a single grid point, corresponding to the average latitude and longitude of the plane's position during ascent. Averaging over a number of grid points was also investigated, this did not notably effect the results.

The skill with which the model is able to represent upper-air soundings varies considerably between cases. The simulated 2006 upwind sounding (Figure 3.5(a)) is able to recreate well both the temperature and moisture profiles in the lower atmosphere. The model predicted ground temperature is within 1°C of the observed and the model temperature trace lies over the measured trace between 900 and

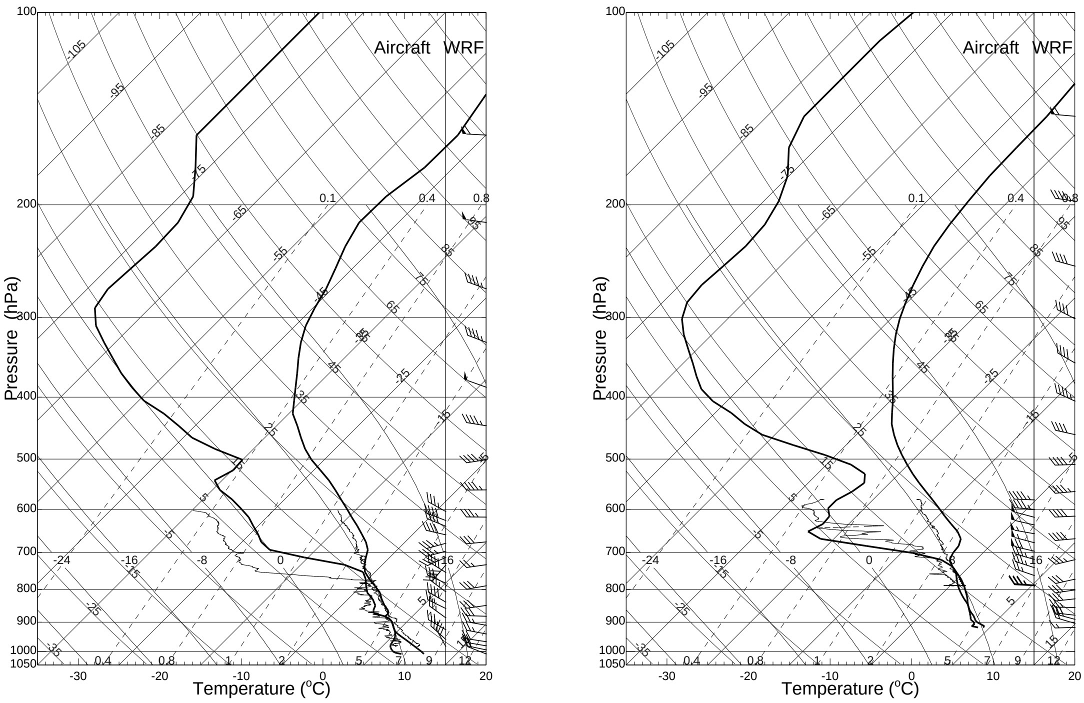

(a) (b)

Figure 3.5: Thermodynamic and wind profiles as measured by aircraft and model. Model predicted temperature profiles extend the full height of the sounding - thick line, aircraft soundings - thin line. Wind profiles are shown on the right. (a) Upwind profile 08/08/2006, (42S,145E). Aircraft sounding 23:00 UTC, model sounding 23:00 UTC, (b) Downwind profile 09/08/2006, (42S,146E). Aircraft sounding 00:25 UTC, model sounding 00:00 UTC.

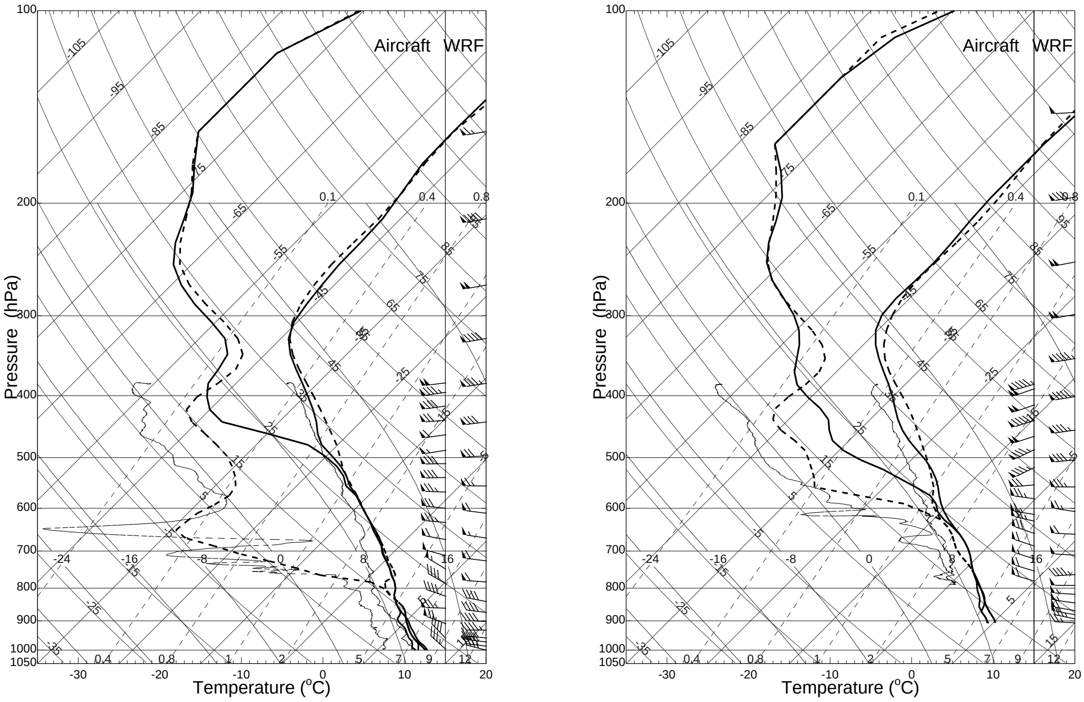

(a) (b)

Figure 3.6: As in Figure 3.5. (a) Upwind profile 04/10/2007, (42.11S,145.17E). Aircraft sounding 2:30 UTC (thin line), model sounding 3:00 UTC (thick line), model sounding 5:00 UTC (dashed line), wind barbs shown for 5:00 UTC model sounding. (b) Downwind profile 04/10/2007, (42.18S,146.14E). Aircraft sounding 3:00 UTC (thin line), model sounding 3:00 UTC (thick line), model sounding 5:00 UTC (dashed line), wind barbs shown for 5:00 UTC model sounding.

750hPa. Cloud base is close to the observed and cloud top is within 20-30hPa of the observed. A temperature inversion of $\sim$2°C is present in the model profile at around 730hPa, but is not present in the observations. The downwind sounding for 2006 is shown in Figure 3.5(b). The observations show a neutrally stable atmosphere between 600-800hPa. The model shows a neutrally stable atmosphere up to around 700hPa then a large inversion is observed. The moisture profile resembles more closely the observations (see Figure 3.5(a)).

Regarding 2007 the model (solid dark line in Figures 3.6(a) and 3.6(b)) shows considerably less skill for a direct comparison. For both the up and downwind soundings the model over predicts temperature and the simulated moisture profile shows little resemblance to the observed. If, however the model sounding is delayed by 2 hours both soundings better resemble the observed, suggesting WRF lagging behind the observations regarding the frontal timing. Further evidence supporting this claim is presented in the following section. Comparison of the delayed upwind model sounding shows that WRF over predicts temperature by approx. 1 °C from the surface to approx. 350hPa (top height of observations). A small temperature inversion is observed at 780hPa that is not present in the observations. The model dew point profile is on average a few degrees above the observed. Qualitatively, the skill associated with the downwind profile shows many similarities with the upwind.

Wind profiles measured by the aircraft and model are also shown for both case studies on the right of Figures 3.5 and 3.6. A notable feature observed during 2006 is the shear layer between 750-650hPa. The largest value for this wind change is $>$25ms^{-1} and occurs in $\sim$100m at an altitude of 2.6km. This phenomenon is also present with less magnitude during 2007. The model fails to reproduce this shear feature in either case study. GFS FNL reanalysis data were studied for the input thermodynamic and wind profiles used by WRF as initial and boundary conditions (see Figures 3.7 (a) and (b)). The observed wind shear is not found in this data

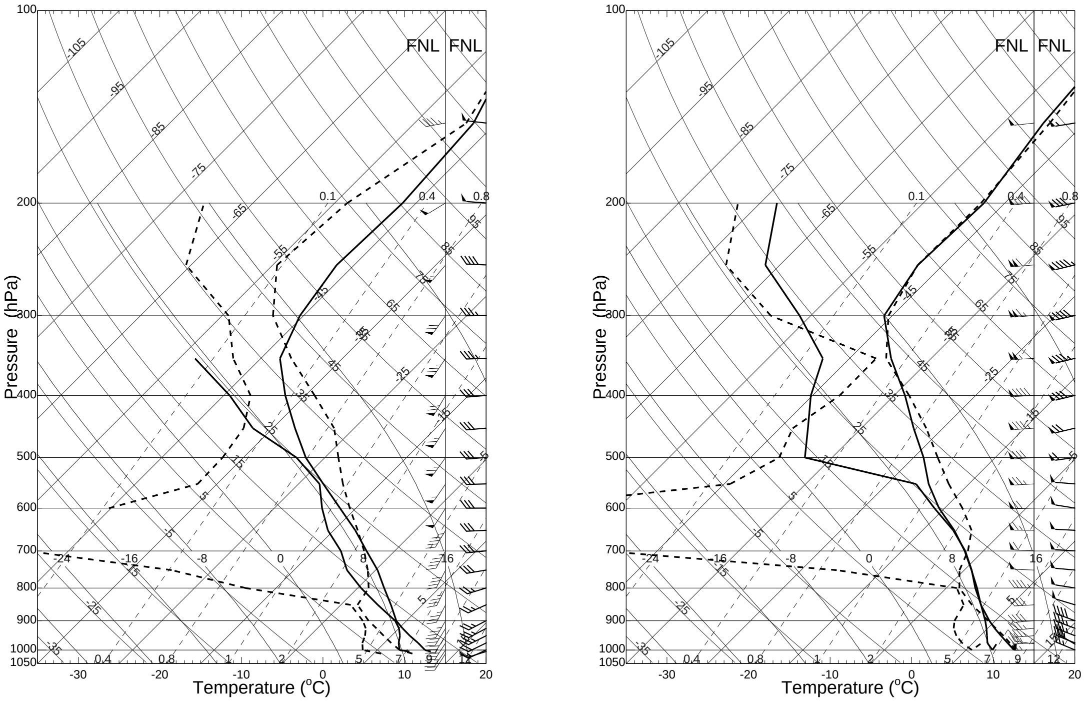

(a) (b)

Figure 3.7: Thermodynamic and wind profiles supplied to the WRF model using the FNL Reanalysis data. The bold line indicates the sounding closest to the observation times, the dashed line indicates the next available sounding, 6 hours later. Wind barbs on the right are associated with the bold sounding, barbs on the left are for the dashed sounding. (a) FNL upwind profile 09/08/2006 00:00 and 06:00, (42S,145E), (b) FNL upwind profile 04/10/2007 00:00 and 06:00, (42S,145.17E).

set. The reason for this mid-tropospheric shear remains unknown. In all, a total of seven aircraft soundings (during different events) have been examined over the west coast of Tasmania, this shear feature is clearly present in five of them.

Throughout the vertical profile the model wind speeds have a maximum error of 15-20 knots with WRF tending to underestimate wind speed. Regarding 2006, the observed wind direction is from the northwest (∼280°, with the exception of the shear layer), the model has winds from the southwest (∼260°). The MSLP analysis in Figure 3.1 indicates that at the time of the sounding the wind direction was transitory and changing from north-westerly to southwesterly. The difference in observed and modelled wind direction is due to WRF slightly leading the observations. WRF soundings produced 1 hour earlier were from the northwest. Regarding 2007, the observed and modelled wind directions agree.

3.3.2 Satellite Observations

Satellite derived cloud top temperature (CTT) from MODIS on the Terra platform are qualitatively compared with model CTT's for domains 3, 4 and 5 (Figure 3.8). A quantitative comparison is implemented for the finest resolution domain (domain 5). For the quantitative comparison two methods were implemented. 1) The WRF model grid cells (dx = 1km) were averaged to the same resolution as the MODIS pixels (dx variable between 5×5km and 5×20km) and 2) the native WRF model resolution was compared with the native MODIS pixel resolution. No appreciable difference was apparent, as such results are presented for the former methodology.

The algorithm used to derive satellite CTT is described in Platnick et al. (2003). The uncertainty in the satellite derived CTT is an interesting problem: most recently Hanna et al. (2008) investigated the difference between satellite derived CTT and upper-air measurements. Differences of approx. 5°C were common, the task here however is to simulate the brightness temperature that a satellite would observe. The algorithm employed uses the temperature of a cloud one unit of optical depth (τ) from the top of the model. Other assumptions are that the zenith angle is zero and cloud absorption coefficients are constant and dependent on specific hydrometeors. Hydrometeors assumed to contribute to cloud optical properties are cloud water, ice, snow and rain, these are assumed to be present in sufficient numbers to affect cloud emissivity. The absorption coefficients are 0.14500 m^2g^{-1}, 0.07350, 0.00234 and 0.00033 respectively (Dudhia, 1989).

Figure 3.8 shows the planar view CTT for both cases, observations and model. The observations for 2006 (Figure 3.8(a)) show relatively cold CTTs most likely

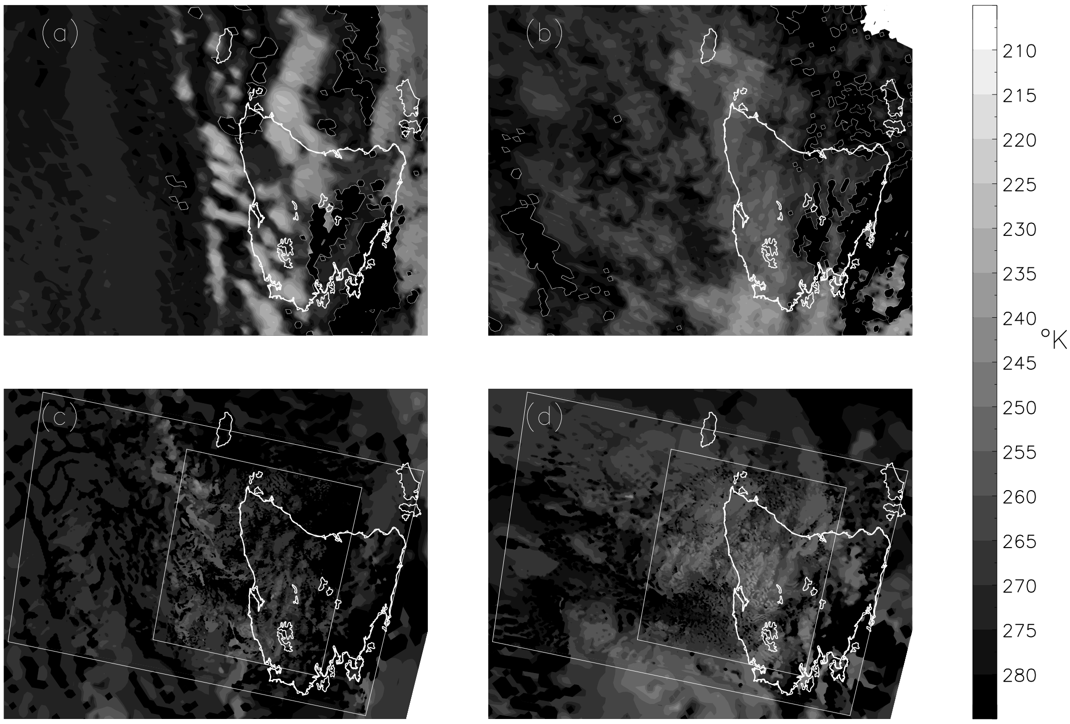

Figure 3.8: Cloud top temperatures. (a) 23:50 08/08/2006 MODIS, (b) 00:05 04/10/2007 MODIS, (c) 00:00 09/08/2006 WRF domains 3, 4 and 5 and (d) 02:00 04/10/2007 WRF domains 3, 4 and 5.

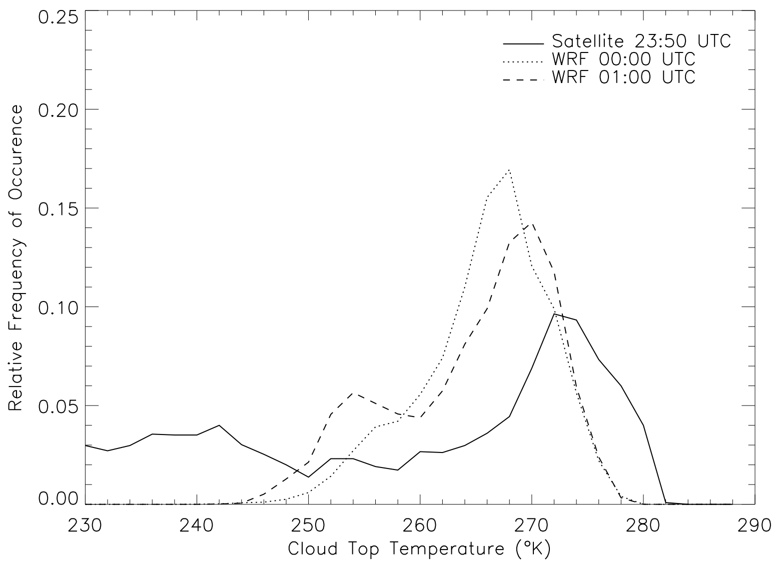

(a)

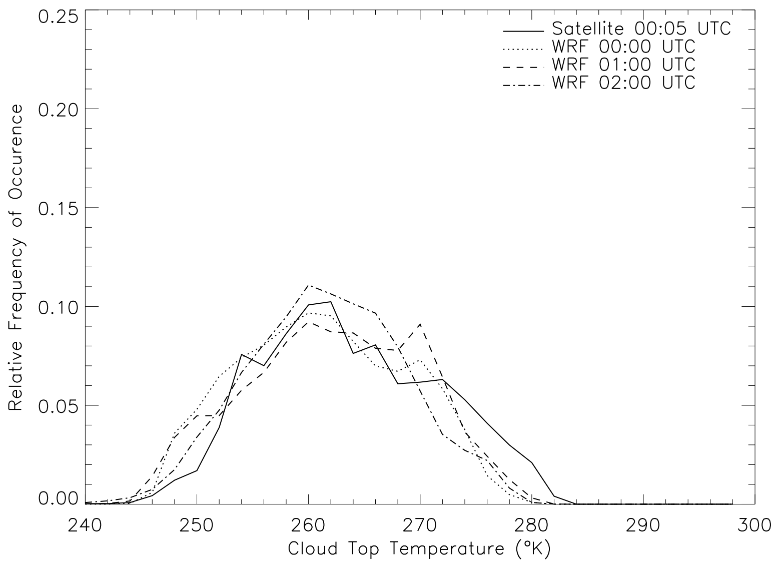

(b)

Figure 3.9: Satellite retrieved and WRF simulated cloud top temperatures for both case studies. Only the region defined by the finest resolution domain is used. One observation time is shown. (a) August 2006, the closest model time and one hour after are shown. (b) October 2007, the closest model time, one and two hours delay are also show.

associated with convective regions along the trough line over the western coast of Tasmania (see Figure 3.1). It is possible that these high cold clouds could have advected in over the trough and be associated with a separate airmass, however this is unlikely. East of this feature over the northeast portion of the island are more cooler clouds (∼240°K) associated with the trailing edge of the front. Figure 3.8(b) shows the frontal cloud band for 2007 over the western region of Tasmania. This shows a cooler distribution of CTTs, however lacking the small localised regions of very cold clouds found in 2006. The simulated cloud field for 2006 (Figure 3.8(c)) shows warmer clouds associated with the trough off the western coast of Tasmania, the position of this feature is well represented. The 2007 simulation (Figure 3.8(d)) shows slightly warmer CTTs associated with the frontal cloud band, this feature is also well positioned over the western portion of the island.

Figure 3.9 shows histograms of MODIS and model CTT for the finest resolution domain (domain 5). For both case studies MODIS finds clouds warmer than 280°K that do not match WRF. Either MODIS is observing fog close to sea level or inferring sea surface temperature as cloud top. The soundings shown in Figures 3.5 and 3.6 indicate that cloud base is at 5 °C, however MODIS is indicating clouds at around 12 °C, this is close to the temperature observed by the aircraft 100m above the ocean surface and below cloud base. Regarding 2006 (Figure 3.9(a)), WRF under predicts warmer clouds above 273°K, then over predicts between 250-273°K. WRF fails to develop clouds with temperatures <245°K, i.e. WRF failed to reproduce the small number of very cold clouds associated with the trough line. The histograms for 2007 are more similar. Sensitivity studies suggest small changes in the magnitude of absorption coefficients do little to alter the distribution of CTTs, increasing confidence in the model CTT algorithm.

Table 3.1 shows the mean, median and standard deviation of CTT together with the total cloud fraction for each case study for the finest resolution domain. Cloud fraction is calculated by simply counting the number of grids that return a CTT at a level above the surface, this number is then normalised by the total number of grid cells within the domain. For the 2006 case the observed skewed distribution is highlighted by the difference in the mean and median CTTs, 261.47 vs. 267.62 °K respectively. WRF manages to replicate some of this skewness, however, with a smaller magnitude, 266.98 vs. 268.97 °K. Cloud fraction is also under predicted. Observations indicate that 94% of the domain is covered in cloud vs. WRF's 69%. (Note that the observed cloud fraction should be lower than 94% due to MODIS incorrectly classifying sea surface as cloud top). For the 2007 case WRF shows much greater skill. The largest error in mean (median) CTT is 2.3 (1.9) °K and cloud fraction is much better represented. WRF's worst prediction is approx. 10% less cloud coverage relative to the observations.

Table 3.1: Mean, median and standard deviation of cloud-top temperature (°K) together with cloud fraction for both case studies for domain 5.

August 2006				
	Mean	Median	Stdev	Cloud Fraction
Obs. 23:50	261.47	267.62	16.69	0.94
WRF 00:00	268.11	268.95	5.91	0.65
WRF 01:00	266.98	268.97	7.46	0.69
October 2007				
Obs. 00:05	265.42	264.78	9.35	0.96
WRF 00:00	263.08	262.85	7.66	0.91
WRF 01:00	264.06	264.23	8.03	0.88
WRF 02:00	263.46	263.42	7.21	0.93

3.3.3 Radar

The West Takone radar located in northwest Tasmania is a 5cm C-band. The minimum detectable signal is relatively high, in the range of 0-10dBz. Observed and simulated radar reflectivities for 16:00 08/08/2006 (UTC) are shown in Figure

3.10. The method for determining the simulated radar reflectivity is described in Blahak (2007). At this time the frontal rain band is passing over the radar domain, enabling a comparison of planar and cross-section view precipitation core structure. The constant altitude plan position indicator (CAPPI) shown in Figures 3.10 (a) and (b) is at a height of 3km, zonal cross-sections along -40.5S are shown in Figures 3.10 (c) and (d) (this latitude was chosen because of clear view, mountains obstruct much of the view to the south).

The simulated radar reflectivities show maximum returns of $\sim$ 22dBz, the observed reflectivity is in the range 24-28dBz. The fine scale precipitation core structure is visually similar in the planar view i.e. localised maxima with horizontal extents of a few kms. It is noted however that this similarity could simply be due to chance. A simulated frontal rain band appears to the west of the observed indicating a possible temporal/spatial displacement of the simulated field. Cross sections show quite different vertical structure. The model replicates precipitation cores extending from the surface to around 5km. However, it also shows mid level precipitation not reaching the ground. This feature is not present in the observations.

The differences between the general shape of the model and observed reflectivity fields are expected. Inspection of the entire simulation (not shown), indicates that the model often shows differences regarding the spatial positioning of precipitating structures. Further, WRF tended to underestimate large dBz returns throughout the frontal passage. Given the uncertainties in initial and boundary fields supplied to the model and the insufficient resolution of updrafts less than $\sim$5km in horizontal extent, it is unsurprising that differences exist.

3.3.4 Aircraft Microphysics Observations

The emphasis of this evaluation is on WRF's ability to simulate aircraft observed cloud structure within the finest resolution domain (domain 5). Initially, a similar

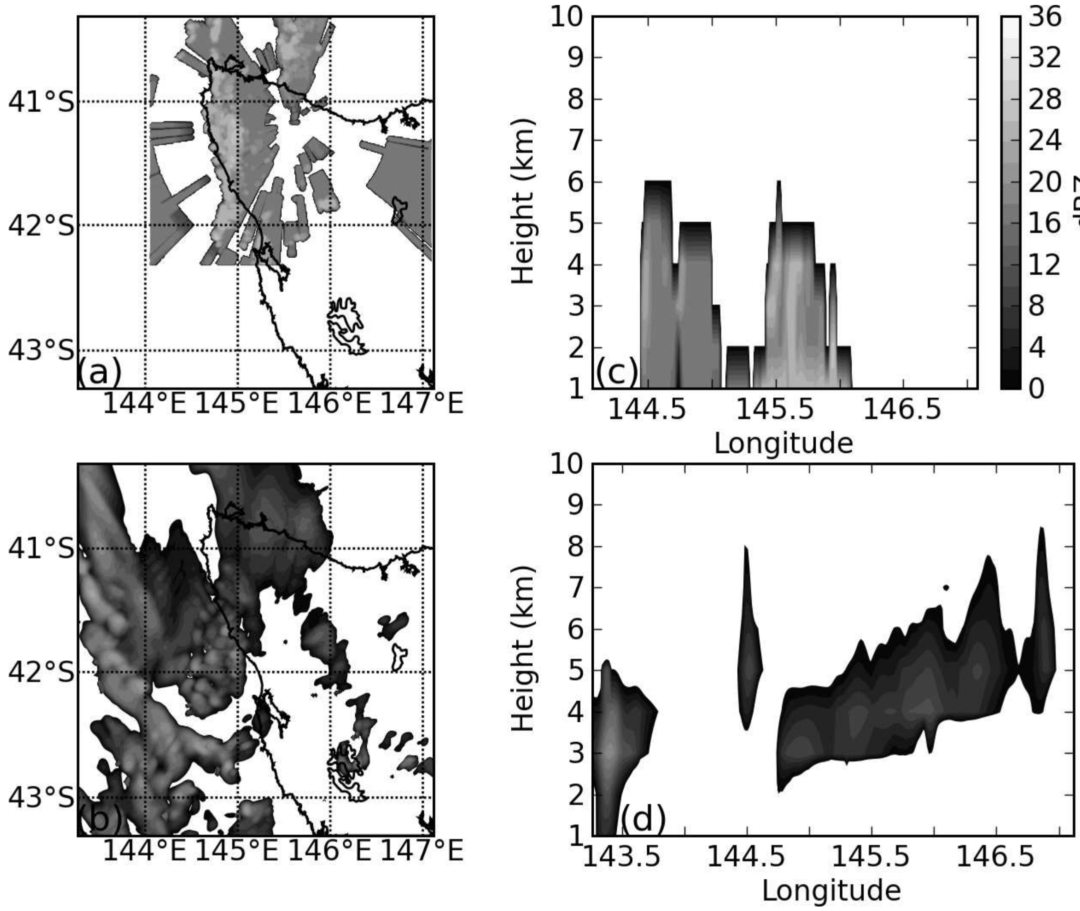

Figure 3.10: Radar reflectivities from the West Takone radar in north west Tasmania for 16:00 08/08/2006 UTC. Precipitation associated with the frontal cloud band is shown. Plots (a) and (c) are observations, (b) and (d) are WRF simulated fields. Constant altitude plan position indicator (CAPPI) is at a height of 3km, cross sections are taken at 40.5S.

evaluation to that presented in Guan et al. (2001, 2002) and Vaillancourt et al. (2003) is carried out. This is a point-by-point direct comparison of aircraft observed variables along the entire flight track with a virtual flight track. Observations of (i) temperature (°C), (ii) dew point temperature, (iii) small hydrometeor particles (0.5-50μm - measured by the CAS) and (iv) liquid hydrometeors (measured with a hot-wire probe) are compared with model fields. The main evaluation however considers only the level flight tracks which were implemented by the aircraft while the seeding burners were aflame. These were conducted over the western region of Tasmania (see Figure 3.3) for 2006 at an altitude of $\sim$2.5km between -4 and -18°C and during 2007 at an altitude of $\sim$2.7km between -8 and -11°C.

The method for obtaining the virtual time series was to input the aircraft trajectory in terms of latitude, longitude, pressure and time (for 2007 the virtual time series was delayed by 2 hours in line with previous findings). The closest latitude, longitude and time grid point from the model was then chosen and linear interpolation used with regard to the height coordinate. This was implemented with the same temporal resolution as the observations (1Hz) i.e. the same grid point is sampled a number of times. As the type of clouds sampled were predominantly cumulus cells having diameters of up to a few km, comparisons along the entire flight track were made using numerous averaging length scales of 1, 2, 4, 8, 16 and 32km.

The model diagnosed variables used for comparison with small hydrometeor particles are cloud water content and small ice particle content ($q_c + q_i$) while for liquid hydrometeors, cloud and rain water content are used ($q_c + q_r$). Note: the model q_i category includes diameters 11-125μm, and is initiated with a density of 890kg m^{-3}. Results presented here assume that all hydrometeors detected by the CAS are spherical and have a density of 1000kg m^{-3}. This is considered a "fair" assumption for 2006 when less ice was present. For the 2007 event however, the validity of this assumption is less robust as there were lower SLW contents and more ice. A lower bound on the bulk density of in-cloud "ice" measured using the CAS (0.5-50μm) is postulated to be 400kg m^{-3} (the term "ice" refers to hydrometeors viewed by the CAS - these can be either water, ice or both). Hence, for both case studies the "true" hydrometeor mixing ratio (as observed by the CAS) is postulated to be somewhere between the values presented herein and a number that is 60% less. Hereafter, discussion of small hydrometeor mixing ratios assumptions that objects viewed by the CAS have a density of 1000kg m^{-3}, unless otherwise stated.

It is noted that for ice particles >100μm, the density is almost certainly lower than 400kg m^{-3} (Heymsfield et al., 2004a,b). However, within the present study the instrument used to measure "ice" particles only measures up to 50μm. Further, Heymsfield et al. (2004a) notes that for pristine ice crystals <100μm, the density can be as much as 910kg m^{-3}. Tasmania, lying within the northern Southern Ocean is considered to be pristine with very few natural CCN and little anthropogenic influence (Gras, 1995). Hence, true "ice" (i.e. frozen hydrometeors <50μm) particles observed by the CAS could potentially have a density ~900kg m^{-3}. Further, as the model ice category is initiated with density of 890kg m^{-3} and the aircraft measurements were made at temperatures >-20°C where mixed phase conditions are not only possible but were almost certainly encountered. The assumption that the true density of objects viewed by the CAS is between 400-1000kg m^{-3} is deemed suitable for a comparison of this nature.

This leads into a necessary discussion on the errors associated with measurements of liquid water using the CSIRO liquid water probe in mixed phase conditions. Cober et al. (1995) found that in mixed phase conditions the King liquid water probe responded to between 5-30% of ice water content, with an average response of ~20%. The uncertainty of the specific probe in use was not evaluated, hence the uncertainty in liquid water contents presented herein is assumed to be that presented by Cober et al. (1995). The uncertainty in this quantity is of greater importance during the 2007 case due to its more mixed phase nature.

Returning to the analysis of the virtual and observed aircraft measurements, regarding both case studies the variables that correlated best were temperature and dew point. Further, this result was independent of spatial averaging, similar to results found in Guan et al. (2001). The correlations regarding the mixing ratios of small and liquid hydrometeors were less impressive. Regarding both case studies a clear dependence on spatial averaging was observed. In general, as the averaging length scale was increased the correlation increased. For temperature and dew point the correlation coefficient was always above 0.85 for 2006 and 0.9 for 2007. Regarding moist fields, at an averaging length scale of 1km the correlation for both case studies was between 0 and 0.2. Averaging over 32km the correlations increased, however all were $\leq$0.65.

The findings regarding the cursory comparison of the real and virtual flight tracks indicated that WRF was able to reproduce the measured temperature and dew point traces with a fair degree of accuracy, quantitatively similar to Vaillancourt et al. (2003), who found average correlations of temperature and dew point to be $>$0.9 and $>$0.85, respectively over 21 flights. The model's ability to reproduce the hydrometeor traces was much poorer ($<$0.2), as was the case in Vaillancourt et al. (2003). As such, a further test is also employed where the observed mixing ratios along the seeding track are compared with those along a virtual seeding track. Both events presented here include at least 4 traverses of a seeding track, for 2006 there is only one seeding track. Regarding 2007 there were two seeding tracks. This analysis considers only the most northerly track as the aircraft made only two traverses of the southerly track. The experimental procedure is to compare the four observational seeding tracks made over the course of approximately one hour with 3 virtual seeding tracks each spaced 1 hour apart (before, during and after the observational period). The comparison is accomplished by averaging the aircraft data over 1km ($\sim$13 seconds).

It is observed (Figures 3.11 and 3.12) that the 2007 event contained smaller concentrations of SLW relative to 2006. Averaged over the entire seeding track the 2006 event contained 0.070g kg^{-1} whereas the 2007 event contained 0.033g kg^{-1}. Virtual seeding tracks are also shown in Figures 3.11 and 3.12. The model is able to replicate qualitatively the different SLW mixing ratios, i.e. the 2007 event contains approximately 50% less SLW than the 2006 event. Quantitatively however, the model overestimates SLW content by $\sim$300% for both events (0.214 and 0.098g kg^{-1}, respectively). Further, the model tends to overestimate the spatial extent of liquid content regions (both case studies). Maximum SLW mixing ratios for 2006 are in close agreement, approx. 1.5g kg^{-1}. For 2007 however the model tends to underestimate maximum SLW contents; observations show peaks of $\sim$1.0g kg^{-1} whereas the model maximum is $\sim$0.5g kg^{-1}.

The results regarding the analysis of small hydrometeors are shown in Figures 3.13 and 3.14. It is noted that the average small hydrometeor mixing ratio during 2006 is approx. half that of 2007. Averaged over the entire seeding track the mixing ratio of all hydrometeors in the range 0.5-50μm for 2006 is 0.077g kg^{-1} (similar to the value measured by the hot-wire), for the 2007 case, 0.140g kg^{-1} (assuming 400kg m^{-3} these reduce to 0.029 and 0.056g kg^{-1}, respectively). As before, model derived virtual CAS traces for three time periods are also shown. The model predicted small hydrometeor mixing ratio for 2006 is 0.156g kg^{-1} (200% more than the observed) and for the 2007 event 0.095g kg^{-1}, well inside the uncertainty of the observed value.

It is noted that the seeding track average mixing ratio values for the hot-wire and the CAS do not agree well for the 2007 case, but are in close agreement for 2006. This finding suggests that the 2006 case is a supercooled event, whereas 2007 is more mixed phase. The positioning of the observed peaks for SLW and small hydrometeors in Figure 3.11 (a,i) with 3.13 (a,i) and 3.12 (a,i) with 3.14 (a,i)

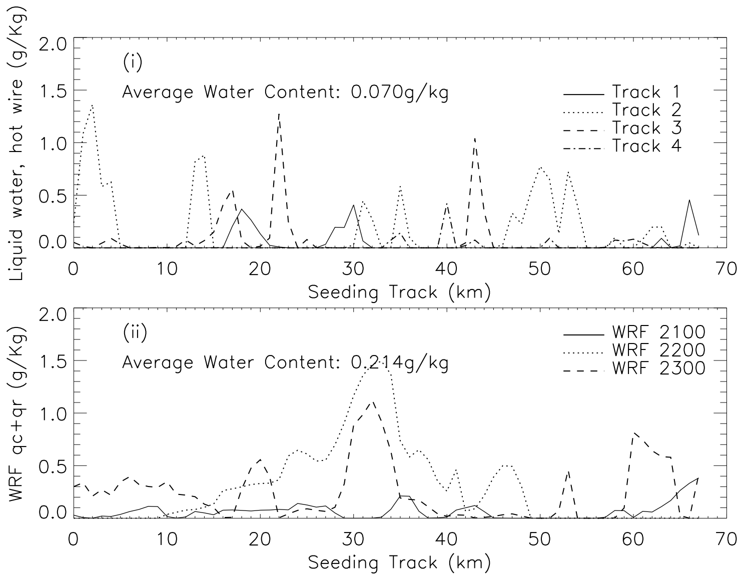

(a) (i) Aircraft, 13 second averages (approx. 1km) and (ii) WRF liquid water trace

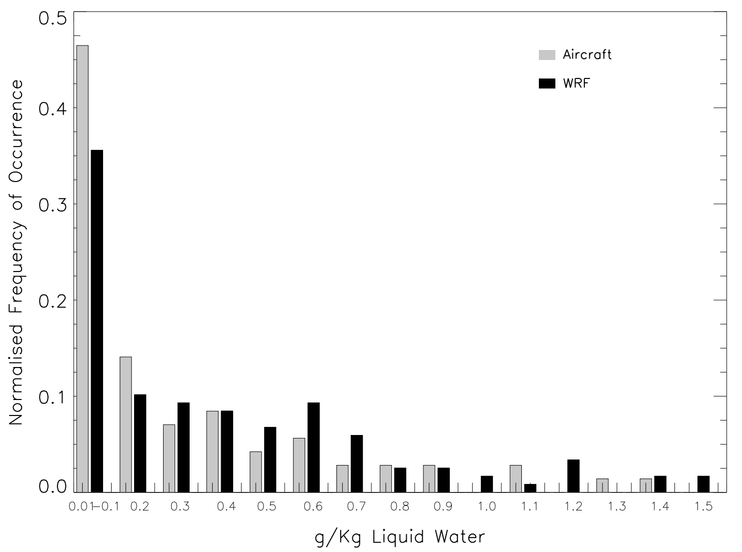

(b) Aircraft and WRF histogram showing probabilities of encountering specific quantities of liquid water

Figure 3.11: Liquid water traces and histograms from the August 2006 case study. The averages shown in (a) i and ii are over all seeding tracks. Measurements were taken at $\sim$ 2.5km altitude at temperatures between -8 and -18°C.

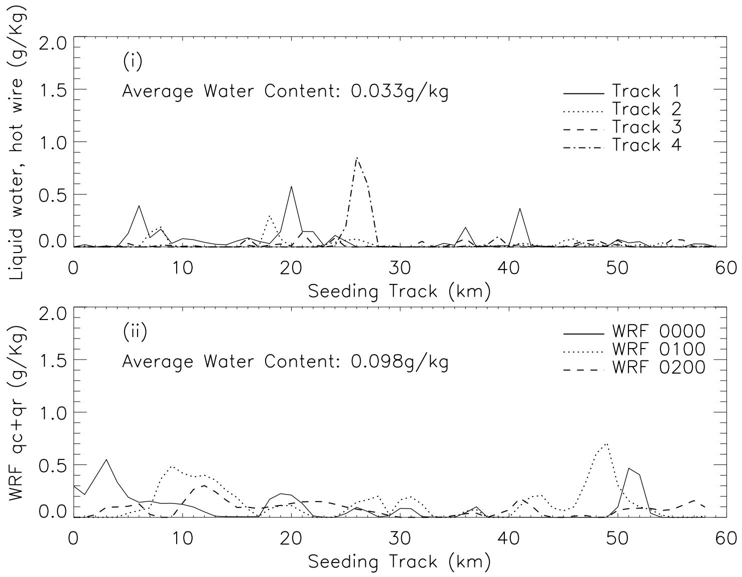

(a) (i) Aircraft, 13 second averages (approx. 1km) and (ii) WRF liquid water trace

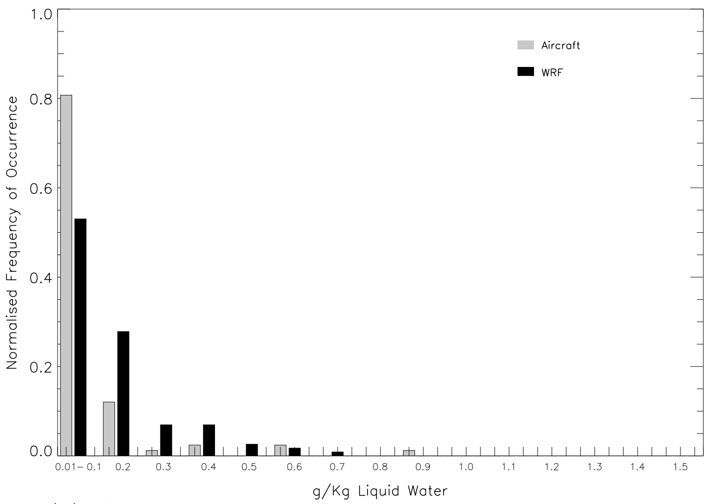

(b) Aircraft and WRF histogram showing probabilities of encountering specific quantities of liquid water

Figure 3.12: Liquid water traces and histograms from October 2007 case study. The averages shown in (a) i and ii are over the all seeding tracks. Measurements were taken at ∼3km altitude at a temperature of approx. -10°C.

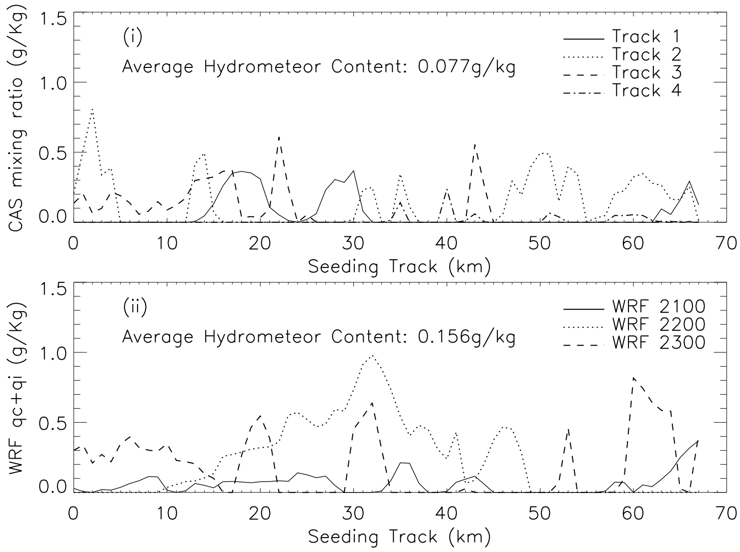

(a) (i) Aircraft, 13 second averages (approx. 1km) and (ii) WRF cloud and ice mixing ratios

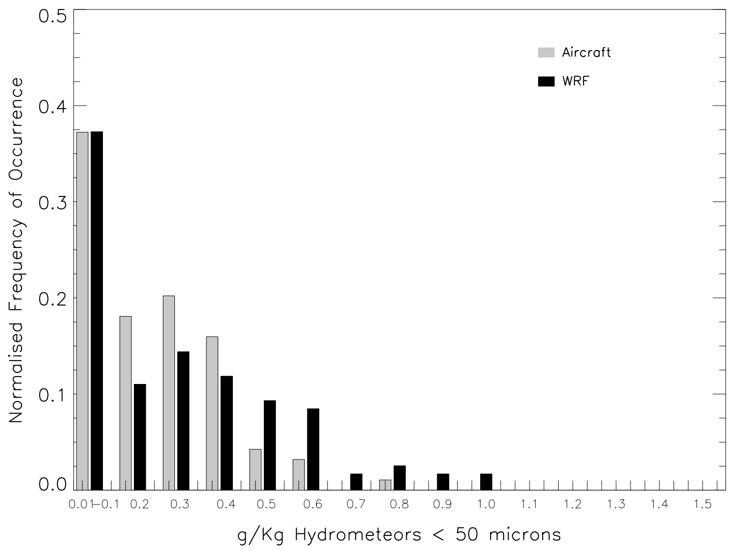

(b) Aircraft and WRF histogram showing probabilities of encountering specific quantities of hydrometeors 0.5-50μm

Figure 3.13: August 2006 case study. CAS small hydrometeor mixing ratio trace and WRF cloud ice + water mixing ratio trace together with histogram showing the relative frequency of encountering specific mixing ratios. Measurements taken in conjunction with Figure 3.11.

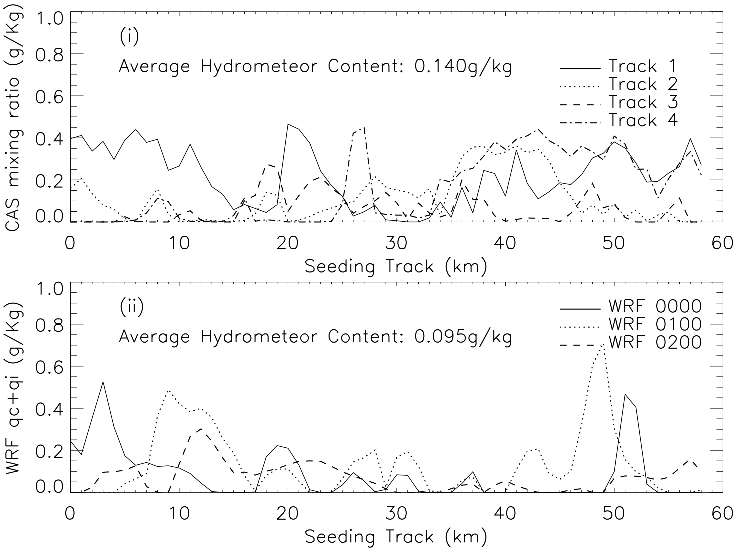

(a) (i) Aircraft, 13 second averages (approx. 1km) and (ii) WRF cloud and ice mixing ratios

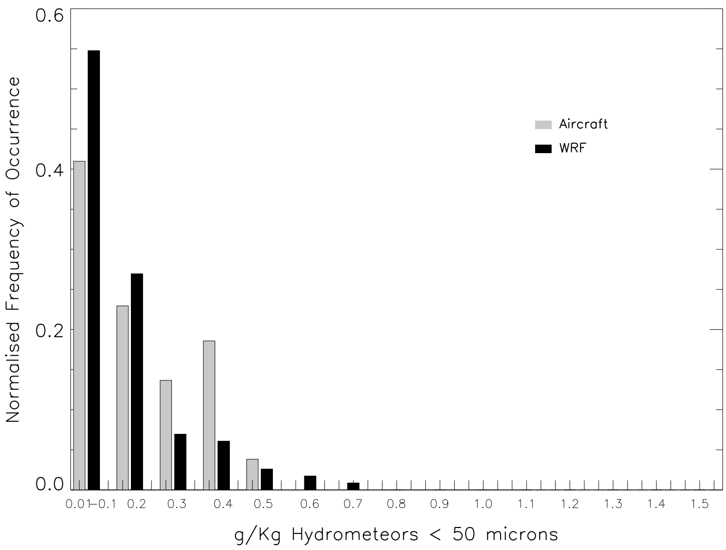

(b) Aircraft and WRF histogram showing probabilities of encountering specific quantities of hydrometeors 0.5-50μm

Figure 3.14: As in Figure 3.13 for the October 2007 case study.

correlate highly. Note: simulated SLW and small hydrometeor time-series are shown in Figures 3.11 (a,ii), 3.13 (a,ii), 3.12 (a,ii) and 3.14 (a,ii). The magnitude of the observed liquid water peaks for "lower" liquid water contents are often lower in magnitude than the CAS. Further, for "lower" magnitude liquid water peaks, the spatial extent is often greater for the CAS relative to the hot-wire. The converse is true for "large" magnitude peaks.

Histograms showing the normalised frequency of occurrence for specific SLW and small hydrometeor mixing ratios during in-cloud conditions regarding both model and observations are shown in Figures 3.11(b), 3.12(b), 3.13(b) and 3.14(b). In-cloud conditions for the observations are defined as liquid water or CAS hydrometeor mixing ratios greater than 0.01g kg^{-1}. In-cloud conditions for the model are defined as having cloud water mixing ratios greater than 0.01g kg^{-1}. The reason for choosing cloud mixing ratio over ice mixing ratio as the indicator for model cloudy conditions is that the TMP has a tendency to produce low ice mixing ratios, hydrometeors tend to move rapidly from the ice to snow category as the diameter increases, this keeps ice mixing ratios low. Using the cumulative mixing ratio of all model moist scalers (including snow and graupel) to define in-cloud conditions was also investigated. This did not noticeably change the results.

The maximum SLW mixing ratio observed during the 2006 event (Figure 3.11) using the hot-wire is $>$ 1.3g kg^{-1} (13 second time constant). Averaged over 5 minute intervals this remains $>$0.3g kg^{-1}. Approximately 55% of in-cloud conditions have SLW mixing ratios $\leq$0.3g kg^{-1} and $>$15% of in-cloud conditions have SLW $>$0.7g kg^{-1}. Regarding the CAS (Figure 3.13), maximum hydrometeor mixing ratios were 0.8g kg^{-1}, approx. half of the value recorded using the hot-wire. A potential reason for this discrepancy is that the CAS cannot detect particles $>$50μm. Regarding the 2006 case, WRF predicted distributions of SLW and small hydrometeors closely resemble the observed. The Kolmogorov-Smirnov (KS) test (Massey, 1951) was used to assess quantitatively the similarity of the distributions. The null hypothesis of the two samples being drawn from the same population could not be rejected at the 0.05 level, for both liquid and small hydrometeors.

The maximum SLW mixing ratio observed during 2007 (Figure 3.12) is ~0.9g kg^{-1}. Here >80% of in-cloud conditions have SLW <0.1g kg^{-1} and less than 10% of values are >0.2g kg^{-1}. WRF-predicted distributions of liquid hydrometeor mixing ratios replicate qualitatively the low SLW contents, however the shape of the distributions are quite different. Approximately 50% of the in cloud conditions have SLW < 0.1g kg^{-1}, hence underestimating the contribution of low liquid water content regions within individual clouds. WRF then over predicts SLW contents between 0.1-0.5g kg^{-1}. Applying the KS test to the distributions of SLW finds the two samples are not drawn from the same population. Regarding the comparison of small hydrometeors (Figure 3.14(b)), WRF over predicts the contribution of low hydrometeor content regions (<0.2g kg^{-1}) and then under predicts the contribution of higher mixing ratio regions. Here the KS test also finds the two samples to be dissimilar. To assess the sensitivity of this result to the bulk density, the lower value of 400kg m^{-3} was used. In this case the observations do not show in-cloud regions with small hydrometeor mixing ratios >0.2g kg^{-1}. This result still fails the KS test.

3.4 Evaluation Summary

Two case studies were used to evaluate cloud structure within the WRF model over the Southern Ocean and Tasmania. The first case during 2006 is characterised by large quantities of SLW and little ice. The second, during 2007 is a more mixed phase event with lower quantities of SLW and larger quantities of ice.

WRF was able to reproduce in-situ soundings with a “fair” degree of accuracy over the west coast and central Tasmania (Section 3.33.3.1). Problems with the timing of the front were highlighted, particularly with regard to the 2007 case.

Temperature inversions, absent in the observations were predicted for 2006 and WRF tended to overestimate temperature for 2007. WRF failed to reproduce a mid-level shear layer present to some degree in both events.

WRF simulated cloud top structure was compared against MODIS data and found to reproduce qualitatively cloud top structure during both cases. Regarding 2006, WRF was able to reproduce a line of convective clouds associated with a trough, but with warmer CTTs. During 2007, when a frontal cloud band was positioned over western Tasmania, WRF was able to reproduce the shape and location of this feature. Quantitatively, for 2006, WRF reproduced the overall shape of the distribution of CTTs, but missed the small number of cold clouds most likely associated with a trough line. The 2007 case was much better represented.

Model simulated radar reflectivities were qualitatively compared for 2006. WRF was able to visually reproduce the precipitation structure, reproducing cores of a few kms. Cross sections demonstrated WRF's ability to reproduce the depth of these features. In general WRF reflectivity values were between 10-20dBz lower than the observed, possibly indicating WRF's inability to capture the more detailed cloud microphysical structure.

Finally, in-situ cloud observations were used to evaluate WRF's microphysics. WRF reproduced the differences between the two events, the more mixed phase nature of 2007 vs. the supercooled environment of 2006. Histograms of in-cloud water and small hydrometeor contents showed that WRF was able to reproduce the relative frequency of high to mid and low hydrometeor content regions. 2006 was especially well represented.

Overall WRF shows some skill at reproducing cloud structure over this region of the world. As such, the following section uses the evaluated cases to investigate the mechanisms which govern cloud properties within the finest resolution domain.

Chapter 4

Numerical investigation

The aims of this Chapter are firstly, to investigate numerically the prevalence of SLW and ice over Tasmania and the ocean to the west. Secondly, to investigate the relationship between SLW, ice and CTT. Third, to evaluate the sensitivity of the model results to changes of the various parameterisations/assumptions the model utilises to represent the cloud microphysics. The final aim is to use the conclusions drawn from the model results to predict thermodynamic and in-cloud microphysical structure for two more case studies. The following sections are organised as follows: First, the model results are presented for the standard configuration (as defined in Section 3.2.1). This is followed by a summary. Section 4.3 presents results illustrating the sensitivity of the model simulations to changes in the number of cloud droplets, ice initiation parameterisation and to use of the Lin microphysics package (Lin et al., 1983). This is followed by a summary.

4.1 Evolution of Mixed Phase Clouds

This section investigates the evolution of mixed phase clouds within the context of the WRF numerical simulations. The aims are firstly, to quantitatively investigate the prevalence of SLW and ice over Tasmania and the ocean to the west, and secondly, to investigate the relationship between SLW, ice and CTT.

Figure 4.1 shows the evolution of the total cloud fraction, mean and median total frozen hydrometeor contents (TFH) and total SLW contents (TSLW), kg m^{-2}. The time series over the 42 hour simulations are taken for the finest resolution domain

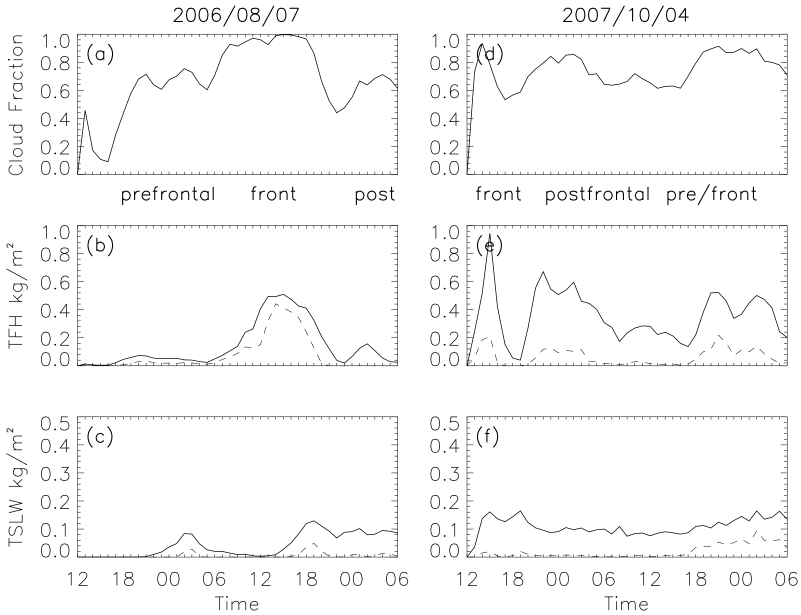

Figure 4.1: Plots showing cloud fraction, mean (solid) and median (dashed) TFH and TSLW for both case studies within the finest resolution domain. The simulation start time is indicated by the dates at the top of the plot and the first time shown on the horizontal axis (in UTC).

(Figure 3.4) which consists of 373×394 1km grids. TFH is defined as:

$$TFH(i,j) = \sum_k (q_i(k,i,j) + q_s(k,i,j) + q_g(k,i,j))\rho\Delta H, \tag{4.1}$$

and TSLW as,

$$TSLW(i,j) = \sum_{k<0^\circ C} (q_c(k,i,j) + q_r(k,i,j))\rho\Delta H. \tag{4.2}$$

Note that TFH is summed over all heights (k), whereas TSLW is summed over all $k < 0$°C. This is due to the existence of frozen hydrometeors at temperatures above freezing, supercooled water does not exist at temperatures >0°C. In Eqns. 4.1 and 4.2, i and j are the horizontal coordinates, q_c, q_r, q_i, q_s and q_g are the mixing ratios of cloud, rain, ice, snow and graupel, ρ is the fluid density and ΔH is the height between η levels. Both TFH and TSLW are defined for in-cloud regions only.

For both case studies the first 12 hours of simulation time are regarded as spin up. For 2006 the time-series of cloud fraction (Figure 4.1a) increases until 03:00 08/08/2006. This first peak is associated with a prefrontal cloud band. About 12 hours after this period (12:00 - 18:00 08/08/2006) cloud fraction (as defined in Section 3.3b) reaches its maximum value of ∼1. This is when the frontal cloud band (shown in Figure 3.2) essentially covers the innermost domain. After this, cloud fraction falls to 0.4, then rebounds to >0.6 with the arrival of the post frontal airmass. The time-series of TFH and TSLW (Figures 4.1b and 4.1c) show the microphysical composition of clouds within the domain. Associated with the prefrontal peak in cloud fraction are clouds that contain similar masses per unit area of frozen and supercooled hydrometeors (∼0.1kg m^{-2}), i.e. potentially mixed phase. Then, associated with the main body of the frontal cloud band are clouds that are composed almost entirely of frozen hydrometeors. The mean and median values of TFH are similar at this time indicating that the majority of clouds have values of ∼0.4kg m^{-2}. As the trailing edge of the frontal cloud band enters the domain (∼ 18:00 08/08/2006) TSLW content increases and TFH content decreases. The final 6 hours of the simulation are entirely postfrontal. The mean TSLW is ∼ 0.1kg m^{-2}; the mean TFH varies between 0.0-0.2kg m^{-2}. The peak at ∼ 01:00 UTC is due to the arrival of the trough, see Figures 3.1, 3.2 and 3.8 (a) and (c).

The 2007 case is shown to the right of Figure 4.1. Total cloud fraction (Figure 4.1d) shows a quite different situation to 2006. At 00:00 03/10/2007 a postfrontal airmass exists within the domain. This continues until 18:00 03/10/2007 when cloud fraction increases to a maximum of 0.9 due to the arrival of a front. Approximately 2-3 hours before the end of the simulation the front exits the domain leaving a post frontal airmass. Throughout the entire simulation cloud fraction is between 0.6-0.9. The mean and median TFH and TSLW suggest that clouds are more likely mixed phase during this case. Between 00:00-18:00 03/10/2007 the mean TSLW is >0.1kg

m^{-2} and the mean TFH is 0.2-0.6kg m^{-2}, however the medians are small, <0.2. This indicates that some clouds have large quantities of ice and/or water but the majority tend to have little quantities of both. The exception is after 18:00 03/10/2007 as the frontal cloud band enters the domain. Here the median TFH increases to 0.2 and TSLW increases to 0.05kg m^{-2}.

Figure 4.1 suggests that the frontal cloud bands for both cases consist of mixed phase clouds with median values of TSLW and TFH of ∼0.1 and 0.2-0.4kg m^{-2}, respectively. Further, when taken over the entire inner domain mixed phase conditions are also indicated to occur during pre/post frontal periods, however, with smaller quantities of liquid and frozen hydrometeors.

Figure 4.2 shows cross sections of total liquid hydrometeor mixing ratio ($q_c + q_r$) and total frozen hydrometeor mixing ratio ($q_i + q_g + q_s$) from domain 4 along 42S for both case studies (2006 and 2007). The figure suggests that during pre/post frontal periods, clouds over the Southern Ocean and Tasmania are capped to heights < 6km, consistent with Mace et al. (2007). Figure 4.2a shows the frontal passage for the 2006 case with a relatively high freezing layer and large amounts of glaciated upper level cloud (frozen hydrometeors (FH) >0.5g/kg). To the west of this feature are lower level mixed phase clouds with smaller quantities of FH (0.05-0.5g/kg) and SLW contents of 1g/kg. Figure 4.2b is during post frontal conditions ahead of the trough and shows relatively little ice, large quantities of SLW (∼ 1.5g/kg) and a low freezing level (∼1km). Figures 4.2c and 4.2d show the 2007 case with moderate quantities of SLW (0.5g/kg) and ice (0.5g/kg), during post-frontal and frontal conditions, respectively. At the times shown for the 2007 case the cross sections imply that mixed phase clouds exist.

A further interesting feature regarding Figure 4.2 is the relative heights of the inversion layer (indicated by the cloud top heights) and the height of the freezing level. During pre and post frontal periods the October 07 case appears to have a

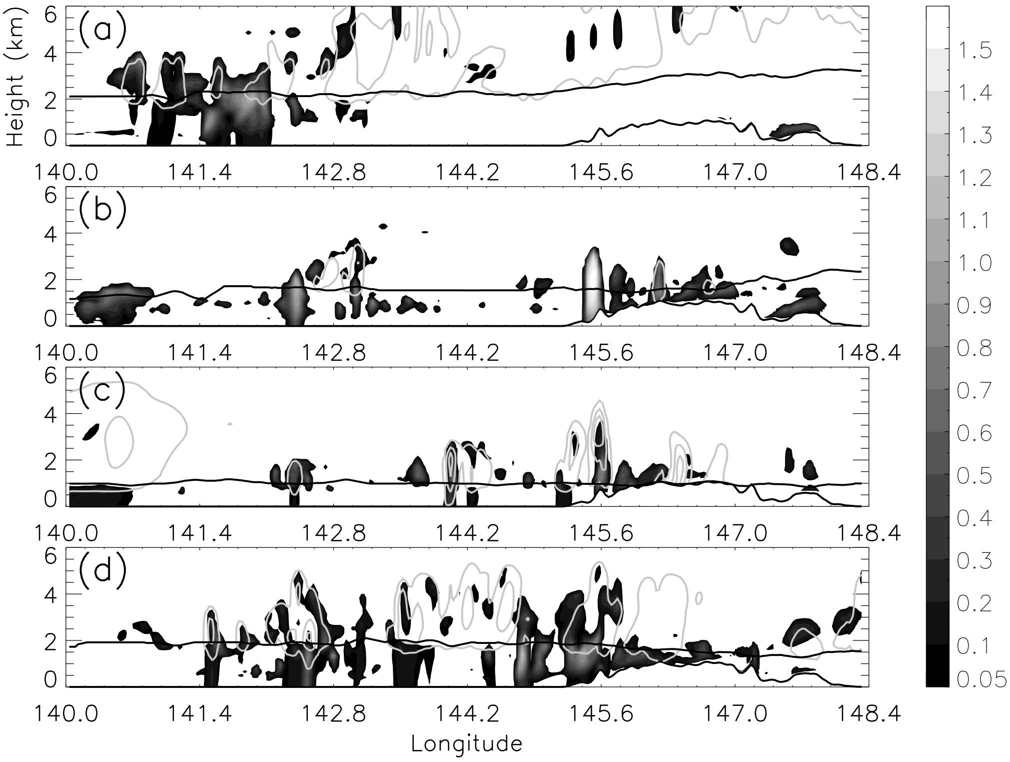

Figure 4.2: Cross sections across 42S for domain 4 showing the Southern Ocean (140-145E) and Tasmania (145-148E). Filled contours show liquid hydrometeors ($q_c + q_r$), grey contours show frozen hydrometeors ($q_i + q_s + q_g$) the first contour is 0.05g/kg larger contours are in steps of 0.5g/kg. The solid black line indicates the height of the freezing layer. (a) 15:00 08/08/2006 UTC frontal, (b) 23:00 08/08/2006 postfrontal, (c) 15:00 03/10/2007 prefrontal and (d) 01:00 04/10/2007, postfrontal.

higher inversion and a lower freezing level, relatively speaking.

Instead of looking at domain wide variables, Figures 4.3 and 4.4 (a) and (c) show time evolution histograms of the ratio of TSLW to TSLW + TFH over land and ocean respectively. The time-series has been separated into components over land and ocean to isolate any orographic effect the island of Tasmania has on cloud structure. Hereafter this ratio is referred to as the ratio of TSLW to all "cold" hydrometeors or RSACH, and is defined as:

$$RSACH(i,j) = \frac{TSLW(i,j)}{TSLW(i,j) + TFH(i,j)}. \tag{4.3}$$

Using the above definition for RSACH, supercooled clouds are defined as having a RSACH >0.7, mixed phase 0.3-0.7 and glaciated clouds <0.3. Figures 4.3 and 4.4 (b) and (d) show the mean and median magnitude of TSLW and TFH over land and water respectively.

The above definition of a mixed phase cloud is unique to this study. Authors such as Spangenberg et al. (2006) have defined mixed phase clouds in a similar way including clouds that are composed of between 10-90% liquid water compared to ice content. Mixed phase clouds over Tasmania however, are quite different to the majority over the Arctic which can exhibit liquid water at cloud top and progressively more ice as cloud base is approached. Another distinct type of Arctic mixed phase cloud which is far less common than the former has a glaciated top and extends from the boundary layer to the mid-troposphere. This type more closely resembles clouds over the Southern Ocean west of Tasmania and over the island itself. This is demonstrated in Figure 4.2 which shows clouds extending from the surface up to <6km in altitude, composed of both frozen and liquid hydrometeors near the freezing layer.

Regarding the 2006 case, Figures 4.3a and 4.3c show that for the majority of the simulation the probability of finding a RSACH close to zero for any grid point is high. This indicates that for the majority of the time either no SLW exists or the mass of SLW is small compared to the mass of frozen hydrometeors. The exceptions to this statement are between 00:00-06:00, 08/08/2006 and 18:00 08/08/2006 until the end of the simulation. The first period coincides with the arrival of prefrontal cloud. Here approximately 40% of grid points have a RSACH >0.8 (i.e. 40% of the grid points contain four times as much TSLW as TFH) and approx. 12% of grid points have a RSACH of 0.5 i.e. mixed phase. Also observed at this time is an increase in the magnitude of the mean and median quantity of TSLW. After this period the frontal cloud arrives $\sim$ 12:00 08/08/2006. During this period the mean

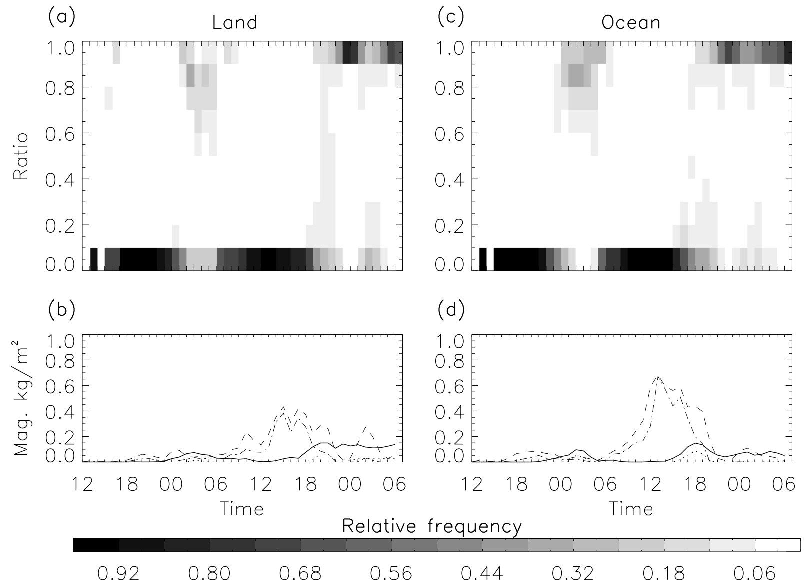

Figure 4.3: Evolution of SLW over land (a) and (b), and Ocean (c) and (d) for the finest resolution domain only during the August 2006 event. Horizontal axis is hours since 12:00 07/08/2006 UTC. Specifically, plots (a) and (c) are histograms showing the time evolution of the ratio of TSLW to sum of TSLW + total frozen hydrometeors (RSACH) for incloud regions only. SLW is integrated from the freezing layer to the top of the model, frozen hydrometeors are integrated throughout the entire model depth, both variables have units kg m^{-2}. In cloud regions are defined as having total liquid/solid hydrometeor contents > 0.05kg m^{-2}. Plots (b) and (d) show the evolution of the mean (solid) and median (dot) TSLW with mean (dash) and median (dash dot) TFH content over land and ocean respectively.

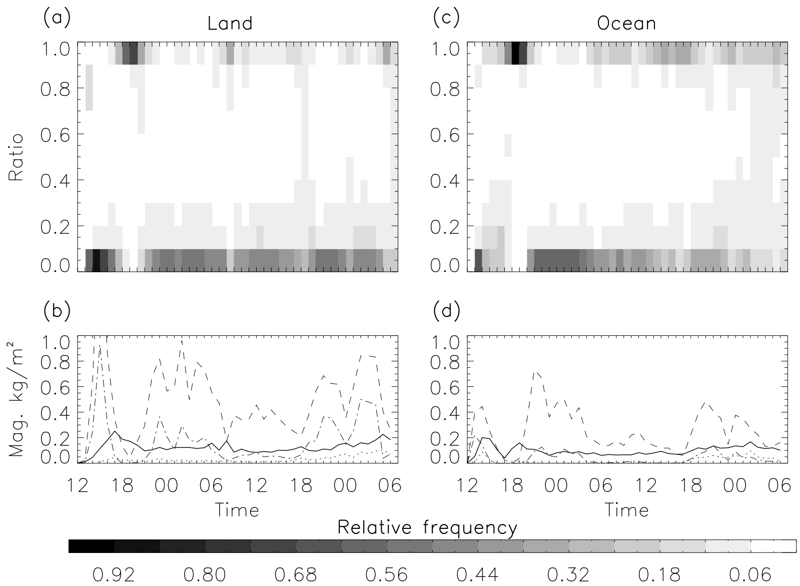

Figure 4.4: As in Figure 4.3, starting 12:00 02/10/2007.

and median magnitude of TFH increases to a maximum, over both land and ocean and the fraction of mixed phase clouds increases once again.

An interesting feature at this time is the discrepancy between the TFH over land vs. ocean. Over ocean the peak TFH increases to $\sim$0.6kg m^{-2}, over land the peak value is 0.4kg m^{-2}. After the frontal cloud leaves the domain ($\sim$ 00:00 09/08/2006) the mean and median magnitude of SLW decreases slightly over land and drops by one-half over ocean. At this time the probability of a cloud having a high RSACH increases. Over both land and ocean from 03:00 09/08/2006 until the end of the simulation over 50% of cloudy grids in the domain are composed almost entirely of SLW. Previously mentioned regarding Figure 4.1b was the peak in TFH at $\sim$ 01:00 UTC 09/08/06, due to the arrival of the trough indicated in Figures 3.1, 3.2 and 3.8 (a) and (c). This feature is also present here. Figures 4.3a and 4.3c show that the trough arrives over ocean before land and is composed of clouds which contain a greater quantity of ice relative to clouds that exist earlier and later.

The 2007 event (Figure 4.4) shows the passage of a front within the first 6 hours of the simulation, during spin up. The second front occurs between 18:00 03/10/07 and 00:00 04/10/2007, TSLW and TFH peak during this time. Throughout the majority of the simulation the probability of a cloud having a high RSACH is low. The highest chance of finding an entirely supercooled cloud is between 12:00-18:00 03/10/2007, Figure 4.4c. >30% of grid points within the domain are composed entirely of SLW. This is the prefrontal time period. The mean and median magnitudes of SLW are generally larger during this case and, in line with the previous case, always have greater magnitudes over land. Mixed phase clouds are predicted by the model in the prefrontal period at 18:00 03/10/2007 over land and in the frontal/postfrontal period between 00:00 04/10/2007 and the end of the simulation over land and water. At this time clouds over ocean tend to favour more mixed phase conditions with lower magnitudes of TFH and TSLW. Over land, clouds favour more glaciated conditions and contain larger magnitudes of both TFH and TSLW.

Regarding both case studies WRF suggests that the probability of finding a mixed phase cloud is much lower than the probability of an entirely glaciated or supercooled cloud. That said, for 2007, throughout the majority of the postfrontal period approximately 12% of grid points have a RSACH of between 0.2-0.3. Cloud grids over land tend to favour more glaciated conditions with greater magnitudes of TSLW and TFH. This difference is not necessarily due to orographic effects, it could be the result of some synoptic forcing like the blocking pattern suggested by Pook et al. (2006).

Figure 4.5 shows time evolution histograms of CTT for both cases (2006 and 2007). The 2006 case (Figure 4.5a and 4.5b) shows that between 00:00-06:00 08/08/2006, >50% (90%) of grid points have CTTs between -10 and -5°C over land (ocean). This corresponds with the initial increase in both the RSACH and TSLW content of Figure 4.3. Between 06:00-12:00 08/08/2006, high cold cloud associated with the frontal cloud band dominates the domain. This cold cloud gradually

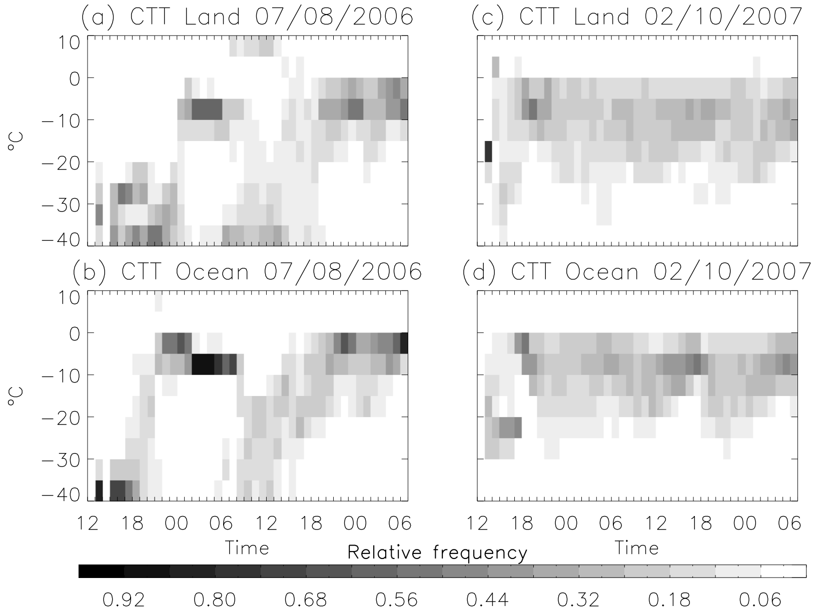

Figure 4.5: Histograms of cloud-top temperature for August 2006 (a and b) and October 2007 (c and d) case studies. Plots (a) and (c) show CTT over land, (b) and (d) over Ocean.

moves to the east leaving the post frontal airmass with relatively warm cloud top temperatures. Here over 80% of grid points have CTTs between −10 and 0°C over land and ocean. Interestingly, clouds over the ocean show a clear preference for warmer tops (lower altitudes). Once again, the trough line that advects into the domain ∼01:00 09/08/06 is present here, demonstrated by the increase in cooler CTTs.

The 2007 event, Figures 4.5c and 4.5d, shows a more homogeneous situation. Little difference in the distributions over land and water is observed. After spin up, the majority of cloud tops have temperatures between -5 and -20 °C throughout much of the simulation. A small increase in cold clouds is observed after 18:00 03/10/2007, associated with the second frontal cloud that advects into the domain. CTTs for this case are cooler and show greater variation. The exception to this statement is between 12:00 and 18:00 03/08/2007 (prefrontal) where over 40% of clouds over the ocean are between −10 and −5°C. This corresponds with a larger

RSACH in Figure 4.4 (c).

The results presented thus far suggest a relationship between CTT and mixed phase conditions. Cloud fields with tops between 0 and -10°C tend to contain predominantly SLW. This is demonstrated in both case studies. Cloud fields with a wider distribution of CTTs including cooler cloud tops tend to be more glaciated, but often contain larger TSLW and TFH contents.

4.2 Summary: Evolution of Mixed Phase Clouds

According to the WRF simulations supercooled liquid water (SLW) exists in pre-frontal, frontal and post frontal airmasses over the Southern Ocean and Tasmania. Simulated cloud top heights are consistent with Mace et al. (2007). Absolute quantities peak within frontal cloud bands, however the proportion of predominantly supercooled clouds is low; conversely the proportion of mixed phase and mostly glaciated clouds is high. During pre/post frontal periods SLW is present mostly in the absence of ice. The probability of a cloud having an equal mass of SLW and frozen hydrometeors (mixed phase) is low for all time, except within frontal cloud structures i.e. the model has a tendency to produce either supercooled or glaciated clouds, mixed phase clouds are rare.

There appears to be a relationship between the microphysical properties of a cloud, cloud top structure and vertical thermodynamic structure. Pre and post-frontal airmasses are found to contain low moisture/temperature inversions just above the freezing layer and convectively unstable boundary layers as shown in Figures 3.5 and 3.6. Clouds developing in the unstable air are unable to penetrate the inversions, hence have narrow distributions of CTTs which are close to the freezing level. These contain supercooled water and little ice.

Regarding 2006, during the pre and postfrontal airmasses the majority of clouds have tops between 0 and -10°C due to strong moisture and temperature inversions in the model. The current method by which ice is initiatied in the Thompson routine uses the Cooper parameterisation (Thompson et al., 2007; Cooper and Lawson, 1984) and in general does not begin to move mass from the liquid to ice categories until temperatures are below -8°C, or the supersaturation w.r.t. ice is greater than 8%. During the prefrontal regime, supersaturations w.r.t. ice exceeded 8% at temperatures warmer than -8°C in approx. 3% of cloudy grids. Throughout the rest of the simulation generally less than 1% of cloudy grids met this criterion. Model simulated clouds for this case study will always show large quantities of SLW and this finding should be relatively insensitive to changes in ice initiation parameterisation, so long as ice does not initiate until cooler than -8°C. Essentially, the model cannot transfer mass from the liquid to the frozen categories until ice is initiated.

For the 2007 case, the inversion height is greater. The majority of clouds are able to obtain altitudes where temperatures are between -10 and -15°C. Further, a larger fraction of cloudy grids obtained supersaturations w.r.t. ice >8% at temperatures warmer than -8°C, approx. 3% throughout much of the simulation, with a maximum of ∼4%. These clouds spend a greater fraction of time transferring mass from the liquid categories to the frozen. This case study should be more sensitive to the ice initiation parameterisation. If ice is initiated at a slower rate then a greater fraction of clouds will contain more supercooled water, should the rate of ice initiation increase the converse is true.

The results presented herein indicate that supercooled and mixed phase clouds exist over Tasmania and the ocean to the west. The results indicate a correlation between atmospheric states possessing convectively unstable boundary layers and inversion heights close to the freezing level with supercooled cloud fields. The magnitude of supercooled water presented in Chapter 3 and simulated herein is consistent with earlier measurements presented in Ryan and King (1997). The observed and simulated cloud microphysical structure is consitent with earlier studies over this region e.g. Mossop et al. (1970). This research provides a physical basis for the long-term success of cloud seeding over this region, as detailed in Chapter 2.

4.3 Model Results: Sensitivity to Changes in CCN, Ice Initiation Parameterisation and Microphysics Routine

The aim of this section is to evaluate the sensitivity of the in-cloud microphysical structure to changes in the number of cloud droplets (a proxy for CCN), the ice initiation parameterisation and the Lin microphysics package (Lin et al., 1983). Initially, the simulations are compared with observations in a manner similar to that detailed in Section 3.3, to evaluate which of the various configurations best represents the observed in-cloud fields. Only results pertaining to the finest resolution domain are presented (domain 5, dx = 1km and dt = 4s, 373×394 grid points). After this the sensitivity analysis focuses on the changes to the broad scale structure as investigated in Section 4.1, demonstrating how the various changes effect the evolution of the cloud fields.

The sensitivity is investigated using five numerical experiments, these are compared with the standard configuration. Four of the experiments use the Thompson microphysics package (Thompson et al., 2007), of these two have the number of cloud droplets changed, these are referred to as experiments Nc=30 and Nc=150 (the standard configuration has Nc=75, where Nc stands for No. cloud drops). The other two have alternate parameterisations for ice initiation, these are referred to as Meyers (Meyers et al., 1997) and Fletcher (Fletcher, 1962) numerical experiments. The standard configuration has ice initiation as described in Cooper (1986). The three ice initiation parameterisations are depicted in Figure 4.6 and are described by the relationships:

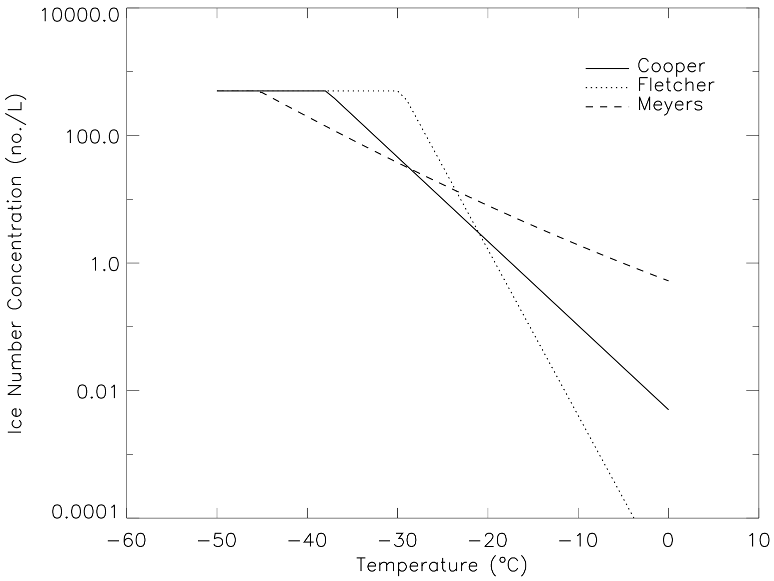

Figure 4.6: Ice nucleation by deposition and condensation freezing. Three parameterisations are shown by Cooper, Fletcher and Meyers. Note: maximum number is set to 500/L, ice does not form until temperatures are below -8°C, or the supersaturation w.r.t. ice >8%. The curve representing the Meyers parameterisation assumes the maximum possible ice supersaturation i.e. water saturation.

$$N_{Cooper} = 0.005exp(0.304(T_0 - T)), \tag{4.4}$$

$$N_{Fletcher} = 10^{-5}exp(0.6(T_0 - T)), \tag{4.5}$$

$$N_{Meyers} = exp(-0.639 + 0.1296S_i). \tag{4.6}$$

Where S_i is the supersaturation w.r.t. ice, T_0 is 273.15 and T is temperature in Kelvin. N is the number of ice crystals initiated (l^{-1}), this is prohibited from reaching erroneously high values at cooler temperatures, the maximum number is $500L^{-1}$ for all parameterisations. Ice forms by the above relationships when the temperature is below -8°C, or the supersaturation w.r.t. ice >8%.

Equations 4.4, 4.5 and 4.6 dictate the number (and mixing ratio) of ice crystals generated for the next model time step. All ice particles are initiated with a diameter of 11μm (10E^{-12} kg), they are assumed to be spherical and have a density of 890kg m^{-3}. This mass is then removed from the cloud mixing ratio. Changing the number of cloud drops changes the shape of the assumed cloud particle size distribution:

$$N(D) = \frac{N_t}{\Gamma(\mu+1)}\lambda^{\mu+1}D^{\mu}e^{-\lambda D}, \tag{4.7}$$

where $N(D)$ is the number of cloud particles of diameter D, Γ is a gamma function, λ is variable and depends on the cloud water mixing ratio q_c and μ, where:

$$\mu = min(15, \frac{10^9}{N_c} + 2). \tag{4.8}$$

Here N_c is the number of cloud particles that are initiated upon saturation. Increasing the value of N_c increases the number of smaller cloud particles and vice versa when the N_c is decreased.

The final numerical experiment was to use the Lin microphysics routine to describe in-cloud processes (Lin et al., 1983). This scheme differs considerably from the Thompson routine having been developed over 20 years earlier and was chosen as a comparison experiment due to its simplicity (and nostalgia, one of the main purposes of this schemes development was for the simulation of cloud seeding experiments). Notable differences include the absence of a prognostic variable for the number concentration of ice particles. Precipitating particles are represented with exponential size distributions with fixed y-intercept parameters (note: cloud water and ice are not assumed to precipitate). This is in contrast to the Thompson routines generalised gamma distribution for all hydrometeors with variable y-intercept parameters.

4.3.1 Sensitivity of In-cloud Conditions

Within this section the differences between the various model runs and in-situ observations collected by the aircraft within the cloud field are evaluated. Table 4.1

uses the Kolmogorov-Smirnov (KS) test (Massey, 1951) to compare the various sensitivity experiments with the observations. Figures 4.7 and 4.8 are histograms of in-cloud supercooled liquid water and small hydrometeor contents (as defined in Chapter 3), for both the 2006 and 2007 cases, respectively. The method used to create these histograms is detailed in Section 3.3.4.

Table 4.1: Comparison of the observed and simulated in-cloud mixing ratio fields for the various numerical experiments. The Kolmogorov-Smirnov test is used for the comparison. The null hypothesis is that the samples are drawn from the same population, 0 indicates that the null hypothesis cannot be rejected at the 0.05 level. The model variables that are compared with the hot-wire probe are q_c and q_r, with the CAS, q_c and q_i, as detailed in Section 3.3.4. The columns titled CAS use a density of 1000kg m^{-3} for objects viewed by the CAS.

	August 2006		October 2007		
	Hot-wire	CAS	Hot-wire	CAS	CAS (400kg m^{-3})
Stand. Conf.	0	0	1	1	1
Nc = 150	1	0	1	1	1
Nc = 30	0	0	0	1	0
Meyers	1	0	1	1	1
Fletcher	1	0	1	1	1
Lin	0	0	1	0	1

The results presented in Table 4.1 show that the numerical experiment Nc=30 most accurately reproduces the in-situ aircraft data. This experiment produces distributions of supercooled water and small hydrometeor contents which according the KS test have a high chance of belonging to the same distributions as the observations. This is true for both case studies. No other numerical experiment compares so well, consistently across case studies. Note: for the 2007 case, when objects viewed by the CAS are assumed to have a density of 1000kg m^{-3}, the null hypothesis that the model and observed in-cloud small hydrometeor mixing ratio distributions come from the same population is rejected. The only other numerical experiment that shows some similarity with observations for the 2007 case is the Lin experiment. Here, the null hypothesis is not rejected if objects viewed by the CAS have a density of 1000kg m^{-3}. This result contradicts the Nc=30 experiment, however the distribution of liquid hydrometeors does not compare well with observations. These results are explored further in the following paragraphs.

Histograms showing the distribution of in-cloud SLW and small hydrometeors for the 2006 case are shown in Figure 4.7. The shape of the simulated distributions closely resemble the observed. The upper-bound for the observed SLW mixing ratio is $\sim$1.5gkg^{-1} and for small hydrometeors $\sim$0.8gkg^{-1}. All simulations that utilise the Thompson microphysics reproduce these values well. The Lin routine does not create in-cloud regions with SLW above 0.9gkg^{-1}. This is the same for small hydrometeor contents and is due to cloud water (q_c) being the dominant term, rain (q_r) and ice (q_i) mixing ratios do not contain sufficient mass to contribute to the shape of these distributions. The other numerical experiments reproduce well the upper-bound of SLW content ($\sim$1.5gkg^{-1}), this is due to mass existing within the rain mixing ratio.

Histograms showing the distribution of in-cloud SLW and small hydrometeors for the 2007 case are shown in Figure 4.8. For this case study a density of 400kg m^{-3} is used for small hydrometeors viewed by the CAS, in-line with more mixed phase/glaciated conditions. All model configurations tend to over predict both SLW and small hydrometeor content regions over 0.2g/kg. Broadly speaking, the traces can be split into 3 groups. 1) The observations, 2) the model results produced with the Thompson microphysics routine and 3) the Lin microphysics. This grouping is not observed for the 2006 case. Results pertaining to the Lin routine show the greatest difference from the observations. As before little (i.e. no) difference is observed between the SLW and small hydrometeor histograms. Interestingly, the observations show $\sim$2% of in-cloud liquid water contents between 0.8-0.9gkg^{-1}. No model configuration replicates this, however the Nc=30 experiment shows $\sim$2% of in-cloud liquid water contents between 0.7-0.8gkg^{-1}, thus adding further evidence in support of this numerical experiment best reproducing the aircraft observations.

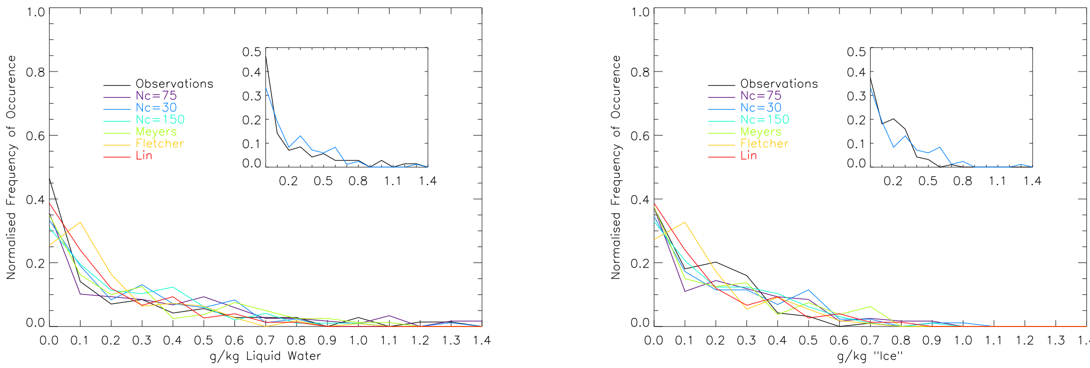

Figure 4.7: Histograms showing distributions of in-cloud supercooled liquid water and small hydrometeor contents for the 2006 case. Measurements were taken at $\sim$ 2.5km altitude at temperatures between -8 and -18°C. Observation hydrometeor content assumes particles observed by the CAS probe have an average density of 1000kg m^{-3}. The smaller plots show the observations and the numerical experiment Nc=30, this was found to most accurately reproduce the observations (Table 4.1). The first bin is 0.01-0.1g/kg, the remaining bins are 0.1g/kg in width with the smaller value shown.

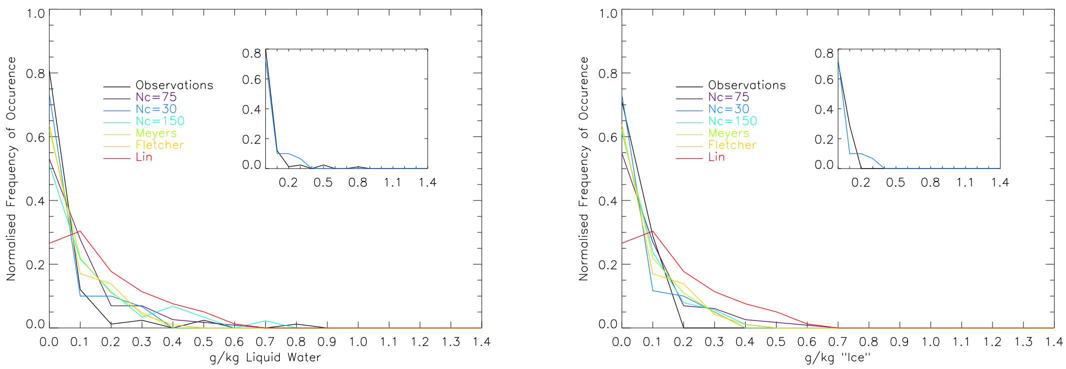

Figure 4.8: Histograms showing distributions of in-cloud supercooled liquid water and small hydrometeor contents for the October 2007 case. Measurements were taken at $\sim$3km altitude at a temperature of approx. -10°C. Observation hydrometeor content assumes particles observed by the CAS probe have an average density of 400kg m^{-3}. The smaller plots show the observations and the numerical experiment Nc=30, this was found to most accurately reproduce the observations (Table 4.1). The first bin is 0.01-0.1g/kg, the remaining bins are 0.1g/kg in width with the smaller value shown.

4.3.2 Broad Scale Cloud Evolution Sensitivity

The sensitivity of the broad scale cloud evolution is evaluated here. Histograms showing the time evolution of cloud-top temperature over the whole domain are presented for both case studies and each numerical experiment in Figures 4.9 and 4.10. In section 4.2 it was concluded that vertical thermodynamic structure was mostly responsible for governing CTT, as such cloud microphysical parameterisations should play a minor role in governing the evolution of this variable. Note that in Section 4.2 the cloud field was split in two using a land mask, for this analysis the histograms represent cloud structure over the whole domain.

Regarding the 2006 case (Figure 4.9), little difference is observed in the evolution of CTTs between the various versions of the Thompson microphysics (Nc=30, 150, Fletcher and Meyers). All show prefrontal, relatively warm clouds between 0 and -10°C with narrow distributions of CTTs. All then make smooth transitions between this regime and the frontal regime at $\sim$ 06:00 08/08/2006. The experiment which shows the most difference at this time, regarding only those that incorporate the Thompson microphysics routine is the Meyers ice initiation parameterisation. At this time a larger fraction of warm clouds are simulated (i.e. at temperatures above 0°C) with fewer colder clouds. Approx. 10% of clouds reach temperatures between -35 and -40°C and only for a short period. All other versions of the Thompson routine show a larger fraction of clouds occupying this temperature band for a longer period of time. Interestingly, the Meyers ice initiation parameterisation produces the lowest number of ice crystals between -30 and -40°C (Figure 4.6). All of the Thompson experiments then go on to develop cooler clouds associated with the postfrontal trough at $\sim$02:00 09/08/2006.

The Lin microphysics routine shows the greatest difference with respect to all other numerical experiments for the 2006 case. As before, a narrow distribution of relatively warm cloud-tops develop in the prefrontal airmass, however unlike the other experiments this regime jumps to the frontal regime. cloud-tops do not gradually move to cooler temperatures but transition quickly missing out the medium range altogether (i.e. cloud-tops between -10 and -30°C). Between 12:00-18:00 08/08/2006 there is a smooth transition to the relatively warmer cloud-tops of the postfrontal regime, similar to the other experiments. The cooler clouds associated with the postfrontal trough line however do not develop in this simulation.

Figure 4.10 shows the time evolution of CTTs for 2007. Interestingly, it was stated in Section 4.2 that this case should be more sensitive to cloud microphysical parameterisations (relative to the 2006 event), in particular the rate of ice initiation. The results indicate that this is not the case, similar to results found in Thompson et al. (2004). In general, all numerical experiments show the majority of cloud-tops at temperatures between -5 and -15°C throughout the entire simulation (excluding spin up, the first 12 hours). Lin shows a slight increase in cooler cloud-tops during the initial postfrontal regime, between 00:00-06:00 03/10/2007 relative to the other experiments. All experiments show an increase in warmer cloud-tops (-5 to -10°C) during the prefrontal regime between 12:00-18:00 03/10/2007.

The relative insensitivity of CTT to the various changes in parameterising the cloud microphysical interactions further supports the conclusion that vertical thermodynamic structure plays the leading role in dictating the evolution of this field. To investigate the sensitivity of in-cloud microphysical structure, the evolution of the ratio of supercooled to all cold hydrometeors (RSACH) is presented.

Histograms showing the time-evolution of the RSACH for 2006 are shown in Figure 4.11. Unlike Section 4.1, these have not been split into land and ocean components but represent the entire domain (for domain 5). It is observed that there is little difference between the standard configuration and the various changes made to the Thompson microphysics, further, the Lin microphysics shows remarkably similar results. All experiments show supercooled/mixed phase conditions in

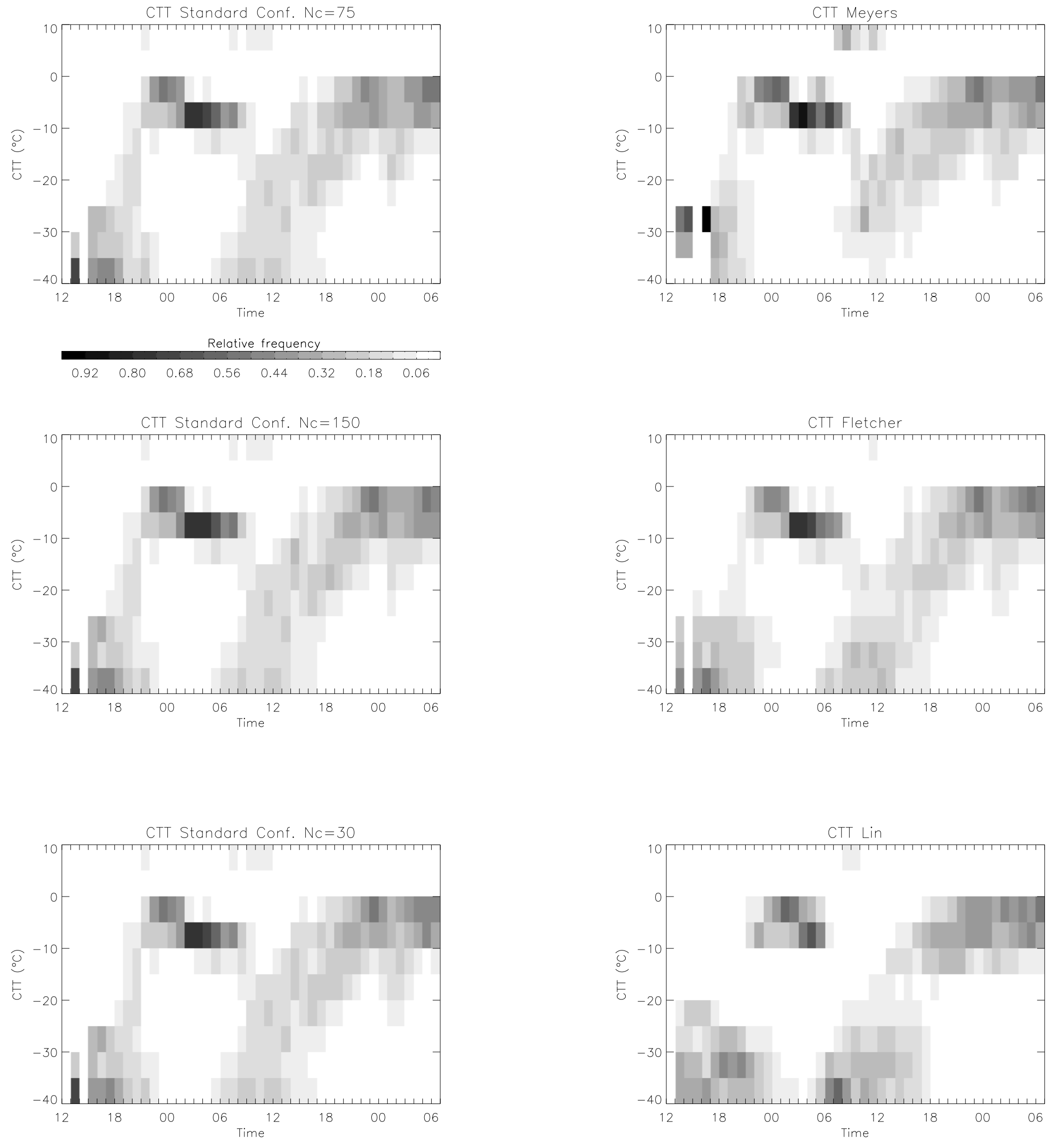

Figure 4.9: cloud-top temperature time evolution histograms for sim. starting 07/08/2006. Top left - standard configuration Nc=75, top right - Meyers, center left - standard configuration Nc=150, center right - Fletcher, bottom left - standard configuration Nc=30 and bottom right - Lin.

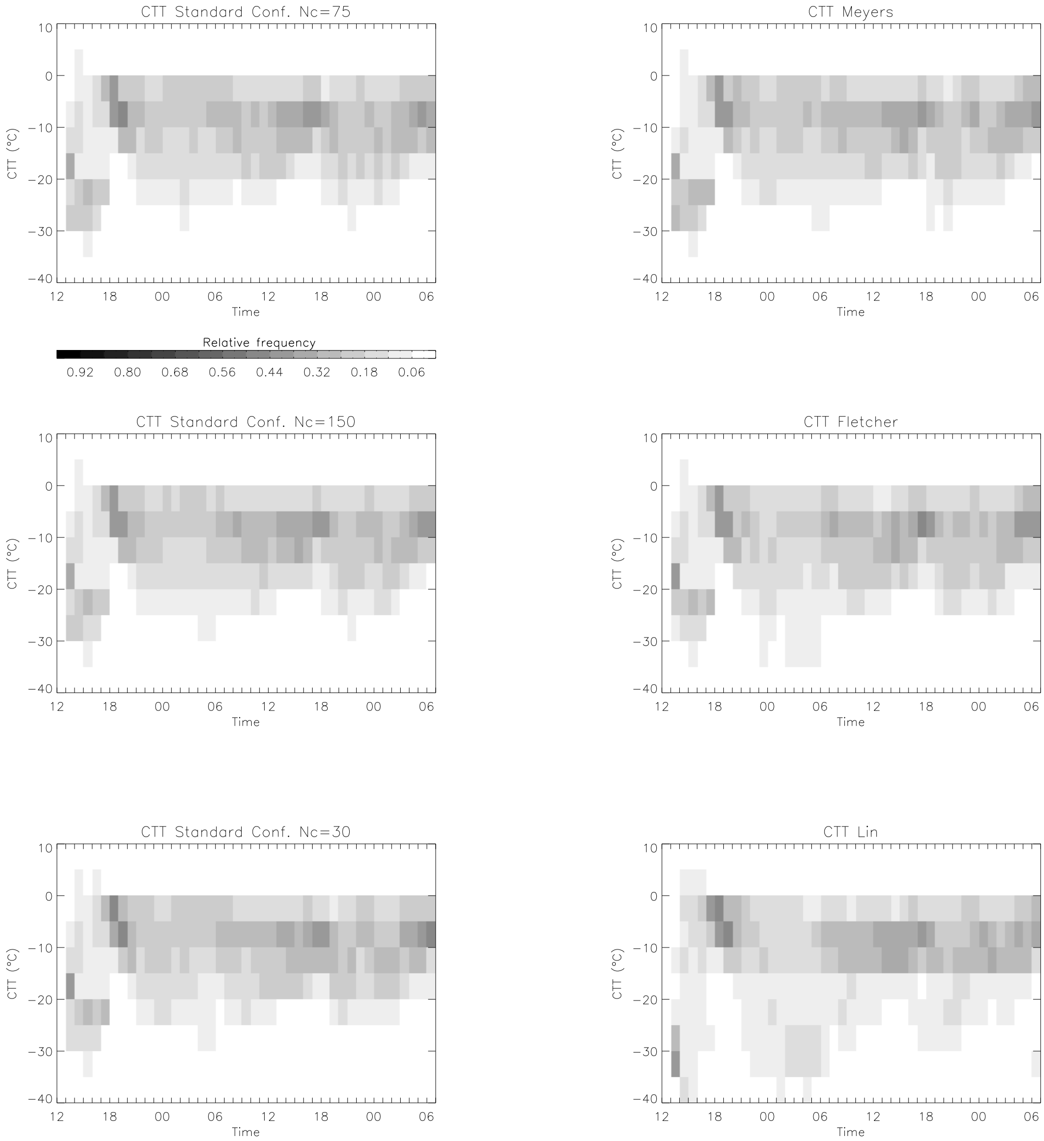

Figure 4.10: CTT time evolution histograms for sim. starting 02/10/2007. Top left - standard configuration Nc=75, top right - Meyers, center left - standard configuration Nc=150, center right - Fletcher, bottom left - standard configuration Nc=30 and bottom right - Lin.

the prefrontal period (00:00-06:00 08/08/2006) and the same again during the post frontal period (∼00:00 09/08/2006 until the end of the simulation). Minor differences are apparent regarding the Lin microphysics, i.e. a slight bias in favour of producing more glaciated clouds, or conversely, few totally supercooled grid points. A notable feature present regarding the Meyers ice initiation parameterisation is the rapid change from supercooled to glaciated conditions as the regime changes from prefrontal to frontal at 06:00 08/08/2006. This is thought to be due to the Meyers parameterisation having the highest rate of ice production at warmer temperatures.

Histograms showing the time-evolution of the RSACH for 2007 are shown in Figure 4.12. Once again the most striking feature between the plots is the similarity between all experiments incorporating the Thompson microphysics, implying the relative insensitivity of the simulations to changes in number concentration of cloud particles or the rate of initiation of ice. The Lin microphysics shows the greatest difference. Throughout the majority of the simulation clouds exist with the full spectrum of RSACH values, indicating the presence of glaciated, mixed phase and supercooled clouds. This is in contrast to various modifications to the Thompson microphysics where few mixed phase clouds exist.

Further results regarding the broad scale sensitivity analysis are presented in Appendix B. Included are thermodynamic profiles, planar view simulated cloud-top temperature plots and cross sections along 42S for domain 4.

4.4 Summary: Sensitivity Analysis

The sensitivity of the simulated cloud fields to changes in the number of cloud droplets (a proxy for CCN), the ice initiation parameterisation and the Lin microphysics is evaluated, within the context of the case studies presented in Chapter 3. The simulations are evaluated within the finest resolution domain with six numerical experiments forming the basis of the evaluation. The first is referred to as the

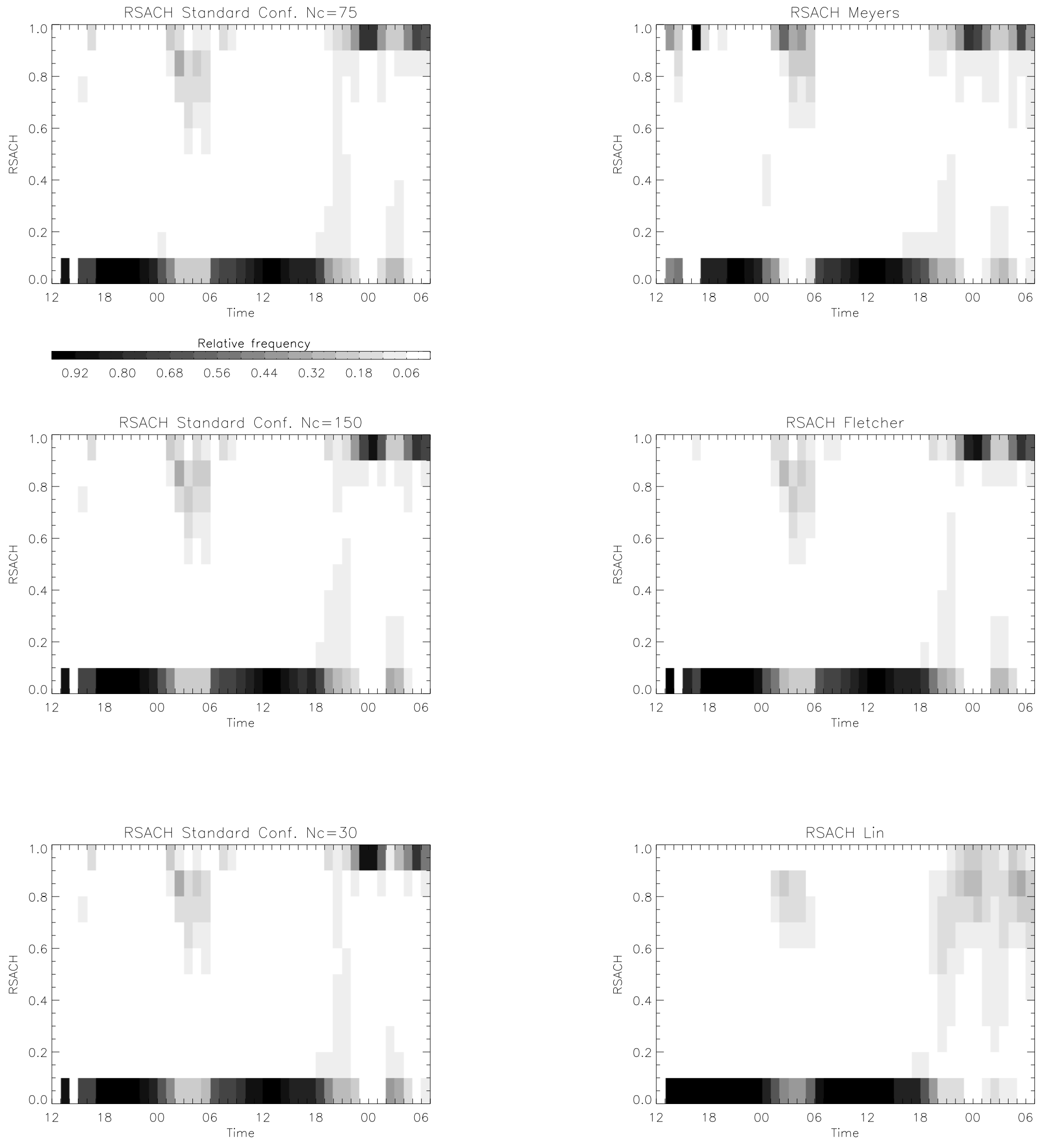

Figure 4.11: Ratio of TSLW to TSLW+TFH evolution histograms for sim. starting 07/08/2006. Top left - standard configuration Nc=75, top right - Meyers, center left - standard configuration Nc=150, center right - Fletcher, bottom left - standard configuration Nc=30 and bottom right - Lin.

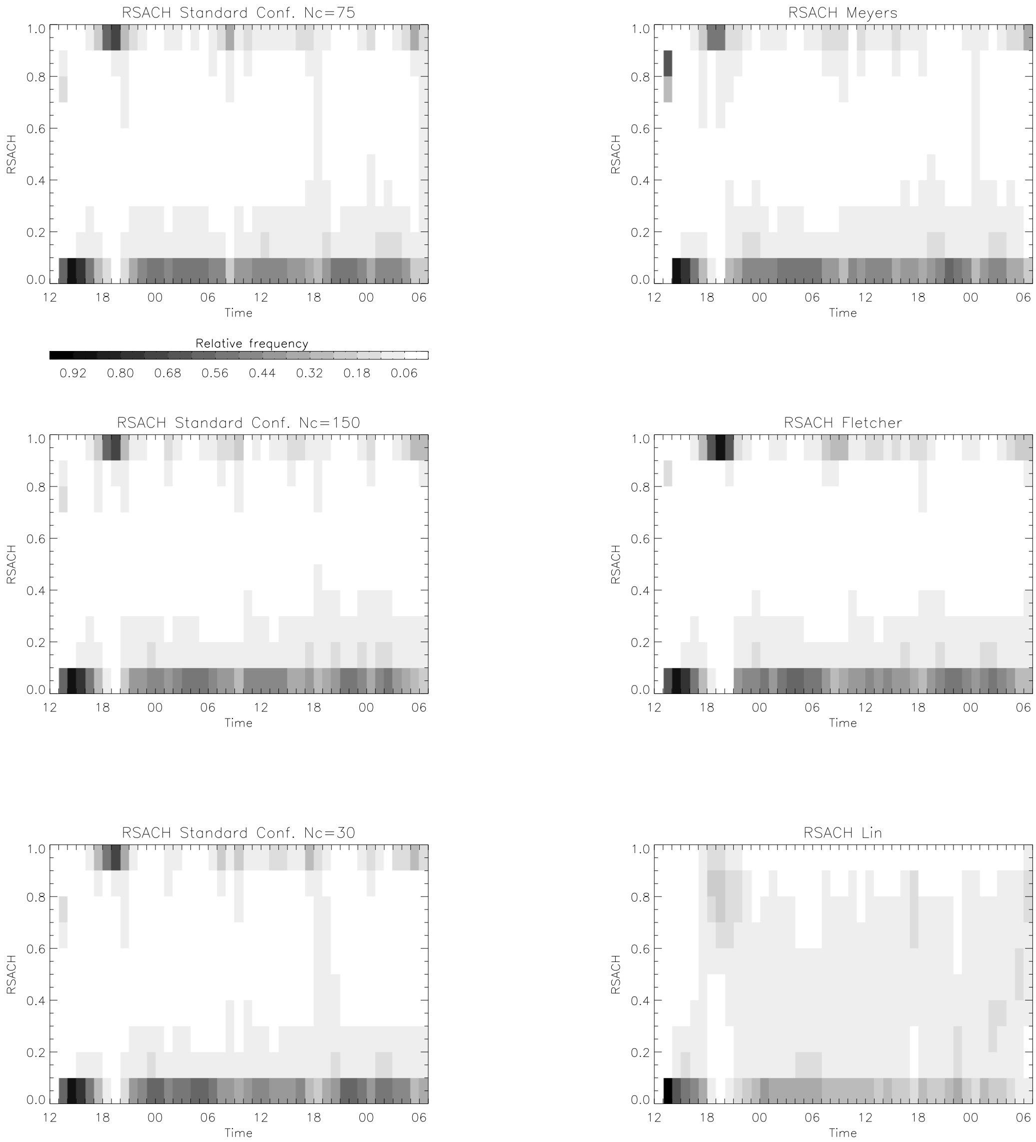

Figure 4.12: Ratio of TSLW to TSLW+TFH time evolution histograms for sim. starting 02/10/2007. Top left - standard configuration Nc=75, top right - Meyers, center left - standard configuration Nc=150, center right - Fletcher, bottom left - standard configuration Nc=30 and bottom right - Lin.

standard configuration and is described in detail in Section 3.2.1, results regarding a comparison of the standard configuration with observations are presented in Section 3.3. Two further numerical experiments have the number of cloud droplets (Nc) altered, Nc=30 and Nc=150 (standard configuration, Nc=75). Two experiments have the ice initiation parameterisation modified; to the Meyers (Meyers et al., 1997) and Fletcher (Fletcher, 1962) parameterisations, the standard configuration uses Cooper (Cooper and Lawson, 1984). The final numerical experiment has the Thompson microphysics routine (Thompson et al., 2007) substituted for the Lin routine (Lin et al., 1983).

Results within Sections 4.1 and 4.2 indicated the evolution of the cloud top temperature distributions were mostly governed by vertical thermodynamic structure. This finding was further substantiated. Little to no difference was observed in the evolution of CTTs between the various numerical experiments. This result supports the conclusion that changes to the rate of ice initiation and number of cloud droplets, and further, changes to the assumed distributions of the cloud particles (exponential vs. gamma) have little to no effect on this field.

The sensitivity of the in-cloud microphysical structure is investigated by comparing simulated in-cloud regions with observations collected by aircraft. The Kolmogorov-Smirnov test was used to assess the similarity of the simulated in-cloud regions with observations. The null hypothesis of the simulated and observed samples belonging to the same population could not be rejected at the 0.05 level for the Nc=30 experiment for both case studies; using the assumption that objected viewed by the CAS had a density of 400kg m^{-3}. Generally speaking the Lin microphysics produced results which least resembled the observations, results produced using the various modifications to the Thompson routine tended to cluster together. For the August 2006 case, all simulated distributions regarding both the simulated hot-wire and CAS fields closely resemble the observed. The October 2007 case showed much greater variability between the various experiments.

Finally, the sensitivity of the broad scale in-cloud microphysical structure to the various numerical experiments was then investigated. Results from the different experiments were remarkably similar. The experiment that showed the greatest difference w.r.t. the standard configuration and all other numerical experiments was the Lin microphysics routine, where the various changes to the Thompson routine were unable to produce mixed phase clouds, generally favouring the extremes of either supercooled or glaciated. The Lin microphysics routine was able to produce clouds with the full spectrum of RSACH values; indicating supercooled, mixed and glaciated conditions simultaneously within the cloud field. The similarities between the different numerical experiments suggests that cloud top temperature is the single most important variable in governing the predominant water phase within the cloud.

Chapter 5

Southern Ocean Cloud Climatology

A climatology of Southern Ocean clouds south of mainland Australia is presented. The MODIS instrument on-board the Terra earth observing satellite is used to investigate the relationship between cloud-top temperature (CTT) and cloud-top phase (CTP) between 30-60S and 100-160E, during the years 2006, 07 and 08. Particular emphasis is placed on supercooled cloud-tops. CTT distributions are constructed with the associated relative frequency of specific CTPs (water/ice/mixed). These are further stratified into latitude bands. The effect the island of Tasmania has on CTTs and phase are assessed and errors in CTT and CTP retrievals due to the MODIS "bow-tie" effect (Platnick et al., 2003) are investigated. Finally, these results are compared with results from the northern Pacific (30-60N, 160-220E).

5.1 Data Preparation

There are currently three separate inferences of cloud phase within the MODIS cloud product, the bispectral IR, which uses inherent differences in water and ice emissions of IR radiation (the difference between the 8.52 and 11 μm bands) to determine the phase. The second algorithm uses shortwave IR bands (1.6 and 2.1 μm), the third method uses a logic-based "decision tree" developed for use with optical thickness and microphysical retrieval algorithms. The phase in this case is a function of spectral band, "shorter" wavelength light is able to penetrate high level cirrus whereas "longer" wavelengths are not. Hence, information contained in the "shorter" wavelength bands will likely correspond to clouds closer to the surface than "longer" wavelength bands. All of these techniques are described in detail in

King et al. (1997) and Platnick et al. (2003).

The method used herein utilises the bispectral IR technique for a number of reasons. Firstly, this method allows for phase retrieval during day and night (the shortwave IR band retrieval only allows for daytime retrievals), secondly, a central aim of this investigation is to compile a climatology of cloud phase at cloud top. As the bispectral IR method uses two longwave IR bands that are readily absorbed by all cloud types, this technique will effectively retrieve a phase at cloud top only. Should thin cirrus partially absorb and re-emit either of the IR bands, this should effectively confuse the phase determination algorithm - resulting in an uncertain cloud top phase retrieval (Platnick et al., 2003). The logic-based "decision tree" algorithm is not used due to uncertainties in exactly which portion of the cloud is emitting the radiation sampled by the detector. Both cloud top temperature and cloud top phase are stored as separate science data sets in the MOD06 level 2 cloud properties data set.

For use in this analysis the native MODIS data which ranges from 5×5km to 5×20km (depending on the detectors viewing angle for the MOD06 level 2 data set) is reprocessed into 1x1° regions. The final data set is the number of times a MODIS pixel appears within a predefined region either as clear or as cloud. If a cloud is detected the temperature and phase are also stored. An example cloud top phase retrieval is shown in Figure 5.1, ~30,000 of these images were used within the present analysis. There are approximately two fly overs per day observing the same region on the earth's surface.

5.2 Results

5.2.1 Southern Ocean Climatology

Figures 5.2, 5.3, 5.4 and 5.5 show cloud fraction and CTP as observed by MODIS (Terra) 2006-2008 inclusive, during the southern hemisphere summer, autumn, winter and spring, respectively. Specifically, cloud fraction refers to the number of times a cloudy pixel is observed within a 1x1 ° grid, normalised by the total number of times a modis pixel obtains an observation within the grid box. Also shown are the fractional occurrences (fraction of the total time) of the CTPs: warm water - i.e. liquid water >0°C (hereafter warm), supercooled liquid water - i.e. <0°C (hereafter SLW), ice, mixed and uncertain. The sum of all phases (including uncertain) equals the cloud fraction. Note that climatological differences due to changes in the Southern Annular Mode, El Nino or Indian Ocean dipole are not considered due the limited number of years in the analysis.

Focusing on Figure 5.2, showing the planar view cloud climatology for the summer months, a clear gradient is observed regarding the number of cloudy pixel observations. Over mainland Australia cloud cover is a minimum with cloud occurring ∼50% of the time, whereas south of the island of Tasmania cloud cover is increases to ∼90%. Warm clouds occur most frequently in the low latitudes and decrease in the poleward direction, all other phase categories have the opposite sign, showing minimum occurrences in the low latitudes and peaks close to the pole.

In general all seasons show fairly similar patterns, cloud fraction is lowest over mainland Australia (and north east Tasmania) reaching a minimum of ∼50% over the central south coast of the mainland. South of Australia cloud fraction increases to >90% in less than 10° of latitude during all seasons. Warm clouds are most prevalent at lower latitudes and decrease in occurrence closer to the pole, the other phases all increase in occurrence closer to the pole. There is a clear preference for

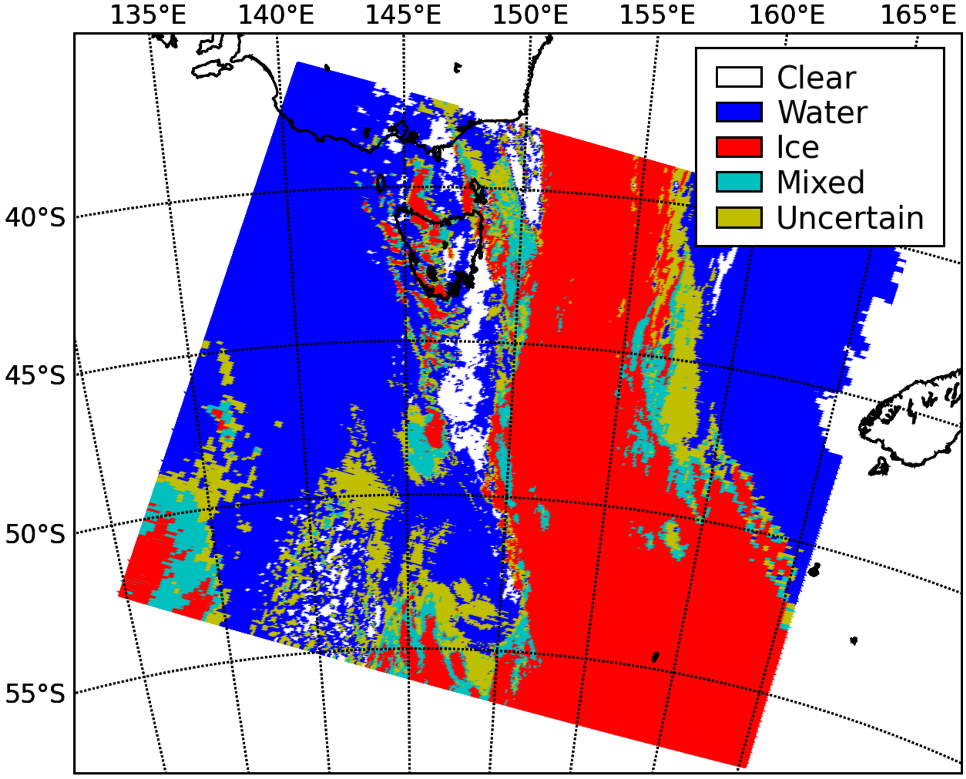

Figure 5.1: Cloud top phase from the MODIS instrument of the Terra satellite 23:50 08/08/2006 (hour:minute dd/mm/yyyy, UTC). A cold front is shown east of Tasmania, much of this cloud mass is glaciated. A post frontal trough line is observed over the west of Tasmania. This image is for the August 2006 case as described in detail in the previous chapters.

warm clouds west of Australia associated with warmer sea surface temperatures (SSTs) in the south Indian Ocean, these also occur along the south west coast of the mainland.

The seasonal cycle over the ocean in general is most pronounced within the occurrence of ice phase, being most prevalent during winter months. Cloud cover tends to be greatest during the winter months and no notable change in the occurrence of warm, SLW, mixed or uncertain cloud types is observed.

Focusing on the island of Tasmania, south east of Australia, a "cloud shadow" (in the same sense as a rain shadow) is observed over north and northeast Tasmania during all seasons, tending closer to north during summer. Relative to a similar latitude over the ocean, there is an increase in supercooled clouds over southwest Tasmania. Here, a seasonal cycle is present, with a minimum in SLW cloud tops during autumn and summer ($\sim$15% of the time) and maximum during winter and spring ($\sim$25%). A further modification to cloud top phase by Tasmania is observed within the ice category. During all seasons, an increase in ice clouds relative to the nearby ocean is observed predominantly over the south east portion of the island and downwind to the east.

The accurate subdivision of the water category about the freezing level depends on the accuracy of the cloud-top temperature retrieval. Hanna et al. (2008) assessed the differences between sounding derived cloud-top temperature and IR brightness temperatures from the Geostationary Operational Environmental Satellite (GOES) over North America. The uncertainty when brightness temperatures were between -5 and 10°C was found to be 'small' relative to cooler temperatures where differences of $\pm$60°C were possible. To address concerns associated with the uncertainty in CTT retrieval, histograms showing the relative frequency of CTP decomposed into equal width temperature bins are shown for summer and winter in Figure 5.6.

Mace et al. (2007) found that the Southern Ocean was predominantly covered

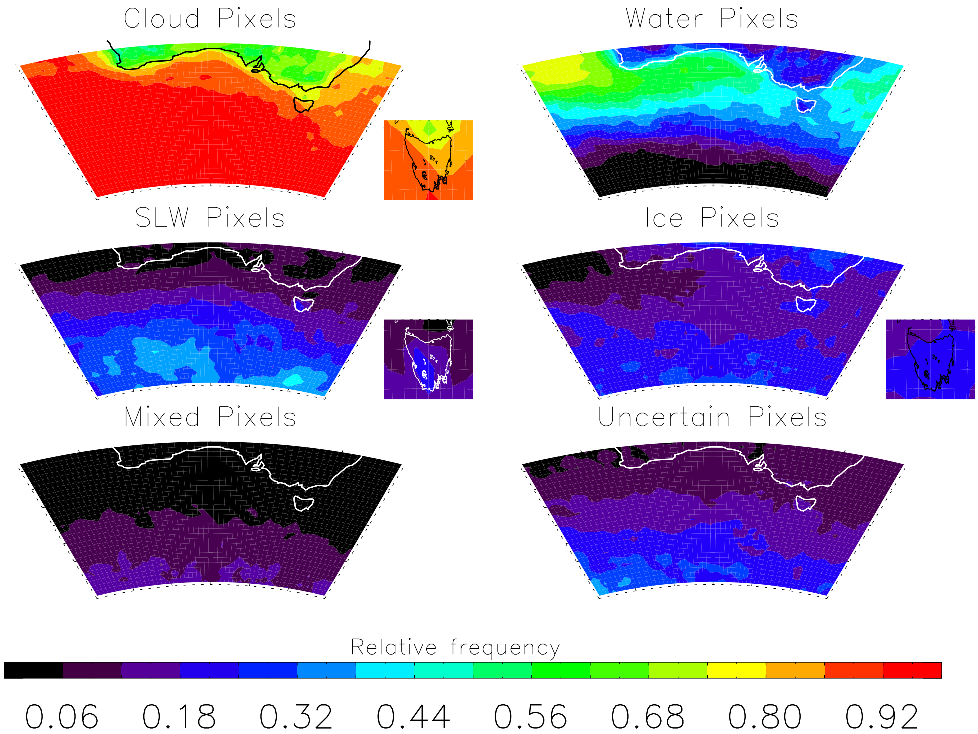

Figure 5.2: Planar view cloud-top phase and cloud fraction DJF (summer), -30 to -60S, 100-160E. Water pixels represent all water clouds at temperatures above 0°C, SLW (supercooled liquid water) is water clouds at temperatures $<$ 0°C. Relative frequency is to the number of observations, i.e. the Southern Ocean south of Tasmania has clouds present $>$ 90% of the time, over Tasmania an ice cloud is observed ~25% of the time. As such, the sum of water, SLW, ice, mixed and uncertain pixels equals the cloud fraction in the top left plot.

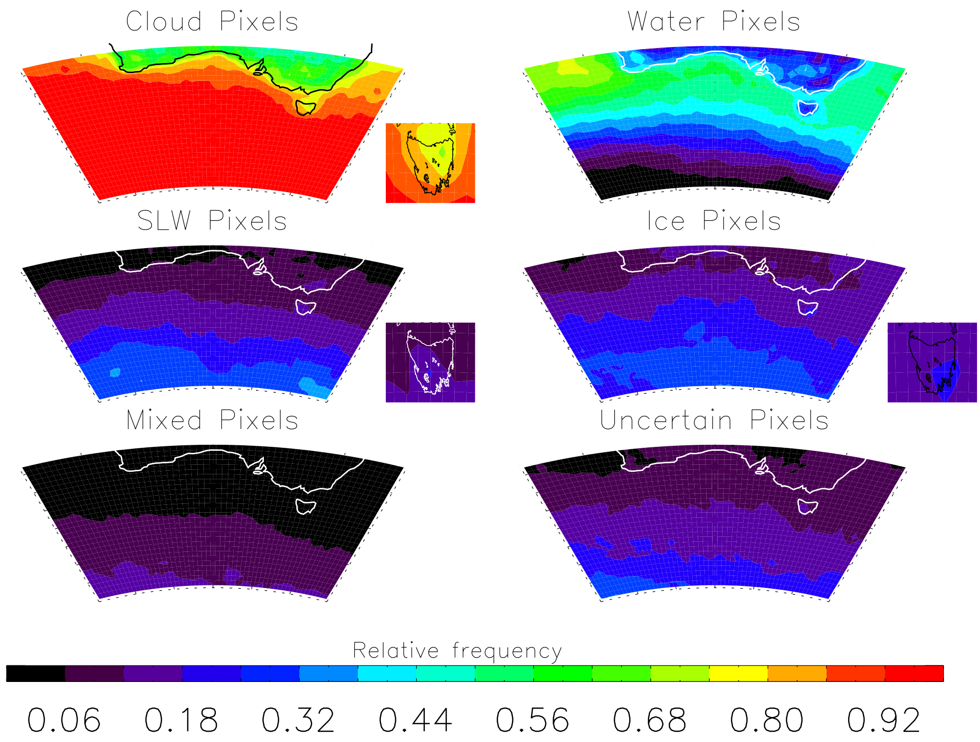

Figure 5.3: Planar view cloud-top phase and cloud fraction MAM (autumn).

in clouds with bases and tops below 3km in altitude. Further, the simulations presented in Chapters 3 and 4 showed for the two case studies, that CTTs during the post-frontal regime (the most prevalent) were generally >-20°C. Figure 5.6 shows that during summer and winter ~50% of the time a cloud exists with a top warmer than -10°C. During summer, a larger fraction of liquid water clouds with temperatures above freezing are observed. Conversely, during winter a greater fraction of glaciated cloud-tops with temperatures <-40°C are apparent. Supercooled cloud-tops are observed at temperatures down to between -30 and -35°C. Further, ~20% of the time a SLW cloud-top is observed with almost half of these occurring at temperatures cooler than -5°C. Mixed phase cloud-tops occur between -5 and -45°C, with a peak between -15 and -25°C. In total a mixed phase cloud-top occurs ~6% of the time during summer and winter. Uncertain CTP retrievals are returned at all temperatures and include CTTs above freezing and below -40°C, where homo-

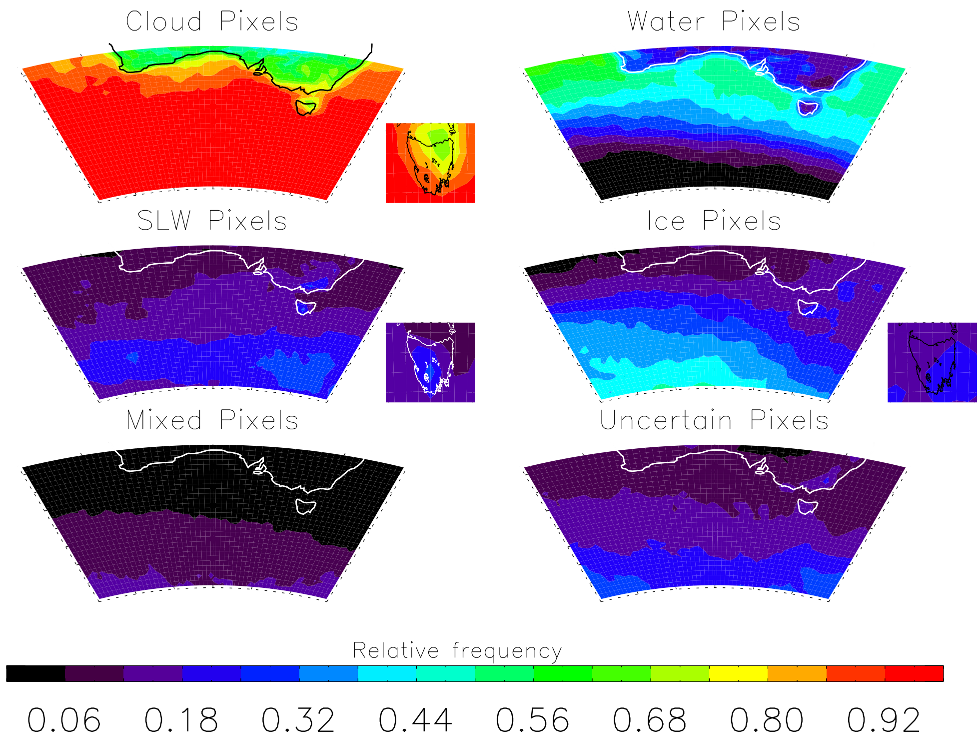

Figure 5.4: Planar view cloud-top phase and cloud fraction JJA (winter).

geneous nucleation should have frozen all liquid phase droplets. The reason for the uncertain CTP retrievals at these extremes is probably due to multilayer or sub-pixel clouds (i.e. clouds with horizontal extent $< 5 \times 5$km at the nadir), the uncertain retrievals between 0 and -40°C however are more ambiguous. Within this temperature range mixed phase clouds are entirely possible, as are double layer clouds. Cloud variability on the sub-pixel scale could also add to uncertain counts as the MODIS resolution varies between 5-20km, the observations and simulations presented in Chapter 3 indicate this is a probable occurrence. This effect is investigated further in Section 5.2.2.

To investigate further how cloud types stratify within latitude bands Figure 5.7 shows the temperature distribution with the relative frequency of CTP for summer and winter within 3 latitude bands: 30-40S, 40-50S and 50-60S. Generally, a clear preference for warmer cloud tops is observed in the lower latitude bands. Between

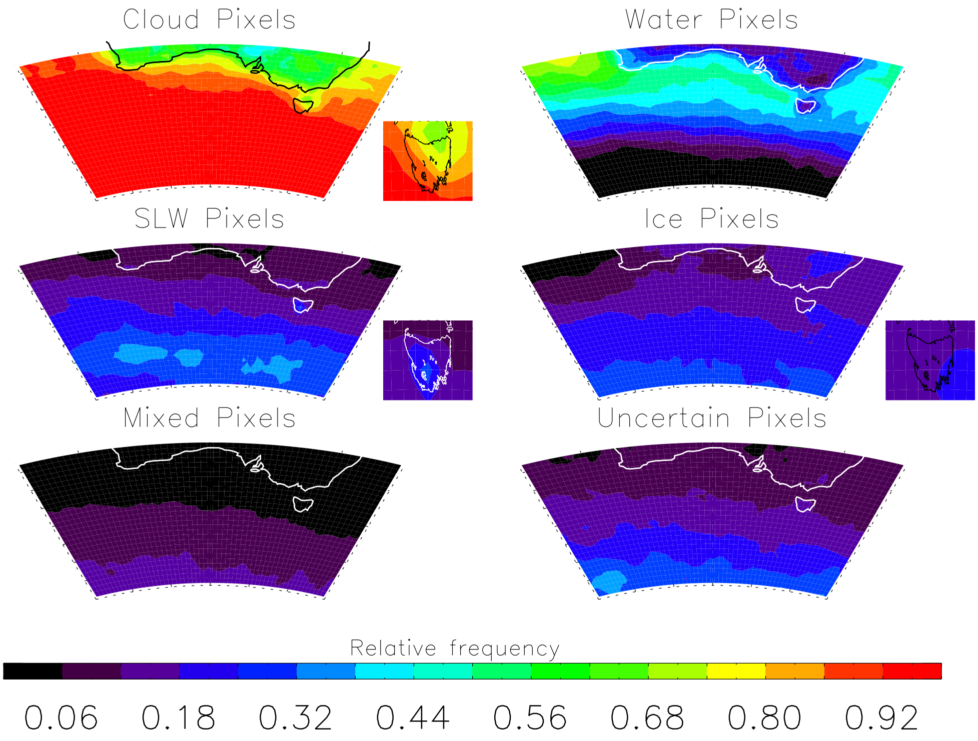

Figure 5.5: Planar view cloud-top phase and cloud fraction SON (spring).

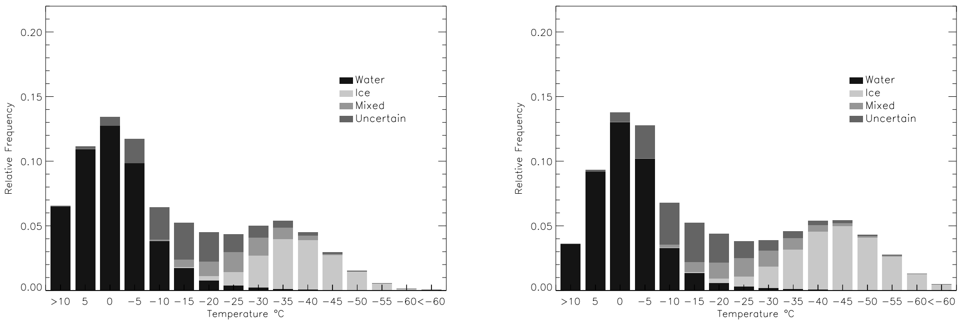

Figure 5.6: Histograms showing the relative frequency of cloud-top phase decomposed into temperatures. The colder bin edge is shown and the bin width is 5°C. Left: summer. Right: winter. The occurrence is relative to the total time, i.e. the sum of all temperature bins is equal to the fraction of time a cloud is observed.

30 and 40S the most common CTT is between 15 and 5°C, between 40 and 50S the most common is 0 to -5°C and between 50 and 60S the most common is -5 to -10°C. This result is seasonally independent. The seasonal cycle is most obvious when considering changes in the frequency of the cooler ice phase clouds (cooler than -40°C) at the higher latitudes (40-50 and 50-60S). The summer-winter variability between 30-40S is much smaller. Here, there is little difference between the summer-winter distributions of cloud-top temperature for cloud-tops cooler than -10°C. Figures 5.2, 5.3, 5.4 and 5.5 indicated the proportion of unclassified (and supercooled) cloud-tops increases in the polewards direction. This result is replicated here. The higher latitude bands contain a higher fraction of clouds tops between -5 and -35°C and considerably more uncertain cloud-top phase retrievals.

5.2.2 MODIS Bow Tie Effect

The MODIS “bow tie” effect is due to the scanning swath nature of the instrument (Platnick et al., 2003). Essentially, pixels near the edges of the scan have increasingly larger coverage on the ground and pixel coverage from subsequent swaths partly overlap. To investigate how this effect affects CTT and CTP retrievals the previous analysis was repeated for the winter months, excluding pixels greater than 5×10km. The results are shown in Figure 5.8. The phase which shows the greatest difference between the distributions is SLW, at temperatures cooler than -10°C the difference for a specific temperature range can be as much as 250%. That said, these large differences only occur when the number of observations are less then 1% of the total. Generally, pixels on the edge are more likely to observe supercooled cloud tops and this difference increases as the temperature decreases (as the number of observations decreases). Ice clouds cooler than -50°C are more likely to be observed by the edge pixels, however ice clouds at warmer temperatures are less likely. A similar pattern is observed regarding mixed phase and uncertain cloud tops, edge pixels are less

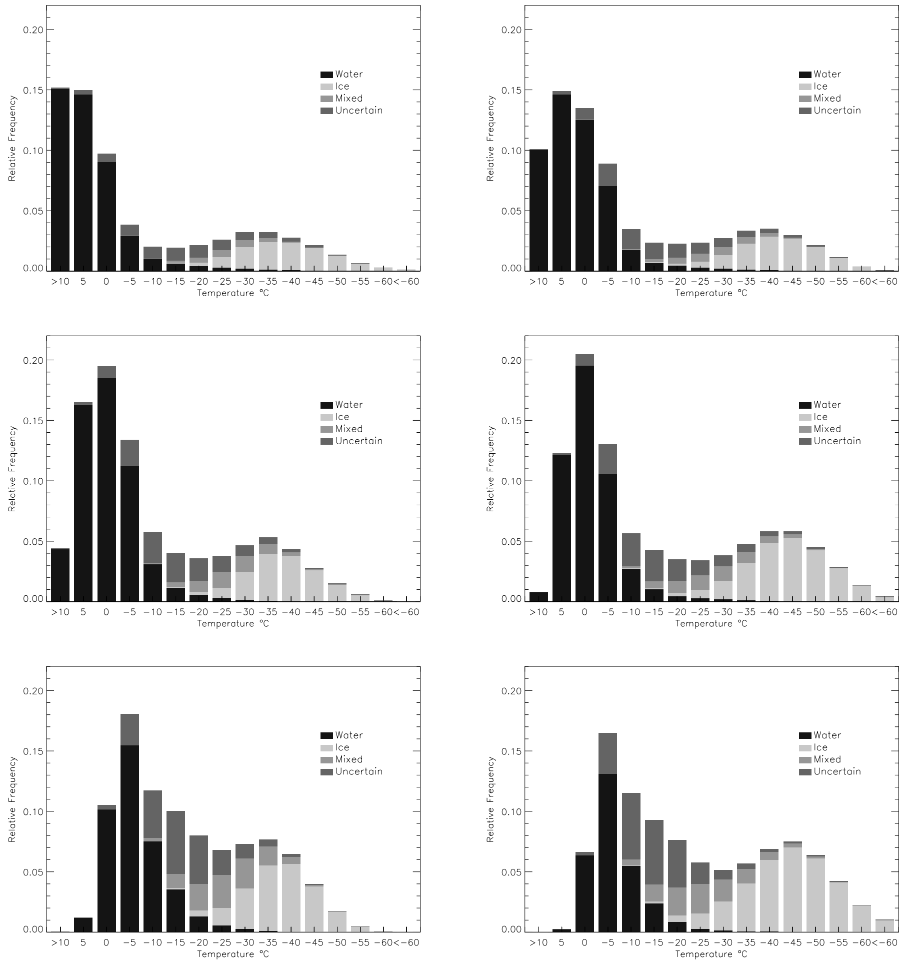

Figure 5.7: Histograms showing the relative frequency of cloud-top phase decomposed into temperature 5°C temperature bins, the colder bin edge is shown. Left: summer. Right: winter. Top: 30-40S, middle 40-50S and bottom 50-60S. The occurrence is relative to the total time, i.e. the sum of all temperature bins is equal to the fraction of time a cloud is observed within a specific latitude band.

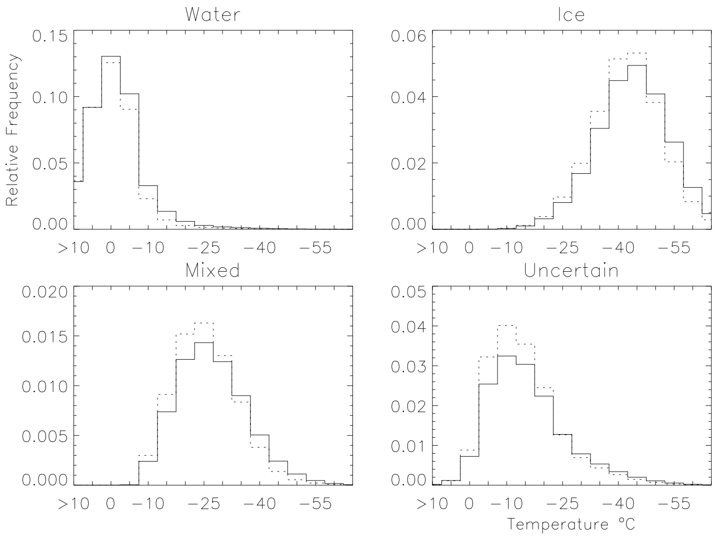

Figure 5.8: Relative frequency of occurrence for specific CTPs during winter (JJA), 30-60S, 100-160E, 2006-2008 inclusive. Solid line uses the entire field of view, the dashed line uses only pixels near to the nadir ($\leq 5 \times 10$km), total cloud cover is 0.88 and 0.87 respectively.

likely to observe these at temperatures warmer than -25°C, and vice versa at cooler temperatures. Despite these differences the general shape of the distributions is similar and the maximum difference between the integrated areas is ∼10%. For the supercooled portion of the water sample the difference is ∼30%.

5.2.3 Pacific Ocean Comparison

As a point of comparison, an analysis for the north Pacific Ocean between 30-60N, 160-220E is presented. The results for summer and winter are presented in Figures 5.9 and 5.10, respectively. Note that the analysis in this part of the world is complicated slightly due to ENSO (El Nino Southern Oscillation), here it is simply noted that 2006 had an extreme SOI index of -10, 2007 +15, and 2008 +15 (Australian Bureau of Meteorology, Accessed 2009). Interannual differences do exist in the data, however, due to the limited sample size it is not possible to analyse these with much confidence.

The most striking result for the north Pacific is the difference between the summer and winter seasons. Whereas the seasonality in the Southern Ocean was small and only notable within the ice CTP, in the northern Pacific large differences are apparent in cloud fraction, water, ice and uncertain CTPs. During summer, cloud cover drops to $\sim$70% between 180-200E south of 40N. The water CTP east of the Kamchatka Peninsula (Russian far east) shows a great deal of variability with a low of $<$6% during winter and a high of $>$50% during summer. The regional peak in the water CTP at 30N, 220E is in close agreement with results presented in Mace et al. (2007). Interestingly, the spacial pattern associated with the occurrences of the ice CTP is quite different from that observed in the Southern Ocean. During the winter months, ice is most common between 30 and 50N, aligned with the North Pacific Drift and decreases in the poleward direction. Over the Southern Ocean the gradient is opposite, the greatest fraction of ice CTP is at the higher latitudes, decreasing as distance from the pole increases. In line with the findings from the Southern Ocean the occurrence of SLW in the north Pacific shows little seasonality.

To further investigate the differences between the northern Pacific and the Southern Ocean, histograms showing the frequency of occurrence of specific CTTs and CTPs are shown for the summer and winter seasons respectively, Figures 5.11 and 5.12. Results from these figures (and previous figures) are summarised in table 5.1. As stated previously, the north Pacific shows greater variability in all CTPs except the SLW category (w.r.t. the Southern Ocean). Both the shape of the histograms and the fractional occurrences of specific CTPs are similar for the Southern Ocean and north Pacific during the local summer season. Winter is when the differences are most apparent. At this time higher temperature clouds are more common over the Southern Ocean, indicating a greater fraction of lower level cloud as found by Mace et al. (2007). A greater fraction of ice, mixed and uncertain CTPs are retrieved over the north Pacific relative to the Southern Ocean during both summer

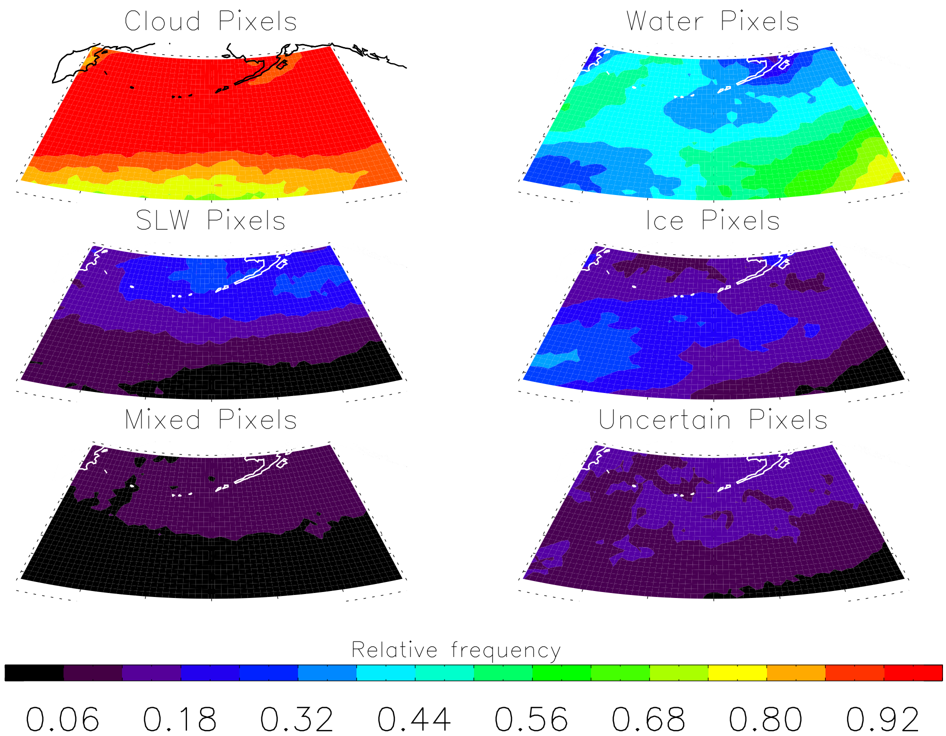

Figure 5.9: Planar view cloud-top phase and cloud fraction JJA (northern hemisphere summer) 2006-2008 inclusive. 30-60N, 160-220E, as described in Figure 5.2.

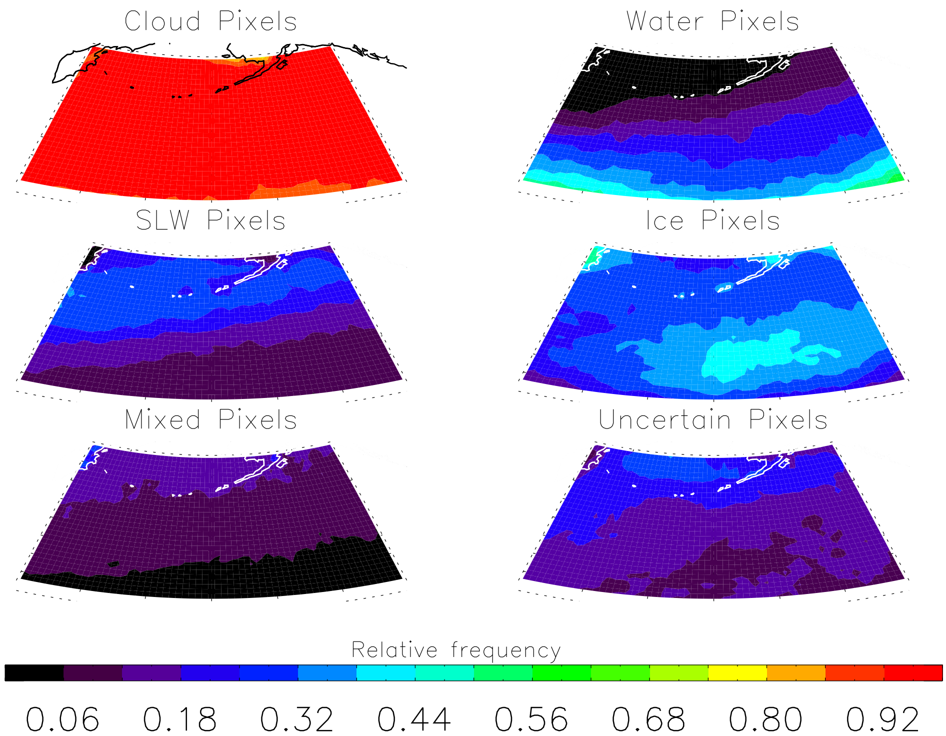

Figure 5.10: Planar view cloud-top phase and cloud fraction DJF (northern hemisphere winter) 2006-2008 inclusive, as described in Figure 5.9.

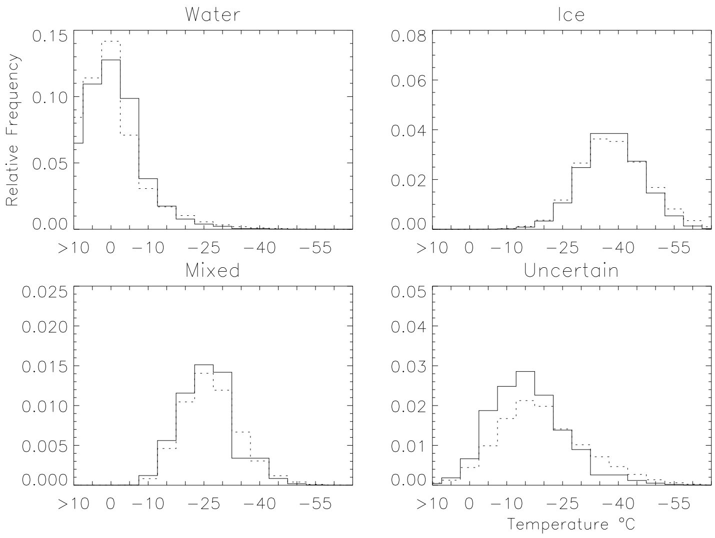

Figure 5.11: Histograms showing the relative frequency of occurrence of CTT and CTP during the summer months for the Southern Ocean (solid line) and the summer months for the north Pacific (dashed), 2006-2008 inclusive.

and winter.

5.2.4 Clouds over Tasmania

Finally, it was noted previously that the island of Tasmania appeared to modify clouds, results regarding this effect are presented for the winter months in Figure 5.13. In general, the island of Tasmania increases the total number of supercooled cloud tops, relative the ocean to the west. This increase persists after the clouds have passed over head and are east of the island. The number of ice clouds over Tasmania is approximately constant relative to the western ocean, however clouds to the east are often cooler and more glaciated. The number of mixed phase and uncertain cloud top retrievals increases over Tasmania, there is little difference between the distributions over the ocean to the west or east.

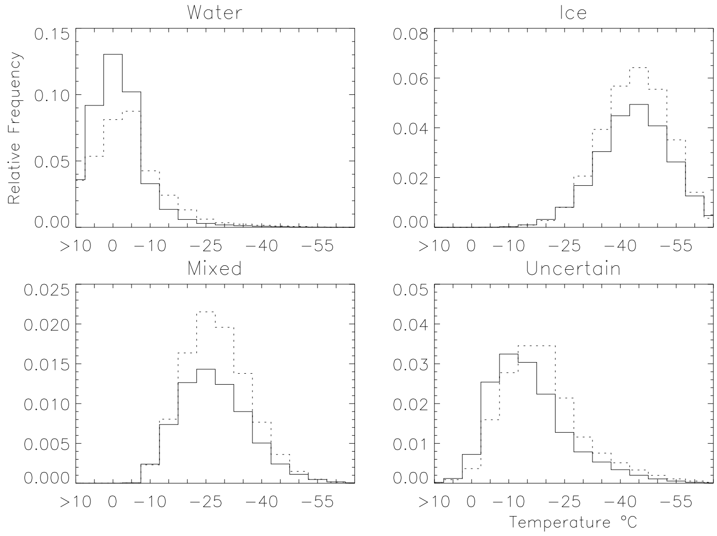

Figure 5.12: As in Figure 5.11 for the winter months.

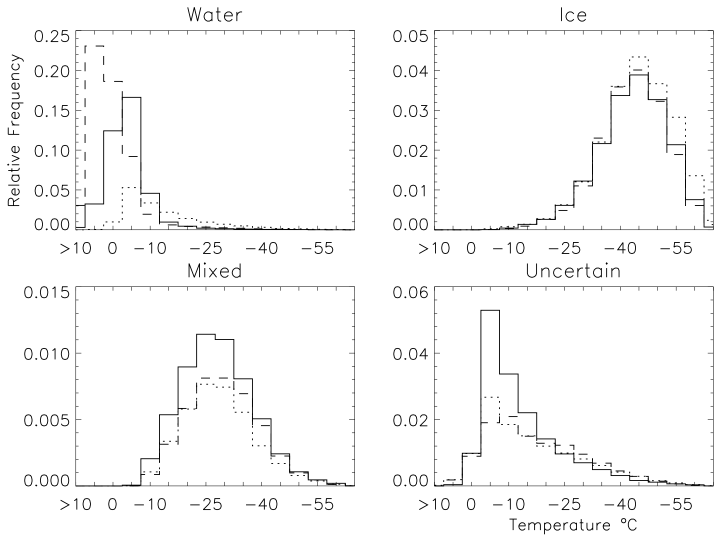

Figure 5.13: Histograms showing the relative frequency of occurrence for specific CTTs and CTPs during the winter months for the region immediately to the west of Tasmania (dashed), over the west coast of Tasmania (dashed) and immediately to the east (dot).

5.3 Summary: MODIS Cloud Climatology

According to the MODIS instrument on-board the TERRA earth observing satellite the Southern Ocean south of mainland Australia is covered by mostly water clouds. Greater than 15% of the time a supercooled water cloud exists over this part of the world. Generally, clouds over this region are low with a large majority having tops at temperatures above freezing, this finding is consistent with Mace et al. (2007). In the higher latitude bands clouds are more likely to have cooler tops that are glaciated. Mixed phase clouds exist approximately 15% of the total time and little seasonal variability is observed between either the distribution of cloud top temperatures or cloud top phase.

The north Pacific between eastern Russia and Alaska/Canada/north west U.S.A is used to compare the results over the Southern Ocean. In general the results are fairly similar, the north Pacific shows greater seasonal variability w.r.t. the distribution of cloud top temperatures and the cloud top phase structure. A slight bias towards more mixed phase/glaciated conditions during the winter months is observed. Approximately 15% of clouds over both oceans return an uncertain phase retrieval - this is predominantly within the 0 to -25°C temperature range. These differences are almost certainly due to the continental influence on airmasses coming off the Asian continent.

The effect of the MODIS "bow-tie" is assessed over the Southern Ocean. There are slight differences in both the distribution of cloud top temperatures and the cloud top phase structure. Finally, the effect the island of Tasmania has on the cloud top structure is assessed. Tasmania is found to increase the number of supercooled clouds over the southwest portion of the island, ∼15% of the time a supercooled cloud is observed over the ocean either to the west or east of Tasmania, a supercooled cloud exists over southwest Tasmania ∼25% of the time. A greater fraction of ice clouds are observed over the ocean to the east, relative to over Tasmania or the ocean to the west.

Table 5.1: Comparison of the various cloud top phases for the Southern Ocean and the north Pacific. The fractions shown are relative to the total number of observations, hence, the sum of Warm, SLW , ice, mixed and uncertain cloud top phases is the total cloud cover (i.e. 1-clear).

Southern Ocean	Warm	SLW	Ice	Mixed	Uncertain	Clear
Summer						
30-60S	0.30	0.17	0.17	0.06	0.13	0.17
30-40S	0.39	0.06	0.12	0.02	0.08	0.34
40-50S	0.39	0.17	0.16	0.05	0.13	0.10
50-60S	0.11	0.29	0.22	0.11	0.20	0.06
West of Tas'	0.49	0.10	0.14	0.03	0.09	0.16
West Tas'	0.28	0.14	0.18	0.03	0.13	0.25
East of Tas'	0.32	0.09	0.21	0.03	0.10	0.25
Winter						
30-60S	0.26	0.16	0.24	0.07	0.15	0.12
30-40S	0.37	0.11	0.13	0.03	0.10	0.26
40-50S	0.32	0.16	0.24	0.06	0.14	0.07
50-60S	0.07	0.22	0.35	0.11	0.22	0.03
West of Tas'	0.45	0.13	0.18	0.04	0.12	0.09
West Tas'	0.16	0.23	0.18	0.06	0.16	0.21
East of Tas'	0.27	0.13	0.21	0.04	0.12	0.24

North Pacific						
Summer						
30-60N	0.34	0.14	0.17	0.05	0.11	0.18
30-40N	0.26	0.06	0.16	0.02	0.09	0.41
40-50N	0.40	0.14	0.20	0.06	0.12	0.07
50-60N	0.36	0.22	0.15	0.07	0.14	0.06
Winter						
30-60N	0.17	0.18	0.30	0.10	0.17	0.08
30-40N	0.30	0.10	0.30	0.05	0.13	0.12
40-50N	0.17	0.20	0.31	0.09	0.16	0.07
50-60N	0.05	0.24	0.29	0.14	0.22	0.06

Chapter 6

Conclusions

The central theme of this work has been cloud seeding over Tasmania. Four separate studies form the main body of work and all are related through this central theme. The aim within Chapter 2 was to analyse long-term Tasmanian precipitation records for a change in precipitation patterns that could be linked with cloud seeding activity. Chapters 3 and 4 then went on to evaluate and use a numerical weather prediction model to better understand the processes and the environment within which clouds over the Southern Ocean and Tasmania form. Essentially, do "seedable" clouds form in the model? When do they occur and in what situations? Finally, within chapter 5 a climatology of Southern Ocean clouds is presented. The aim here was to find out how prevalent supercooled clouds are over Tasmania, the Southern Ocean west of Tasmania and other parts of the world.

To some readers it might have made more sense to evaluate Southern Ocean and Tasmanian clouds for their "seedability" before commencing work that asks questions like "how do seedable clouds form over Tasmania?". However the present structure is maintained as it is an excellent display of how Science progresses. Initially, an answer was sought to the question "does cloud seeding over Tasmania work?". The short answer to this is, "probably, yes". However, there are many caveats to the analysis upon which this statement is based, namely the lack of physical evidence demonstrating physical changes to seeded clouds. The opinion of this author is that future work regarding cloud seeding over Tasmania should focus heavily on obtaining this evidence, through detailed observations during a random seeding experiment. What is presented in the current work is a significant amount of circumstantial evidence that shows the necessary ingredients for effective cloud seeding are in place over Tasmania.

The MODIS satellite climatology presented in Chapter 5 shows that between 20-25% of the time a supercooled cloud top exists over west Tasmania. Further, approximately 33% of the time a cloud exists between 0 and -15°C. This result implies that a significant proportion of clouds over Tasmania meet the criteria needed for effective seeding with artificial ice nuclei. The climate is found to be more similar to the far south Southern Ocean, between 50 and 60S and the far north Pacific between 50 and 60N. The conclusion here is that clouds over Tasmania aren't special, however the fact that these clouds exist over Tasmania is.

Given that the satellite climatology finds a significant proportion of seedable clouds over Tasmania, what processes or environmental factors exist to bring about these clouds? The answer here is due to a combination of factors. First, Tasmania is an island in the northern regions of the Southern Ocean, where the boundary layer is cold, moist and thermodynamically unstable. Secondly, a regular procession of cold fronts pass over Tasmania with a period of 1 or 2 a week. The postfrontal airmasses assessed here contained both temperature or moisture inversions just above the freezing level, these factors inhibit the evolution of 'deeper' clouds and promote cloud structures that have low altitude bases and tops. When modelled, these clouds did not readily glaciate.

Unresolved questions persist however. Significant wind shear is found in conjunction with temperature and moisture inversions, this feature was not reproduced by the model. The effect this has on cloud evolution and development, even precipitation development is unknown. Further, the effect this has on the dispersion on the seeding material is an unknown. More research and field work is needed to isolate the spatial pattern of this feature and its relationship with either large mesoscale systems or possibly even waves associated with the orography of Tasmania.

Many questions still remain regarding cloud seeding over Tasmania. In the opinion of this author future research would ideally focus on using the A-train satellite constellation to further study cloud microphysics over the Southern Ocean and Tasmania. The origin of the mid-level shear layer remains a mystery and warrants further investigation. The use of dual polarised, Doppler radars is strongly encouraged as a method to document in-cloud microphysical changes associated with seeding and precipitation formation mechanisms in general over the Southern Ocean.

Bibliography

Austin, R. T., 2008: CloudSat 2B-CWC-RVOD Algorithm Process Description Document. *CloudSat Data Processing Center (http://www.cloudsat.cira.colostate.edu)*.

Australian Bureau of Meteorology, Accessed 2009: Recent Climate Summaries, http://www.bom.gov.au/climate/current/.

Baumgardner, D., H. Jonsson, W. Dawson, D. O'Conner, and R. Newton, 2001: The Cloud Aerosol and Precipitation Spectrometer: A new instrument for cloud investigators. *Atmospheric Research*, **59-60**, 251–264.

Bennartz, R., 2007: Global assessment of marine boundary layer cloud droplet number concentration from satellite. *Journal of Geophysical Research*, **112**, D02 201.

Blahak, U., 2007: RADAR MIE LM and RADAR MIELIB, Calculation of Radar Reflectivity from Model Output. *Internal Rep., Institute for Meteorology and Climate Research, University/Research Center Karlsruhe.*

Boe, B., R. Bomar, W., R. Cotton, W., L. Marler, B., D. Orville, H., and A. Warburton, J., 2004: The Weather Modification Association's response to the National Research Council's Report titled: "Critical issues in weather modification research". *Journal of Applied Meteorology*, **26**, 53–82.

Boers, R., J. B. Jensen, and P. B. Krummel, 1997: A line of convection embedded in a stratocumulus-topped boundary layer. *Quartly Journal of the Royal Meteorological Society*, **123**, 207–221.

Boers, R. and P. B. Krummel, 1998: Microphysical properties of boundary layer clouds over the southern ocean during ace 1. *Journal of Geophysical Research*, **102**, 97JD03 280.

Cober, G. C., G. A. Isaac, and J. W. Strapp, 1995: Aircraft icing measurements in east coast winter storms. *Journal of Applied Meteorology*, **34**, 88–100.

Cooper, W. A., 1986: Ice Initiation in Natural Clouds. *Precipitation Enhancement - A Scientific Challenge, Meteor. Monogr., Amer. Meteor.*, **43**, 29–32.

Cooper, W. A. and R. P. Lawson, 1984: Physical interpretation of results from HIPLEX-1 experiment. *Journal of Climate and Applied Meteorology*, **23**, 523–540.

Deshler, T. and D. W. Reynolds, 1990: The persistence of seeding effects in a winter orographic cloud seeded with silver iodide burned in acetone. *Journal of Applied Meteorology*, **29**, 477–488.

Deshler, T., D. W. Reynolds, and A. W. Huggins, 1990: Physical response of winter orographic clouds over the Sierra Nevada to airborne seeding using dry ice or silver iodide. *Journal of Applied Meteorology*, **29**, 288–330.

Dudhia, J., 1989: Numerical study of convection observed during the winter monsoon experiment using a mesoscale two-dimensional model. *Journal of Atmospheric Science*, **46**, 3007–3107.

Efron, B. and R. J. Tibshirani, 1993: *An Introduction to the Bootstrap*. Monographs on Statistics and Applied Probability 57, Chapman and Hall/CRC.

Ek, M. B., K. E. Mitchell, Y. Lin, E. Rogers, P. Grunmann, V. Koren, G. Gayno, and J. D. Tarpley, 2003: Implementation of noah land surface model advances in the national centers for environmental prediction operational mesoscale eta model. *Journal of Geophysical Research*, **108**.

Ferrier, B. S., 1994: A double-moment multiple-phase four-class bulk ice scheme. part 1: Description. *Journal of Atmospheric Science*, **51**, 249–280.

Fletcher, N. H., 1962: *The Physics of Rain Clouds*. Cambridge University Press, 386 pp.

Gabriel, K. R., 1998: Ratio statistics for randomized experiments in precipitation stimulation. *Journal of Applied Meteorology*, **38**, 290–301.

Gabriel, K. R. and D. Rosenfeld, 1990: The second Israeli rainfall stimulation experiment: Analysis of precipitation on both targets. *Journal of Applied Meteorology*, **29**, 1055–1067.

Garstang, M., R. Bruintjes, R. Serafin, H. Orville, B. Boe, W. Cotton, and J. Warburton, 2005: Finding common ground. *Bulletin of the American Meteorological Society*, **86**, 647–655.

Gras, J. L., 1995: CN, CCN and particle size in Southern Ocean air at Cape Grim. *Atmospheric Research*, **35**, 233–251.

Guan, H., S. G. Cober, and G. A. Isaac, 2001: Verification of supercooled cloud forecasts with in situ aircraft measurements. *Weather and Forecasting*, **16**, 145–155.

Guan, H., S. G. Cober, G. A. Isaac, A. Tremblay, and A. Methot, 2002: Comparison of three cloud forecast schemes with in-situ aircraft measurements. *Weather and Forecasting*, **17**, 1226–1235.

Hanna, J. W., D. M. Schultz, and A. R. Irving, 2008: Cloud-top Temperatures for Precipitating Winter Clouds. *Journal of Applied Meteorology and Climatology*, **47**, 351–359.

Heymsfield, A. J., A. Bansemer, and C. Schmitt, 2004a: Effective Ice Particle Densities Derived from Aircraft Data. *Journal of Atmospheric Science*, **61**, 982–1003.

Heymsfield, A. J., C. Schmitt, and A. Bansemer, 2004b: Effective Ice Particle Densities for Cold Anvil Cirrus. *Geophysical Research Letters*, **31**, L02 101.

Hines, K. M. and D. H. Bromwich, 2008: Development and Testing of Polar Weather Research and Forecasting (WRF) Model. Part I: Greenland Ice Sheet Meteorology. *Monthly Weather Review*, **136**, 1971–1989.

Hong, S. Y., Y. Noh, and J. Dudhia, 2006: A new vertical diffusion package with an explicit treatment of entrainment processes. *Monthly Weather Review*, **134**, 2318–2341.

Janjic, Z. I., 2000: Comments on "development and evaluation of a convection scheme for use in climate models". *Journal of Atmospheric Science*, **57**, 3686.

Jarque, C. M. and A. K. Bera, 1980: Efficient tests for normality, homoscedasticity and serial independence of regression residuals. *Economics Letters*, **6**, 255–259.

Jensen, J. B., S. Lee, P. B. Krummel, J. Katzfey, and D. Gogoasa, 2000: Precipitation in marine cumulus and stratocumulus part 1: Thermodynamic and dynamic observations of closed cell circulations and cumulus bands. *Atmospheric Research*, **54**, 117–155.

Jiang, H., W. R. Cotton, J. O. Pinto, and W. M. J. Curry, J. A., 2000: Cloud Resolving Simulations of Mixed-phase Arctic Stratus observed during BASE: Sensitivity to Concentration of Ice Crystals and Large-scale Heat and Moisture Advection. *Journal of Atmospheric Science*, **57**, 21052117.

Justice, C. O., et al., 1998: The moderate resolution imaging spectroradiometer (modis) land remote sensing for global change research. *IEEE transactions on geoscience and remote sensing*, **36**, 1228–1249.

King, M. D., S. Tsay, S. E. Platnick, M. Wang, and K. Liou, 1997: Cloud Retrieval Algorithms for MODIS: Optical Thickness, Effective Particle Radius, and Thermodynamic Phase. *MODIS Algorithm Theoretical Basis Document No. ATBD-MOD-05, MOD06 - Cloud product.*

Kraus, E. B. and P. Squires, 1947: Experiments on the stimulation of clouds to produce rain. *Science*, **159**, 489–491.

Lavery, B., G. Joung, and N. Nicholls, 1997: An extended high-quality historical rainfall dataset for Australia. *Australian Meteorological Magazine*, **46**, 27–38.

Lin, Y. L., R. D. Farley, and H. D. Orville, 1983: Bulk parameterization of the snow field in a cloud model. *Journal of Applied Meteorology*, **22**, 1065–1089.

Long, A. B. and A. W. Huggins, 1992: Australian Winter Storms Experiment 1: Supercooled liquid water and precipitation-enhancement opportunities. *Journal of Applied Meteorology*, **31**, 1041–1055.

Mace, G. G., R. Marchand, Q. Zhang, and G. Stephens, 2007: Global hydrometeor occurrence as observed by CloudSat: Initial observations from summer 2006. *Geophysical Research Letters*, **34**.

Massey, F. J., 1951: The kolmogorov-smirnov test for goodness of fit. *Journal of the American Statistical Association*, **46**, 68–78.

McGregor, J. L. and M. R. Dix, 2007: *High Resolution Numerical Modelling of the Atmosphere and Ocean. Chapter: An Updated Description of the Conformal-Cubic Atmospheric Model.* Springer New York.

Mellor, G. L. and T. Yamada, 1982: Development of a turbulence closure model for geophysical fluid problems. *Reviews of Geophysics and space physics*, **20**, 851–875.

Meyers, M. P., J. Y. Harrington, and W. R. Cotton, 1997: New rams cloud microphysics parameterization. part 2: the two-moment scheme. *Atmospheric Research*, **45**, 3–39.

Michalakes, J., J. Dudhia, D. Gill, J. Klemp, and W. Skamarock, 1999: *Towards teracomputing: Design of a next-generation regional weather research and forecast model*. World Scientific, River Edge, New Jersey, 117-124.

Mlawer, E. J., S. J. Taubman, P. D. Brown, M. J. Iacono, and C. S. A., 1997: Radiative transfer for an inhomogeneous atmosphere: Rrtm, a validated correlated-k model for the longwave. *Journal of Geophysical Research*, **102**, 16 663–16 682.

Morrison, A. E., S. T. Siems, M. J. Manton, and A. Nazarov, 2009: On the analysis of a cloud seeding data set over Tasmania. *Journal of Applied Meteorology*, **48**, 1267–1280.

Morrison, H. and J. O. Pinto, 2005: Mesoscale modelling of springtime arctic mixed-phase stratiform clouds using a new two-moment bulk microphysics scheme. *Journal of Atmospheric Sciences*, **62**, 3683–3704.

Mossop, S. C., A. Ono, and E. R. Wishart, 1970: Ice Particles in Maritime Clouds near Tasmania. *Quarterly Journal of the Royal Meteorological Society*, 487–508.

National Climate Centre, Bureau of Meteorology, 2006: An exceptionally dry decade in parts of southern and eastern Australia: October 1996-2006, special climate statement 9.

Nirel, R. and D. Rosenfeld, 1995: Estimation of the effect of operational seeding on rain amounts in Israel. *Journal of Applied Meteorology*, **34**, 2220–2229.

Platnick, S., M. D. King, S. A. Ackerman, W. P. Menzel, B. A. Baum, J. C. Riedei, and R. A. Frey, 2003: The modis cloud products: Algorithms and examples from terra. *IEEE Transactions on Geoscience and Remote Sensing*, **41**, 459–473.

Pook, M. J., P. C. McIntosh, and G. A. Meyers, 2006: The Synoptic Decomposition of Cool-Season Rainfall in the South eastern Australian Cropping Region. *Journal of Applied Meteorology and Climatology*, **45**, 11561170.

Rauber, R. M. and L. O. Grant, 1987: Supercooled liquid water structure of a shallow orographic cloud system in southern Utah. *Journal of Applied Meteorology*, **26**, 208–215.

Reisner, R., R. M. Rasmussen, and R. T. Bruintjes, 1998: Explicit forecasting of supercooled liquid water in winter storms using the mm5 mesoscale model. *Quarterly Journal of the Royal Meteorological Society*, **124**, 1071–1107.

Reynolds, D. W. and A. W. Dennis, 1986: A review of the Sierra Cooperative Pilot Project. *Bulletin of the American Meteorological Society*, **67**, 513–523.

Rosenfeld, D. and W. L. Woodley, 1989: Effects of cloud seeding in west Texas. *Journal of Applied Meteorology*, **28**, 1050–1080.

Russell, M. L., D. H. Lenschow, K. K. Laursen, P. B. Krummel, S. T. Siems, A. R. Bandy, D. C. Thornton, and T. S. Bates, 1998: Bidirectional mixing in an ACE 1 marine boundary layer overlain by a second turbulent layer. *Journal of Geophysical Research*, **103**, 16 411–16 432.

Ryan, B., K. Wilson, J. Garratt, and R. Smith, 1985: Cold Fronts Research Programme: Process, Future Plans and Research Directions. *Bulletin of the American Meteorological Society*, **66**, 1116–1122.

Ryan, B. F. and W. D. King, 1997: A critical review of the Australian experience in cloud seeding. *Bulletin of the American Meteorological Society*, **78**, 239–254.

Schaefer, V. J., 1946: The production of ice crystals in a cloud of supercooled water droplets. *Science*, **104**, 457–459.

Shaw, D. E., W. D. King, and E. Turton, 1984: Analysis of Hydro-Electric Commission cloud seeding in Tasmania 1979-83. Tech. rep., CSIRO Division of Cloud Physics CP 394, pp 33.

Silverman, A., B. and W. Sukarnjanasat, 2000: Results of the Thailand warm-cloud hygroscopic particle seeding experiment. *Journal of Applied Meteorology*, **39**, 1160–1175.

Simmonds, I. and K. Keay, 2000: Mean Southern Hemisphere Extratropical Cyclone Behaviour in the 40-Year NCEP-NCAR Reanalysis. *Journal of Climate*, **13**, 873–885.

Skamarock, W., J. Klemp, J. Dudhia, D. Gill, D. Barker, W. Wang, and J. Powers, 2005: *A Description of the Advanced Research WRF Version 2*. National Center for Atmospheric Research, Boulder, Colorado, USA.

Smith, E. J., E. E. Adderley, and D. Walsh, 1963: A cloud-seeding experiment in the Snowy Mountains. *Journal of Applied Meteorology*, **2**, 324–332.

Smith, E. J., L. G. Veitch, D. E. Shaw, and A. J. Miller, 1979: A cloud-seeding experiment in tasmania. *Journal of Applied Meteorology*, **18**, 804–815.

Solomon, S., D. Qin, M. Manning, Z. Chen, M. Marquis, K. B. Averyt, M. Tignor, and H. L. Miller, 2007: IPCC, 2007: Climate Change 2007: The Physical Science Basis. Contribution of Working Group I to the Fourth Assessment Report of the Intergovernmental Panel on Climate Change. *Cambridge University Press*.

Spangenberg, D. A., P. Minnis, S. Sun-Mack, and P. M. R. Shupe, M. D., 2006: Characterisation of Mixed-Phase Clouds During Mixed-Phase Arctic Cloud Experiment from Satellite, Ground-Based, and In-Situ Data. *Proceedings of the sixteenth ARM science team meeting*.

Stephens, G., et al., 2002: The CLOUDSAT Mission and the A-Train. *Bulletin of the American Meteorological Society*, **83**, 1771–1790.

Thompson, G., P. R. Field, R. M. Rasmussen, and W. D. Hall, 2007: Explicit forecasts of winter precipitation using an improved bulk microphysics scheme. part 2: Implementation of a new snow parameterization. *Submitted to Monthly Weather Review.*

Thompson, G., R. M. Rasmussen, and K. Manning, 2004: Explicit forecasts of winter precipitation using an improved bulk microphysics scheme. part 1: Description and sensitivity analysis. *Monthly Weather Review*, **132**, 519–542.

Tremblay, A., A. Glazer, and L. Garand, 2001: Comparison of three cloud schemes in winter storm forecasts. *Monthly Weather Review*, **129**, 2923–2938.

Vaillancourt, P. A., A. Tremblay, S. G. Cober, and G. A. Isaac, 2003: Comparison of aircraft observations with mixed-phase cloud simulations. *Monthly Weather Review*, **131**, 656–671.

Walko, R., W. R. Cotton, and M. P. Meyers, 1995: New rams cloud microphysics parameterization. part 1: the single-moment scheme. *Atmospheric Research*, **38**, 29–62.

Wapler, K., T. P. Lane, P. T. May, C. Jakob, S. T. Siems, and M. J. Manton, 2008: WRF Model Simulations of Tropical Cloud Systems observed during TWP-ICE. *28th Conference on Hurricanes and Tropical Meteorology, AMS.*

Watkins, A. and B. Trewin, 2007: Australian climate summary: 2006. *Bulletin of the Australian Meteorological and Oceanographic Society*, **20**, 10–17.

Weisstein, W. E., Accessed 2008: Bonferroni correction, from MathWorld–A Wolfram Web Resource, http://mathworld.wolfram.com/BonferroniCorrection.html.

Yum, S. S. and J. G. Hudson, 2004: Winter/summertime contrasts of cloud condensation nuclei and cloud microphysics over the southern ocean. *Journal of Geophysical Research*, **109**, D06 204.

Zhang, R., G. Li, J. Fan, D. Wu, and M. Molina, 2007: Intensification of Pacific Storm Track Linked to Asian Pollution. *The National Academy of Sciences of the USA*, **104**, 52955299.

Appendix A: Cloud Seeding Evaluation Sensitivity Analysis

Results not presented in Morrison et al. (2009) are included here. Tables A1, A2, A3 and A4 extend the analysis presented in detail in Section 2.4. Presented are the double ratios, and associated levels of significance, for the two target regions (HECA and CSIRO) with the various controls. The sensitivity to the inclusion/omission of Hydro Tasmania (HT) operated sites is investigated. Further, the effect of changing the longevity criteria, the period of assessment (1950/60-2005, 1950/60-1985 and 1980-2005) and the number of seeding events required for a month to be classed within the seeded sample is assessed.

From Tables A3 and A4, it is observed that for the majority of tests, changes in either the longevity, period of assessment or inclusion/omission of HT operated sites has little effect. The results presented in Section 2.4 are tests numbered 5 and 17 in the below tables, these results are generally consistent with the other tests. Tests numbered 15, 20, 21, 23 and 24 show the greatest difference in results. In these cases the double ratios of the west and north west with the CSIRO target are below 1.0, none of these results are significant. Tests with a probability of occurrence smaller than 0.05 indicate a result which has a less than 5% chance of being due to random processes. However, multiple comparisons are being considered here. Applying the Bonferroni adjustment (Weisstein, Accessed 2008) for multiple comparisons to a 95% significance level for 120 tests produces an alpha of 0.0004. A result with a probability of occurrence less than this is significant, even when comparing such a large number of tests. It is noted that over 20% of the tests remain significant at the adjusted alpha level. Interestingly, the tests in Tables A1, A2, A3 and A4 that have the highest longevity requirement during the more recent period 1960-2005 (when the rain gauge network was changing least), with the largest number of sites (Tests 6 and 18) all show positive results; with all except one being significant.

Table A5 shows a sensitivity analysis where the data set has been split into two parts. 1950/60-1985, incorporating the first two Tasmanian cloud seeding experiments and 1980-2005, mostly incorporating the recent years of operational seeding. It is noted that in general the earlier years of seeding (1950/60-1985) do not show strong increases and sometimes show decreases with double ratios <1.0, only two of these results are significant (CSIRO vs. SE control, 1950 and 1960-1985). The more recent years of seeding often show increases in precipitation associated with cloud seeding activity, however many of these results are also not significant. This analysis emphasises the need for a sufficiently long time series to achieve significant results and further for a static and numerous rain gauge network to reduce the possibility of ambiguous results.

Finally Tables A6 and A7 show how successively increasing the number of seeded events needed to define a seeded month changes the results, HECA and CSIRO targets respectively. The first rows are results that have already been presented i.e. that a single seeding event in a month defines that month as seeded. All other results generally indicate that as the number of seeding events increases within a seeded month, the magnitude of the double ratio also increases. The notable exception to this is the double ratio between either the CSIRO or HECA targets and the west control, a possible reason for this effect is the inadvertent seeding of this control region.

Table A1: Table showing the different analyses performed. The experiment number is on the left, numbers indicated with an asterisk are the tests presented in Chapter 2. Columns from the left are: the experiment reference number, period, sites included (B - Bureau of Meteorology, H - Hydro Tasmania), longevity threshold (0.25, 0.50 and 0.75) and target area (HECA). The following columns detail the average numbers of sites used throughout the analysis for: T - target (HECA), W - west, NW - north west, HQ - high quality, NE - north east and finally SE - south east.

Exp	Period	Sites	Thres.	Type	T	W	NW	HQ	NE	SE
1	1950-2005	B+H	0.25	HECA	20.40	12.83	35.70	9.56	90.40	102.79
2	1950-2005	B+H	0.50	HECA	15.74	10.29	29.65	9.56	71.75	84.52
3	1950-2005	B+H	0.75	HECA	3.17	4.34	21.88	9.56	49.40	61.20
4	1960-2005	B+H	0.25	HECA	24.28	13.77	37.57	9.50	96.97	109.98
5*	1960-2005	B+H	0.50	HECA	19.55	10.44	30.78	9.50	78.19	90.90
6	1960-2005	B+H	0.75	HECA	11.36	5.52	28.18	9.50	63.96	68.75
7	1950-2005	B	0.25	HECA	11.05	9.89	35.19	9.56	89.91	101.67
8	1950-2005	B	0.50	HECA	8.07	8.37	29.65	9.56	71.75	83.72
9	1950-2005	B	0.75	HECA	2.40	3.56	21.88	9.56	49.40	60.41
10	1960-2005	B	0.25	HECA	11.80	10.19	36.95	9.50	96.37	108.36
11	1960-2005	B	0.50	HECA	9.69	8.10	30.78	9.50	78.19	89.92
12	1960-2005	B	0.75	HECA	4.12	4.57	28.18	9.50	63.96	67.78

Table A2: As in TableA1 for the CSIRO target.

Exp	Period	Sites	Thres.	Type	T	W	NW	HQ	NE	SE
13	1950-2005	B+H	0.25	CSIRO	11.83	12.83	35.70	9.56	90.40	102.79
14	1950-2005	B+H	0.50	CSIRO	10.05	10.29	29.65	9.56	71.75	84.52
15	1950-2005	B+H	0.75	CSIRO	1.85	4.34	21.88	9.56	49.40	61.20
16	1960-2005	B+H	0.25	CSIRO	14.04	13.77	37.57	9.50	96.97	109.98
17*	1960-2005	B+H	0.50	CSIRO	12.13	10.44	30.78	9.50	78.19	90.90
18	1960-2005	B+H	0.75	CSIRO	5.82	5.52	28.18	9.50	63.96	68.75
19	1950-2005	B	0.25	CSIRO	8.41	9.89	35.19	9.56	89.91	101.67
20	1950-2005	B	0.50	CSIRO	6.87	8.3	29.65	9.56	71.75	83.72
21	1950-2005	B	0.75	CSIRO	1.85	3.56	21.88	9.56	49.40	60.41
22	1960-2005	B	0.25	CSIRO	9.04	10.19	36.95	9.50	96.37	108.36
23	1960-2005	B	0.50	CSIRO	8.25	8.10	30.78	9.50	78.19	89.92
24	1960-2005	B	0.75	CSIRO	2.67	4.57	28.18	9.50	63.96	67.78

Table A3: Table showing the results for the tests described in Table A1. Results indicated with an asterisk indicate tests presented in Chapter 2. No results are presented for test no. 9, due to incomplete data.

Exp.		W	NW	HQ	NE	SE
1	DR	1.053	1.091	1.152	1.177	1.157
	Sig.	0.0128	0.0041	<0.0001	<0.0001	0.0013
2		1.034	1.070	1.128	1.147	1.147
		0.0723	0.0248	<0.0001	0.0003	0.0017
3		1.004	1.029	1.075	1.108	1.098
		0.4432	0.2526	0.0201	0.0263	0.041
4		1.053	1.088	1.147	1.151	1.134
		0.0121	0.0097	<0.0001	0.0008	0.0036
5*		1.053*	1.088*	1.136*	1.144*	1.129*
		0.0156*	0.0098*	<0.0001*	0.0022*	0.0040*
6		1.056	1.061	1.105	1.114	1.104
		0.0115	0.0553	0.0004	0.011	0.0246
7		1.080	1.074	1.133	1.160	1.136
		0.001	0.0259	0.0001	0.0008	0.0045
8		1.089	1.105	1.166	1.185	1.183
		0.0002	0.0069	<0.0001	0.0003	0.0003
9		N/A	N/A	N/A	N/A	N/A
		N/A	N/A	N/A	N/A	N/A
10		1.093	1.096	1.156	1.161	1.139
		0.0003	0.0123	0.0001	0.0019	0.0028
11		1.099	1.125	1.175	1.183	1.167
		0.0004	0.0038	<0.0001	0.0006	0.0009
12		1.067	1.073	1.117	1.126	1.116
		0.0081	0.0696	0.0015	0.0171	0.0205

Table A4: Table showing the results for the tests described in Table A2. Results indicated with an asterisk indicate tests presented in Chapter 2.

Exp.	W	NW	HQ	NE	SE
13	1.084	1.123	1.186	1.211	1.191
	0.0033	0.0017	<0.0001	<0.0001	0.0001
14	1.055	1.091	1.151	1.170	1.170
	0.0308	0.0117	<0.0001	0.0004	0.0001
15	0.965	0.989	1.034	1.065	1.055
	0.8207	0.5805	0.1885	0.125	0.1394
16	1.0788	1.114	1.175	1.179	1.161
	0.0067	0.0062	<0.0001	0.0003	0.0009
17*	1.047*	1.081*	1.129*	1.137*	1.122*
	0.0710*	0.0228*	<0.0001*	0.0026*	0.0046*
18	1.085	1.091	1.136	1.145	1.135
	0.0037	0.0235	0.0004	0.0048	0.0047
19	1.075	1.070	1.129	1.155	1.131
	0.0109	0.0414	<0.0001	0.0005	0.0016
20	0.960	0.973	1.027	1.044	1.042
	0.8922	0.7277	0.1776	0.162	0.1598
21	0.979	0.989	1.034	1.065	1.053
	0.7173	0.5823	0.1877	0.1224	0.1471
22	1.066	1.068	1.126	1.132	1.111
	0.0261	0.0477	0.0001	0.0025	0.0051
23	0.970	0.993	1.037	1.044	1.030
	0.8033	0.5617	0.1182	0.1751	0.2406
24	0.971	0.977	1.017	1.025	1.016
	0.7919	0.6778	0.3227	0.326	0.3764

Table A5: Table showing double ratios and probabilities of occurrence for the period 1950/1960-1985 and 1980-2005. The data used to create these results included both BoM and HT sites, with a threshold longevity criteria of 0.5 (either 1950-2005 or 1960-2005).

Start	End	Type		W	NW	HQ	NE	SE
1950	1985	HECA	DR	0.961	0.954	0.997	1.036	1.124
			Sig.	0.8636	0.8522	0.5108	0.2750	0.0626
1950	1985	CSIRO	DR	0.993	0.976	1.041	1.042	1.128
			Sig.	0.5586	0.6894	0.3384	0.2276	0.0342
1960	1985	HECA	DR	0.991	0.974	1.013	1.040	1.126
			Sig.	0.6040	0.7236	0.3588	0.2548	0.0550
1960	1985	CSIRO	DR	0.993	0.976	1.015	1.042	1.128
			Sig.	0.5636	0.6862	0.3322	0.2212	0.0322
1980	2005	HECA	DR	1.054	1.060	1.103	1.122	1.047
			Sig.	0.0322	0.1262	0.0066	0.0302	0.1946
1980	2005	CSIRO	DR	1.047	1.053	1.097	1.116	1.041
			Sig.	0.1294	0.1984	0.0206	0.058	0.2184

Table A6: Table showing the results using successively greater number of seeded events to define a seeded month for the HECA target. Results are for the 50% longevity threshold, 1960-2005 including both Hydro Tasmania and BoM sites. Columns from the left are either double ratio or significance, no. of seeded events used to define a seeded month, number of seeded months in the seeded sample then results relative to the west, northwest, high quality, northeast and southeast controls.

HECA	Seed	No.	W	NW	HQ	NE	SE
DR	1	130	1.054	1.089	1.137	1.145	1.130
SIG			0.017	0.0118	<0.0001	0.0026	0.004
DR	2	95	1.020	1.153	1.168	1.217	1.233
SIG			0.219	<0.0001	<0.0001	<0.0001	<0.0001
DR	3	70	1.026	1.104	1.133	1.149	1.235
SIG			0.1746	0.0106	0.0002	0.003	<0.0001
DR	4	49	1.014	1.124	1.141	1.167	1.212
SIG			0.3104	0.0064	0.001	0.0058	0.0006
DR	5	30	1.042	1.175	1.171	1.219	1.186
SIG			0.1292	0.0032	0.0004	0.0032	0.013
DR	6	23	1.035	1.285	1.235	1.410	1.217
SIG			0.1998	0.0002	<0.0001	<0.0001	0.0082

Table A7: As in Table A6 for the CSIRO target.

CSIRO	Seed	No.	W	NW	HQ	NE	SE
DR	1	130	1.047	1.081	1.129	1.137	1.122
SIG			0.0658	0.0292	<0.0001	0.0026	0.003
DR	2	95	1.002	1.133	1.148	1.196	1.212
SIG			0.48	0.0026	<0.0001	<0.0001	<0.0001
DR	3	70	1.010	1.086	1.115	1.130	1.215
SIG			0.3772	0.0378	0.0018	0.0096	<0.0001
DR	4	49	1.007	1.116	1.133	1.158	1.203
SIG			0.422	0.0178	0.0016	0.0068	0.0002
DR	5	30	1.079	1.217	1.212	1.262	1.228
SIG			0.06	0.0018	0.0002	0.0016	0.001
DR	6	23	1.075	1.335	1.284	1.466	1.265
SIG			0.0964	<0.0001	<0.0001	<0.0001	0.001

Appendix B: Sensitivity Analysis

Within this section results associated with the sensitivity analysis of Section 4.3 are presented. Figures 1, 2, 3 and 4 show thermodynamic profiles associated with the various sensitivity experiments, detailed in Section 4.3. Figures 1 and 2 are associated with the upwind soundings of the August 2006 and October 2007 cases respectively. Figures 3 and 4 are associated with the downwind soundings. Little difference is observed between the various sensitivity experiments. No attempt to quantitatively compare thermodynamic profiles is made. The profiles are included for completeness.

Figures 5 and 6 show planar view cloud-top temperatures for August 2006 and October 2007, respectively. The observations for the times shown are presented in Figure 3.8. Little difference is observed between the different numerical experiments. With the exception of the Lin microphysics package (Lin et al., 1983) all experiments clearly show a line of cooler clouds associated with a post frontal trough during the August case. The Lin microphysics produces a cloud field with the greatest difference relative to the other experiments.

October 2007 planar view cloud-top temperatures are shown in Figure 6. All experiments show the frontal cloud band well positioned over the western side of the island of Tasmania. The Lin microphysics package appears the most different, clearly showing an underestimate regarding total cloud cover relative to the other simulations.

Tables A8 and A9 quantitatively describe the bulk statistical properties of the cloud-top temperature fields for all numerical experiments and observations.

Regarding August 2006, all numerical experiments underestimate cloud fraction by $\sim$30%, with the Lin microphysics producing the lowest value. There is little difference between the variations based on the Thompson microphysics. The observed distribution of CTT is highly skewed with the mean temperature being 6°C below the median. No simulation reproduces this difference well. Further, the observed standard deviation of CTT is $\sim$17°K. The largest simulated standard deviation is $\sim$ 7.5, approximately half the observed value. The Lin microphysics experiment has the smallest spread in the distribution of CTTs.

October 2007 is much better represented by all numerical experiments. Cloud fraction is close to the observed often $>$0.9, with the exception of Lin which is $\sim$0.8. In this case the observed mean and median are close, $\sim$265°K and the standard deviation is $\sim$9°K. The simulations generally reproduce this well with a slight bias to cooler cloud-tops. The standard deviation in simulated CTTs is generally underestimated by between 1-2°K.

Figures 7 and 8 show cross sections along 42S within domain 4 for both case studies. As was the case for the thermodynamic profiles, no attempt to quantitatively compare the cross sections is made. They are included for completeness.

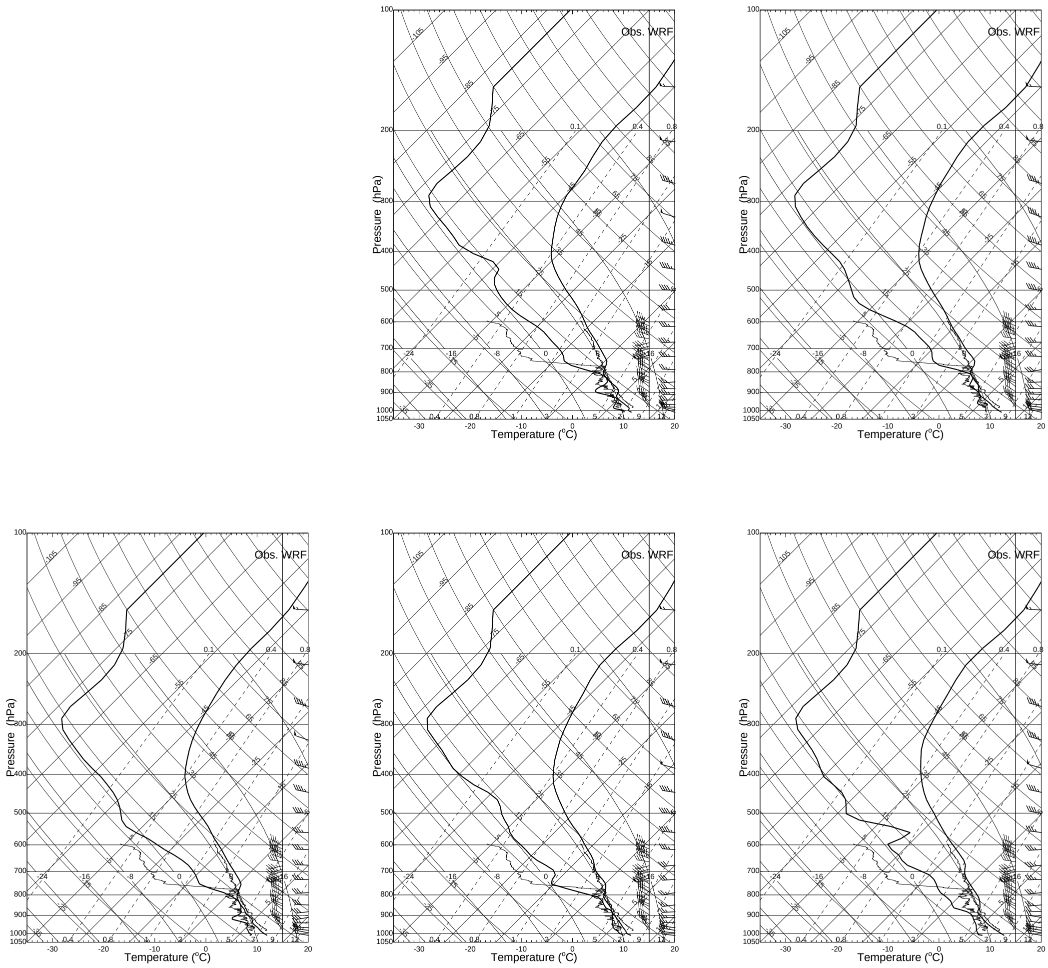

Figure 1: Upwind soundings comparison 23:00 08/08/2006. Standard configuration is shown in Figure 3.5 (a). Top middle - Meyers, top right - Fletcher, bottom left - Standard Configuration Nc=150, bottom middle - Standard Configuration Nc=30 and bottom right - Lin.

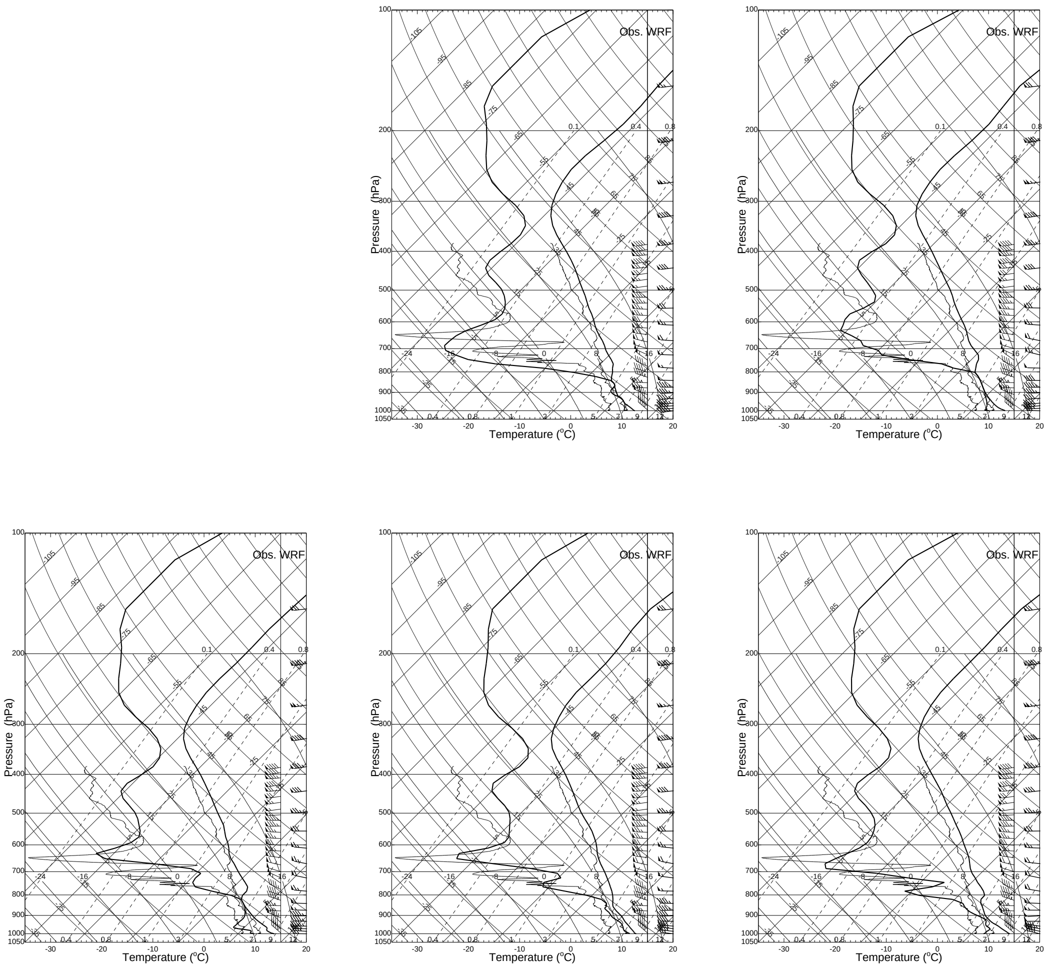

Figure 2: Upwind soundings comparison aircraft, 03:00, model 05:00 04/10/2007. Standard configuration is shown in Figure 3.6 (a). Top middle - Meyers, top right - Fletcher, bottom left - Standard Configuration Nc=150, bottom middle - Standard Configuration Nc=30 and bottom right - Lin.

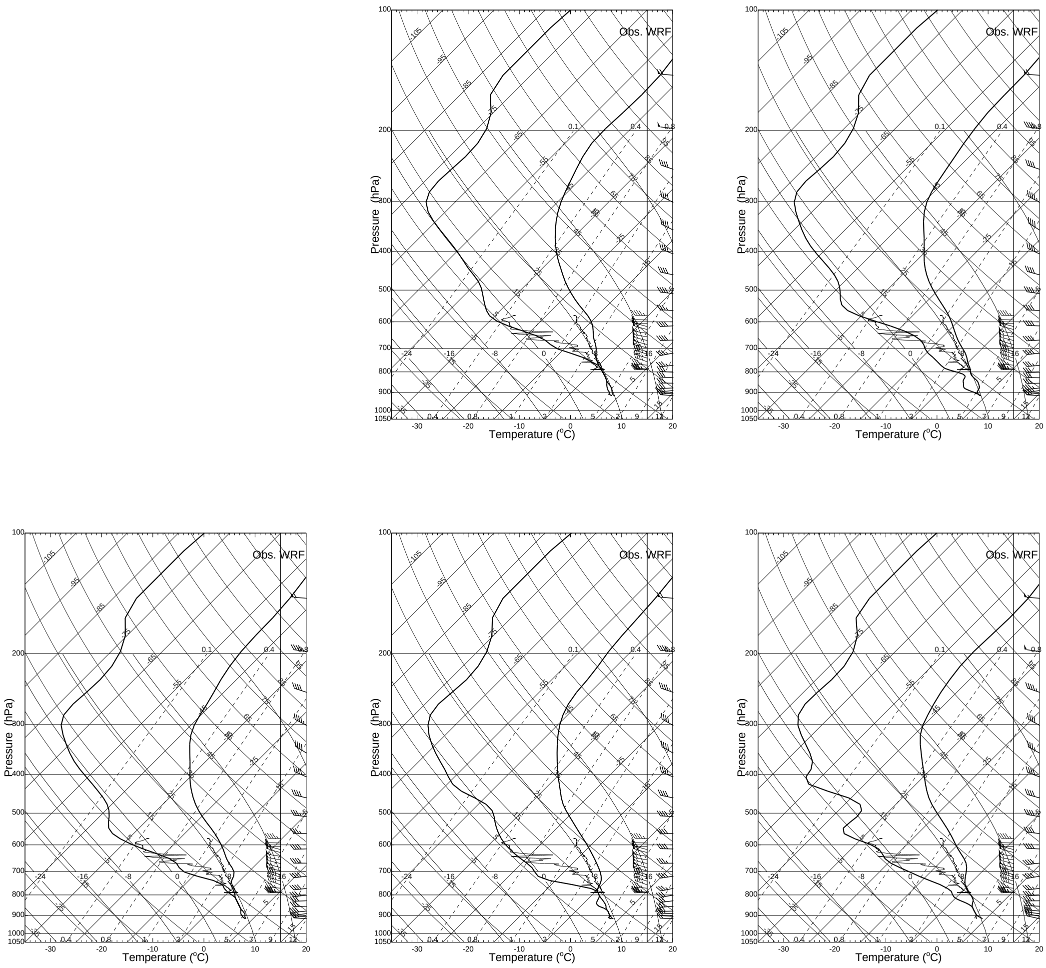

Figure 3: Downwind soundings comparison 00:00 09/08/2006. Standard configuration is shown in Figure 3.5 (b). Top middle - Meyers, top right - Fletcher, bottom left - Standard Configuration Nc=150, bottom middle - Standard Configuration Nc=30 and bottom right - Lin.

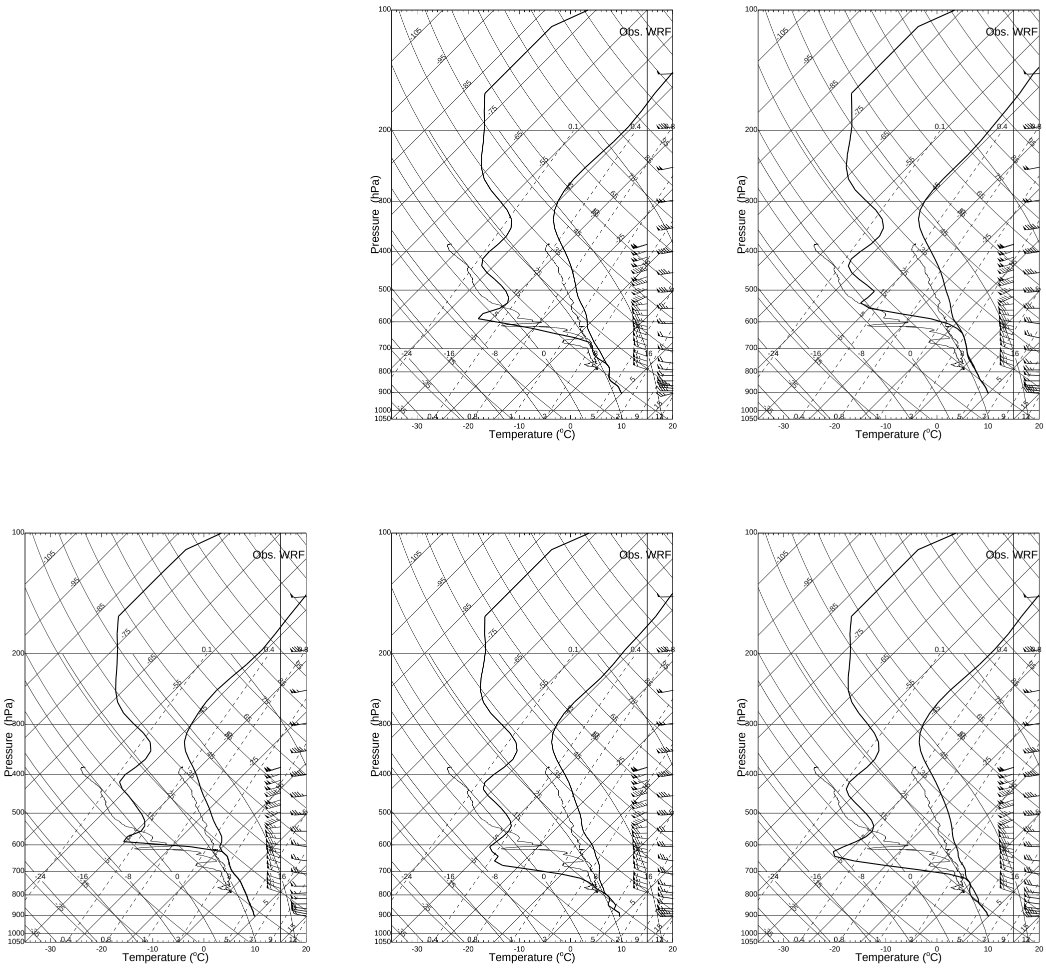

Figure 4: Downwind soundings comparison, aircraft 03:00, model 05:00 04/10/2007. Standard configuration is shown in Figure 3.6 (b). Top middle - Meyers, top right - Fletcher, bottom left - Standard Configuration Nc=150, bottom middle - Standard Configuration Nc=30 and bottom right - Lin.

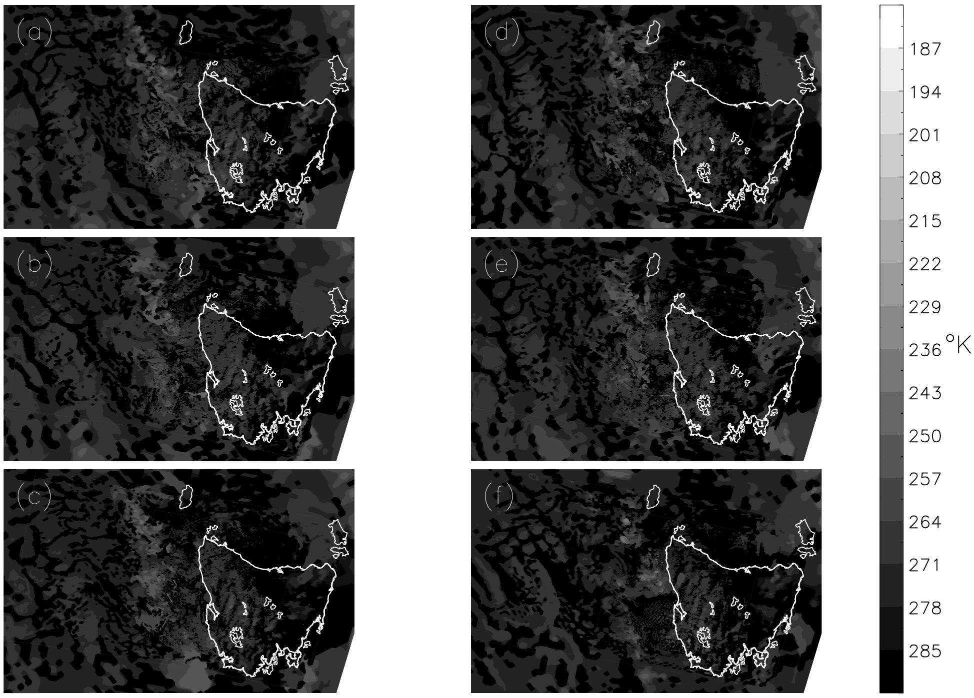

Figure 5: Planar view cloud-top temperature for 00:00 09/08/2006. (a) is for the standard configuration, (b) standard config. with CCN = 150, (c) standard config. CCN=30, (d) Meyers, (e) Fletcher and (f) Lin.

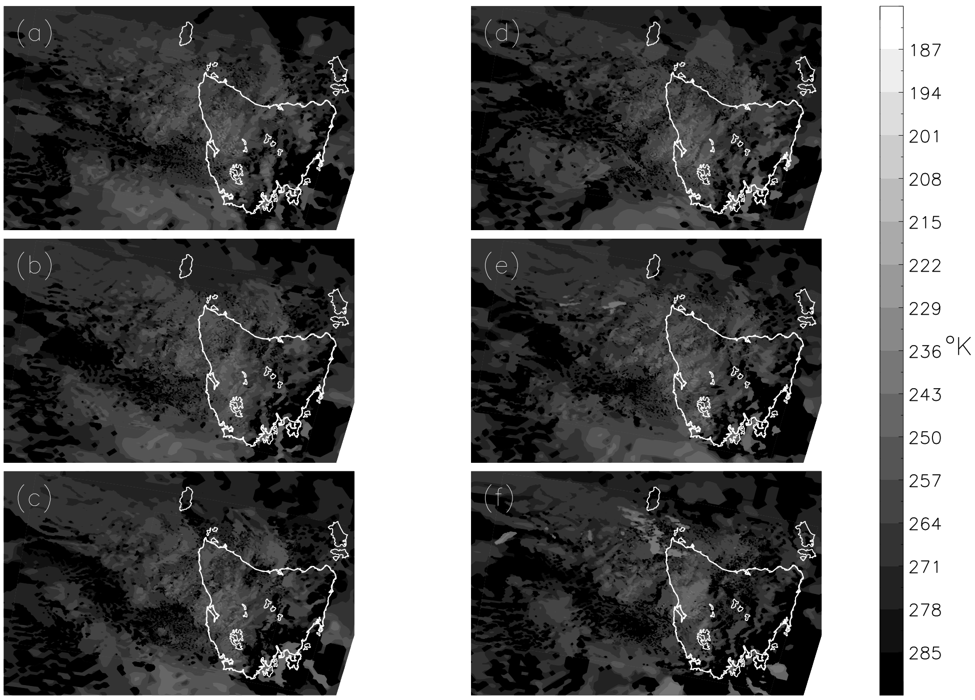

Figure 6: Planar view cloud-top temperature for 02:00 04/10/2007. (a) is for the standard configuration, (b) standard config. with CCN = 150, (c) standard config. CCN=30, (d) Meyers, (e) Fletcher and (f) Lin.

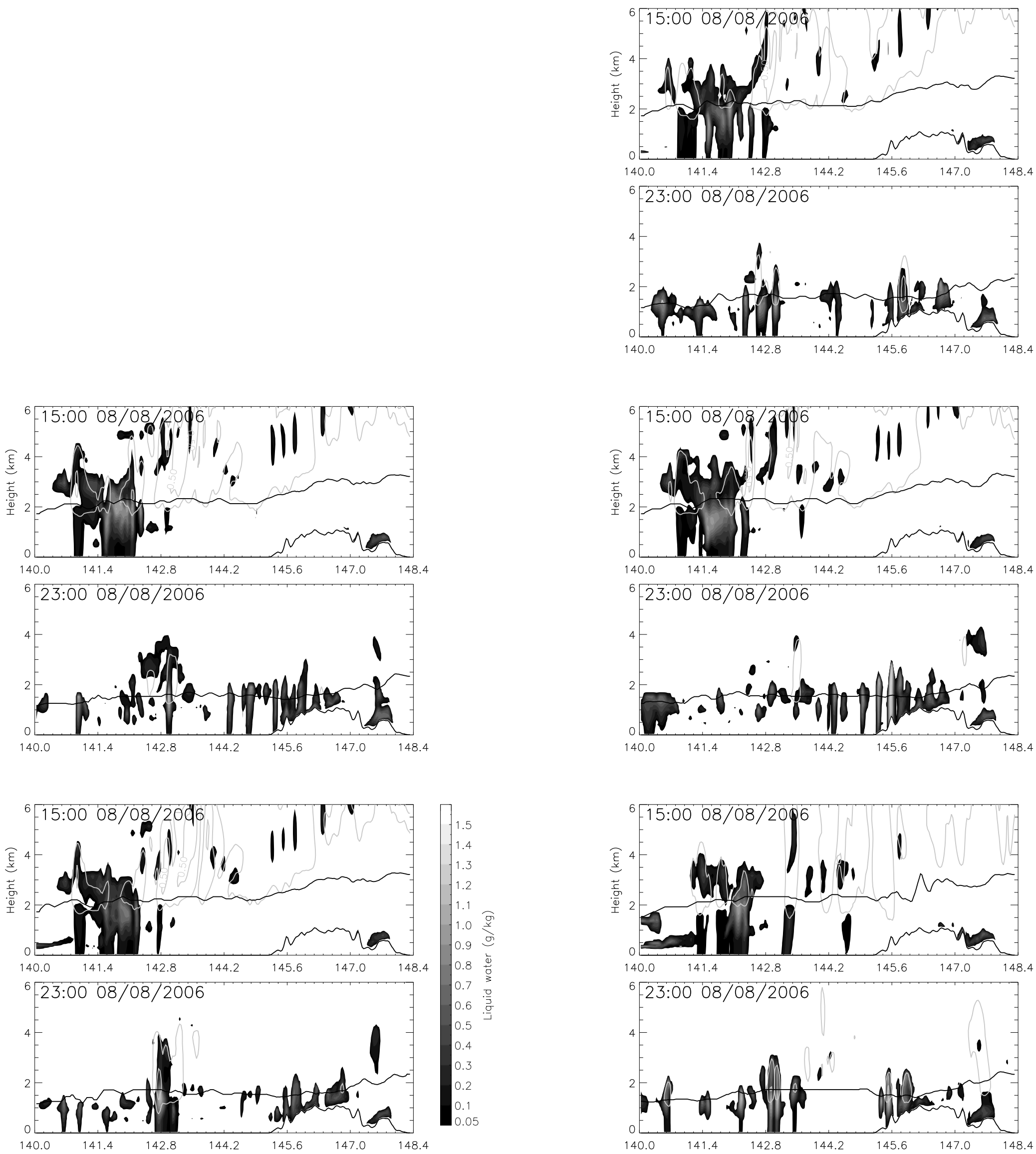

Figure 7: Cross sections across 42S for the August 2006 case, for domain 4 showing the Southern Ocean (140-145E) and Tasmania (145-148E). Filled contours show liquid hydrometeors ($q_c + q_r$), grey contours show frozen hydrometeors ($q_i + q_s + q_g$) the first contour is 0.05g/kg larger contours are in steps of 0.5g/kg. The solid black line indicates the height of the freezing layer. The standard configuration is shown in Figure 4.2, plots (a) and (b). 15:00 is during the passage of the frontal cloud band, 23:00 is postfrontal. Top right - Meyers, center left - standard configuration Nc=150, center right - Fletcher, bottom left - standard configuration Nc=30 and bottom right - Lin.

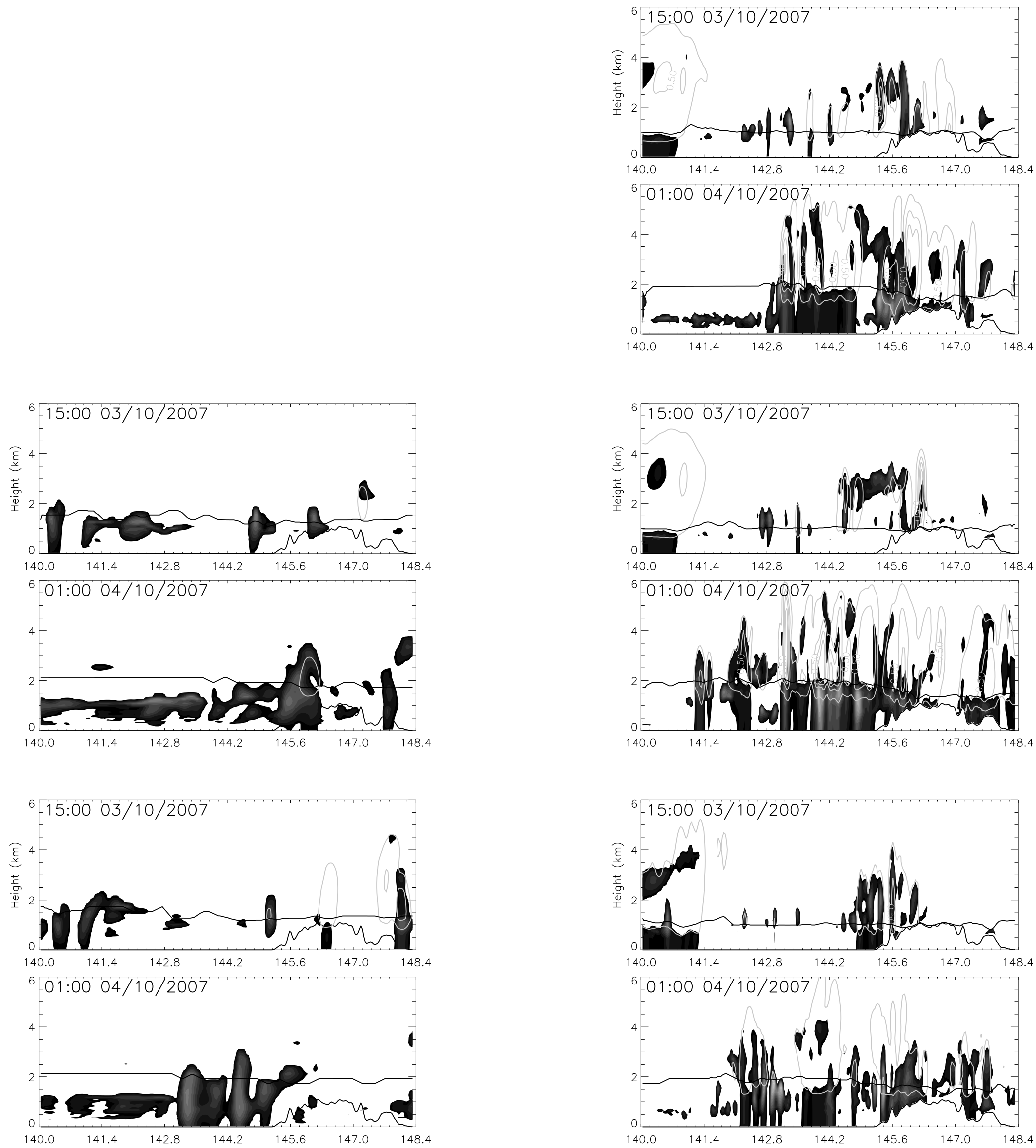

Figure 8: As in Figure 7 for October 2007. The standard configuration is shown in Figure 4.2, plots (c) and (d). 15:00 03/10/07 is prefrontal, 01:00 04/10/2007 is postfrontal. Top right - Meyers, center left - standard configuration Nc=150, center right - Fletcher, bottom left - standard configuration Nc=30 and bottom right - Lin.

Table A8: August 2006 case. Mean, median and standard deviation of cloud-top temperature (°K) together with cloud fraction for domain 5. Results are shown for the observations and all numerical sensitivity experiments.

August 2006	Mean	Median	Stdev	Cloud Fraction
Obs. 23:50	261.47	267.62	16.69	0.94
Stand. Conf.				
WRF 00:00	268.11	268.95	5.91	0.65
WRF 01:00	266.98	268.97	7.46	0.69
Nc=150				
WRF 00:00	268.66	269.43	5.52	0.67
WRF 01:00	266.85	268.92	7.43	0.68
Nc=30				
WRF 00:00	269.06	269.74	5.67	0.59
WRF 01:00	266.70	268.80	7.61	0.67
Meyers				
WRF 00:00	268.88	269.87	5.65	0.62
WRF 01:00	267.61	269.80	7.10	0.71
Fletcher				
WRF 00:00	268.48	269.12	5.27	0.67
WRF 01:00	266.90	268.54	7.20	0.69
Lin				
WRF 00:00	269.68	270.96	5.45	0.54
WRF 01:00	268.82	270.75	6.03	0.60

Table A9: October 2007 case. Mean, median and standard deviation of cloud-top temperature (°K) together with cloud fraction for domain 5. Results are shown for the observations and all numerical sensitivity experiments.

October 2007	Mean	Median	Stdev	Cloud Fraction
Obs. 00:05	265.42	264.78	9.35	0.96
Stand. Conf.				
WRF 00:00	263.08	262.85	7.66	0.91
WRF 01:00	264.06	264.23	8.03	0.88
WRF 02:00	263.46	263.42	7.21	0.93
Nc=150				
WRF 00:00	262.75	262.84	7.54	0.90
WRF 01:00	262.62	262.70	8.04	0.88
WRF 02:00	263.48	263.17	7.22	0.91
Nc=30				
WRF 00:00	263.82	263.76	7.46	0.86
WRF 01:00	264.00	263.81	8.31	0.86
WRF 02:00	264.14	263.86	7.63	0.88
Meyers				
WRF 00:00	263.80	263.95	7.71	0.88
WRF 01:00	263.77	263.95	7.63	0.91
WRF 02:00	263.50	263.44	7.35	0.92
Fletcher				
WRF 00:00	264.00	263.96	7.28	0.90
WRF 01:00	263.42	263.42	8.10	0.87
WRF 02:00	263.16	263.15	7.44	0.92
Lin				
WRF 00:00	264.82	265.10	6.74	0.80
WRF 01:00	264.78	264.54	7.22	0.82
WRF 02:00	263.89	264.77	8.45	0.82